Core conductor theory and cable properties of neurons

WILFRID RALL | *Mathematical Research Branch, National Institute of Arthritis, Metabolism, and Digestive Diseases, National Institutes of Health, Bethesda, Maryland*

CHAPTER CONTENTS

INTRODUCTION

Core Conductor Concept

A simple core conductor can be described as a long thin tube of membrane that is filled with a core of electrically conducting medium (e.g., axoplasm) and is bathed on the outside by another electrically conducting medium (e.g., extracellular fluid). This membrane tube is typically a cylinder whose length is very much greater than its diameter. For nerve axons or dendrites, the resistance to electric current flow across the membrane is much greater than the core resistance for short length (i.e., small, compared with the length constant λ) increments along the cylinder. Because of these relative resistances, it follows that electric current inside the core conductor tends to flow parallel to the cylinder axis for considerable distance before a significant fraction can leak out across the membrane. It is this simple physical concept that provides the basis for a cable theory treatment of steady-state distributions of current and potential in neuronal core conductors; for transient cable properties, the membrane capacitance must also be taken into consideration. An explicit mathematical derivation of cable theory from these physical concepts is provided later in this chapter (see the section ASSUMPTIONS AND DERIVATION OF CABLE THEORY).

Perspective

Both the concepts and the mathematical theory of core conductors have played an important role in neuroscience for over 100 years. They have provided a basis for the interpretation of electrophysiological observations in terms of the underlying anatomic structures. The early mathematical theory was a remarkable achievement that arose (ca. 1870) from a need to interpret early experiments made on whole nerve trunks (see references in section BRIEF HISTORICAL NOTES). Not until the introduction of single axon preparations and electronic instrumentation (ca. 1930) did detailed quantitative testing of theoretical predictions become possible.

Both theory and experiment underwent complementary development during the period before and after World War II (1930–1950). Cable theory predictions were elaborated mathematically, computed numerically, and displayed graphically and thus provided the basis for improved experimental designs. This led to remarkable success in the characterization of axonal membrane properties and cable properties. It is relevant here to note that the most sophisticated studies of active (i.e., nonlinear) membrane properties were made under experimental conditions (space clamp and voltage clamp) designed to eliminate cable properties. Although this was highly successful with excised giant axons, such space clamping was not applicable to cells with dendritic trees.

The use of intracellular micropipettes began (ca. 1950) to provide a wealth of new electrophysiological data from neuromuscular junctions and from motoneuron somas. Correct interpretation of these data depended on a careful consideration of the cable properties to be expected in these experimental situations. With the nerve-muscle preparations, it was found that the cable properties of the muscle fiber corresponded (at least in first approximation) to a core conductor of effectively infinite length; that is, the length was many times the length constant (λ), as was also true for axons. With motoneurons, however, the situation was complicated by the unknown contribution of the dendrites and by the fact that the intracellular recording site was usually restricted to the soma. It was necessary to apply cable theory to extensively branched dendritic trees and to consider such problems as the following. How significant is the contribution of dendritic cable properties to observations recorded at the soma? How should the dendrites be included in our efforts to estimate motoneuron membrane properties? How important are dendritic synapses to the integrative performance of the neuron? Also, how well can a dendritic tree be represented as an equivalent cylinder? How long are the individual dendritic branches relative to their length constant (λ) values, and what is the effective length of a dendritic tree or its most nearly equivalent cylinder?

The theoretical and experimental efforts of the past 15 years have provided some of the answers for motoneurons of cat spinal cord and some general results and conceptual models that should be useful with other neuron types as well.

Comment

Considerations of space, time, and the differing needs of various readers all share responsibility for the fact that different portions of this chapter are written at different levels. The historical notes skip lightly over the efforts of many people. The mathematical derivation of the cable equation is rather detailed (probably too pedantic for some readers); it represents an attempt to meet a need that has been expressed to me by numerous colleagues. In contrast, the mathematical solutions for various particular boundary conditions and initial conditions are presented with less explanatory comment, but further details are available in the recent literature. Also many interesting topics and examples have been mentioned only very briefly or not at all.

Reviews and Monographs

Taylor (182) has reviewed many aspects of cable theory and also has provided references to the older reviews of the 1920's and 1930's. The bibliographies and comments on historical aspects of cable theory by Brazier (12), Harmon & Lewis (64a), Hodgkin (71–

76), Katz (97, 99), Lewis (107), Lorente de Nó (113), Scott (169a) Stämpfli (176), and Tasaki (179, 181) are useful. A valuable monograph by Cole (24) provides unique insights, knowledge, and review of membrane biophysics and cable theory.

Some review of dendritic neuron models is provided by Barrett & Crill (6, 7), Jack & Redman (92, 93), and Rall (142, 143, 147, 148). A monograph by Hubbard, Llinás, and Quastel (82) includes some cable theory, as well as some aspects of dendritic neuron models. A monograph by Jack, Noble, and Tsien (91) provides a valuable presentation of many aspects of cable theory, neuron models, and membrane biophysics.

With regard to the contrast of dendritic synaptic function with axonal function, the ideas of the late 1950's were discussed by Bishop (10), Bullock (15) Eccles (37, 38), Fadiga & Brookhart (44), Fatt (46, 46a, 46b), Frank & Fuortes (54), Grundfest (64), Lorente de Nó & Condouris (116), and Rall (138–142). By the mid 1960's an increased understanding of the dendritic contribution to synaptic potentials in motoneurons was both documented and reviewed in a series of five related papers (17, 129, 144, 149, 174). The role of dendritic cable properties in the generation of cortical field potentials has been elucidated with application to the olfactory bulb (147, 151, 152, 170) and then to the cerebellum (110, 190). Both the experimental evidence and the implications of various recently discovered synaptic arrangements, some of which include dendrites as both presynaptic and postsynaptic, have been reviewed in a recent monograph by Shepherd (171).

Terms used in this chapter are defined in the LIST OF SYMBOLS.

BRIEF HISTORICAL NOTES

Early Electrophysiology

It is remarkable that not only electrophysiology, but also electrochemistry and much of electrophysics, can be traced back to a common origin (ca. 1790) in the provocative observations and arguments of Galvani (Professor of Anatomy at Bologna) and Volta (Professor of Physics at Pavia). Systematic physical measurements of electric currents generated by nerve and muscle were begun in the 1840's by Matteucci (Professor of Physics at Pisa) and by du Bois-Reymond (in the Berlin physiological laboratory of Johannes Müller); many references and comments on this early period can be found in a historical chapter by Brazier (12).

Electrotonus

Electrotonus has had various meanings over the years, sometimes descriptive and sometimes theoretical. In a two-volume treatise in 1848–1849, du Bois-Reymond (36) dealt at great length with his observa-

tions and his theory of the electrotonic state of nerve tissue (des elektrotonischen Zustandes des Nerven). To him this meant the state of changed electromotive forces (emf's) in the tissue during steady applied current. His theory involved polarizable "*Molekeln*" that were supposed to align themselves longitudinally under applied longitudinal current (in analogy with the magnetization of iron by a magnetic field); this theory lost in competition with core conductor and cable theory. It may be noted that in 1859 Pflüger (133) also wrote a book devoted to this early physiology of electrotonus.

Passive Membrane Electrotonus

With the development of core conductor theory and the improvement of experimental techniques over the years, it became recognized that linear aspects of the observed phenomena (those explainable in terms of a core conductor having a passive membrane) should be distinguished from the nonlinear aspects. A classic example was provided by the asymmetry found beneath the cathode and the anode when externally applied current was just below the threshold for initiation of a propagated impulse. Such local nonlinearity was referred to as the "local response" by Hodgkin, Katz, and Rushton (72, 80, 96, 163) and was sometimes characterized as an active membrane property.

Passive Versus Active Membrane

A passive membrane can be defined as one whose transmembrane impedance and emf remain constant (independent of transmembrane potential and time). An active membrane exhibits changing impedance, and/or emf, and regenerative coupling to the transmembrane potential. The active membrane state defined by Hodgkin & Katz (79) differs from the resting state by the greatly increased permeability to sodium ions; this changes the resultant effective membrane emf by changing the relative weighting of the parallel sodium and potassium emf's in their version of the Goldman equation (58, 79). With this distinction between passive and active membrane properties, the early confusion between different aspects of empirical electrotonus can be understood. Most physiologists now restrict the adjective "electrotonic" to passive membrane core conductor properties. This applies to present terminology, such as electrotonic distance and electrotonic length.

Cable Theory

Cable theory dates back to 1855 when Professor William Thomson (later to become Lord Kelvin) presented to the Royal Society a series of excerpts of his correspondence with Professor Stokes (101). This provided a mathematical theory and practical applications for the submarine (transatlantic) telegraph ca-

ble then being planned. Thomson not only derived the cable equation, but also, being thoroughly familiar with the mathematical advances made around 1822 by Fourier (55) for problems in heat conduction, he presented both steady-state and transient solutions for particular cable boundary conditions and initial conditions.

An important merit of cable theory is the simplifying assumption that reduces the problem to a single spatial dimension, namely, distance along the cable; this greatly facilitates the theoretical treatment of transients, as well as steady states. The advantage to be gained by applying cable theory to neuronal core conductors was not explicitly recognized until about 1900 (30, 68–70, 81). Since 1945 the two most important presentations of cable theory (with application to transients in axons) have been provided by the now classic papers of Hodgkin & Rushton (80) and Davis & Lorente de Nó (33).

Core Conductor Concept

The idea of accounting for nerve electrotonus by means of a core conductor model was first proposed and demonstrated in 1863 by Matteucci (122). This suggestion was further developed, tested, and vigorously defended by Hermann (67-70) in the 1870's and on through 1900. The core conductor model (*Kernleiter*) consists of a long, thin electrically conducting core that is encased by a thin membrane (or sheath) and placed in a solution of electrolytes. The earliest models were made of platinum wire encased in a moistened cloth sheath; a more realistic model was made with a hollow grass stem (natural straw) filled with and soaked in electrolyte solution. When current is applied between two electrodes placed along the outside of the membrane sheath (see Fig. 1), much of this current flows directly through the external electrolytic medium from the anode to the cathode, but some current flows from the anode inward across the membrane, then along the core conductor, and outward across the membrane to the cathode. Because the membrane offers significant resistance, the current flowing across it becomes spread out over a considerable membrane surface area. This spread of membrane current extends into extrapolar regions, as well as the interpolar region, which means that extracellular current must also flow into these extrapolar regions, thereby providing an important point of agreement between experiment and the core conductor model. Quantitative testing depends on a mathematical core conductor theory and careful experiments. Early testing was necessarily qualitative; quantitative testing had to wait for the development of single-fiber preparations and modern electronic instrumentation.

Core Conductor Theory

A mathematical treatment of core conductors was published in 1873 by Weber (184) who was a close
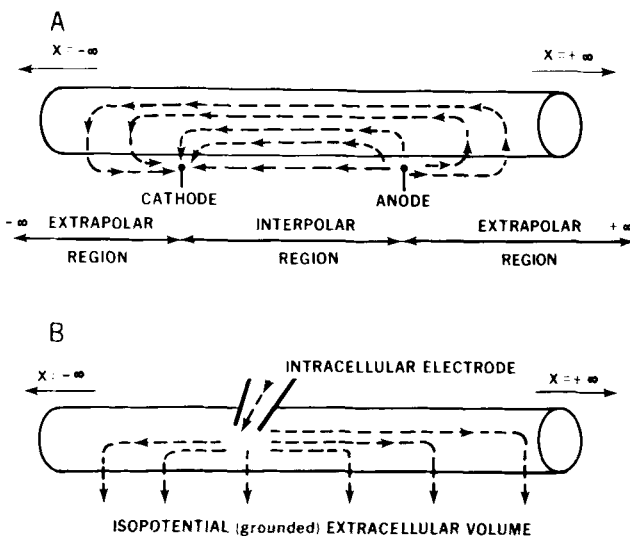
FIG. 1. Cylindrical core conductor with the spreading distribution of electric current indicated (only roughly) by *dashed lines*, for 2 arrangements of electrodes; cylinders extend to (±) infinite length. A: both electrodes (cathode and anode) are extracellular; some current flows entirely extracellularly, directly from anode to cathode in the interpolar region; some extracellular current flows out into the extrapolar region before crossing the membrane. B: intracellular (micropipette) electrode provides source of current that spreads along the core before crossing the membrane to the extracellular volume that is isopotential with a ground electrode.

colleague of Hermann in Zurich. Weber provided a thorough three-dimensional analysis that is now recognized as classical mathematical physics: the application of Bessel functions to the steady flow of electricity in a cylindrical coordinate system. Whenever one is interested in analyzing the distribution of electric current and potential in the external volume or within the cylindrical core cross section, it is necessary to use such a three-dimensional theory (22, 41, 45, 132, 134-136, 146, 186). Weber's solutions also make explicit the nonuniformity of potential and current density in cylindrical cross sections near an electrode. Weber himself pointed out that, with increasing distance from the electrode, the potential within cylindrical cross sections becomes more nearly uniform and the (extrapolar) potential approaches an exponential decrement with distance along the core conductor (184). Thus, for locations not too close to an electrode, the steady-state results of three-dimensional core conductor theory do approach the simpler results of one-dimensional cable theory. Recently the differences between a three-dimensional and a one-dimensional treatment have been reexamined, both theoretically and computationally [for axons of infinite length, see (22, 41, 57, 65, 132, 134-136); for passive decay transients in core conductors of finite length, see (134a, 145, 146)]. The conclusion is that one-dimensional cable theory provides an excellent approximation for most purposes (which involve longitudinal distances that are many times the cylinder diameter) but that significant differences can occur at locations close to point sources of current and in

problems where the distribution of potential in a large extracellular volume is of primary importance.

Estimation of Membrane Capacitance

The importance of electric capacitance for the time course of passive electrotonic spread and of impulse propagation in a core conductor was recognized and discussed by Hermann (69). He presented diagrams and equations for core conductor local circuits which demonstrated that extra charge (or depolarization) at one location would produce local electric currents whose effect is to charge (or depolarize) the membrane capacity at successive locations along the core conductor. He reported overall capacitance values of the order of 0.5 μF for a whole nerve trunk but emphasized the unreliability of the measurements and the difficulty of estimating values for single fibers from nerve trunk measurements. These difficulties were not overcome until 1937 when Curtis & Cole (31) performed transverse AC impedance measurements with a squid giant axon and obtained a value of 1.3 μF/cm² for its membrane capacitance. Cole (24) provides a detailed account of the history of cell membrane capacity measurement and credits Fricke with the earliest reliable measurements and interpretations, made in 1922 with red blood cell suspensions. Additional measurements by Fricke and others on red cells of many species all provided a membrane capacitance value of about 0.8 μF/cm², which was independent of frequency and variations in the suspending solution. These results, together with those that Cole and his collaborators obtained with suspensions of sea urchin eggs and later with *Nitella* and squid axons, all pointed to values of the order of 1 μF/cm² as the membrane capacitance of living cell membrane. Cole (24) regards this as a biological constant, with extreme values of about 0.5 and 2.0 μF/cm². This is recognized as primarily a property of the thin lipid layer (inner biomolecular layer) that is common to all cell membranes.

The representation and interpretation of tissue impedances and membrane impedances in the complex plane have been reviewed and discussed by both Cole and Schwan (24, 26, 166–168). The estimation of

nerve membrane capacitance by means of a cable theory analysis of transients in single large axons of lobster and crab was provided by Hodgkin & Rushton (80), Hodgkin (73), and Katz (98); these estimates agree with a C_m value of the order of 1 μF/cm². Space-clamped squid axons have provided estimates of the same order. (See LIST OF SYMBOLS at the end of this section for definitions).

It may be noted that similar experiments with muscle fibers yielded significantly larger membrane capacitance values (98); subsequent research accounts for much of this difference in terms of the sarcoplasmic reticulum and t tubes that are peculiar to muscle (see the chapter by Costantin in this *Handbook*).

Resting Membrane Resistivitiy

The concept of a thin membrane having low permeability to ions and consequently a relatively low electric conductivity (or high electric resistivity) was already contained in the resting membrane concept of Bernstein (8) and in the core conductor concept. The early experimental determinations of membrane capacitance also assumed and supported this idea. However, not until the squid giant axon preparation became available (189), could Cole & Hodgkin (27) obtain the first good estimate of nerve membrane resistivity in 1939. Using steady-state cable theory, they obtained a value of about 1,000 Ω cm² for resting squid axon membrane resistivity. This order of magnitude has been confirmed by many subsequent experiments with squid giant axons, in which space clamping with current or voltage clamping was used (24, 99). This value is included in the representative set of passive cable parameter values for squid giant axon listed in Table 1.

Passive Cable Parameters of Invertebrate Axons

The values already noted for squid giant axon were obtained before World War II. The study by Hodgkin & Rushton (80) was begun before the War but not published until 1946. In this paper they demonstrated how the several passive cable parameters can be

TABLE 1. *Cable Parameters for Invertebrate Giant Axons*

Parameter	Symbol	Units	Squid[1]	Lobster[2]	Crab[3]	Lobster[4]	Earthworm[5]	Marine worm[6]
Axon diameter	d	μm	500	75	30	100	105	560
Length constant, with $r_e = 0$	λ	cm	0.65	0.25	0.23	0.51	0.4	0.54
Input resistance, for x to $\pm\infty$, with $r_e = 0$	$R_{\pm\infty}$	Ω	5×10^3	1.8×10^5	1.5×10^6	2.5×10^5	4.6×10^5	6.2×10^3
Core resistance, per unit length	r_i	Ω/cm	15×10^3	1.4×10^6	13×10^6	1×10^6	2.3×10^6	23×10^3
Membrane resistance, for unit length	r_m	Ω cm	6.5×10^3	9×10^4	0.7×10^6	0.23×10^6	0.37×10^6	6.8×10^3
Intracellular resistivity	R_i	Ω cm	30	60	90	80	200	57
Membrane resistivity	R_m	Ω cm²	1×10^3	2×10^3	7×10^3	8×10^3	12×10^3	1.2×10^3
Membrane time constant	τ	ms	1	2	7		3.6	0.9
Membrane capacitance	C_m	μF/cm²	1	1	1		0.3	0.75

Representative rounded values. [1] *Loligo paelei* (24, 27, 31, 74, 76). [2] *Homarus vulgaris* (80, 99). [3] *Carcinus maenas* (73, 76, 98, 99). [4] *Homarus americanus* (13). [5] *Lumbricus terrestris* (59). [6] *Myxicola infundibulum* (9, 57a, 61).

estimated from a single axon by making several different extracellular measurements and by using theoretical expressions from cable theory to solve for the several unknown basic parameters. They applied this method to the 75-μm diameter axon in the walking legs of the lobster (*Homarus vulgaris*); the same methodology was subsequently applied to the 30-μm diameter axon of crab (*Carcinus maenas*) by Hodgkin (73) and by Katz (98). This milestone in establishing cable theory for single nonmyelinated axons is summarized by rounded representative values of cable parameters included in three columns of Table 1. Definitions of symbols and the theoretical relations between these parameters are provided in later sections of this chapter (Eqs. 3.15-3.22). It should be noted that these values have been adjusted, as in a previous tabulation by Katz in 1966 (99), to correspond to negligible extracellular resistance ($r_e = 0$). More recent experiments using intracellular electrodes (Fig. 1B) have provided the additional values listed in the last three columns of Table 1—for a different lobster (*Homarus americanus*) and for the annelid worms *Lumbricus terrestris* and *Myxicola infundibulum* (9, 13, 57a, 59, 61).

Importance of Single Axon Preparations

It may be noted that Davis & Lorente de Nó (33) provided a useful presentation of cable theory results at about the same time as Hodgkin & Rushton (80). Their experimental applications, however, were not carried out with a single axon, but with a vertebrate nerve trunk (peroneal nerve of bullfrog) consisting of many axons of different diameters, some myelinated and some nonmyelinated. This made it extremely difficult to estimate the cable parameters for any one axon, and it was later found that serious complications also resulted from the significant resistance of the epineural sheath that encloses this nerve trunk (157).

Estimation of Parameters for Myelinated Axons

Success with myelinated axons of vertebrate nerves depended also on experiments performed with single axons. The technique was introduced in 1934 by Kato, and further developed and applied by Tasaki and colleagues (178-181) and by Huxley & Stämpfli (84, 85). Based on this research, a useful set of estimated parameters for a frog myelinated axon was assembled by Hodgkin [(76); cf. (24)] and is here summarized in Table 2.

The idea of saltatory propagation of action potentials in myelinated axons seems to have originated in 1925 with Lillie, but a detailed review of this subject is outside the scope of this chapter (see the chapter by Hille in this *Handbook*). Useful references to the cable aspects are provided by Rushton (164), Tasaki (181), Hodgkin (76), and FitzHugh (50-52); recent

computations of saltatory propagation are provided by Goldman & Albus (60) and by Koles & Rasminsky (104). Properties of active nodal membrane are treated in the chapter by Hille in this *Handbook*.

Space and Voltage Clamp

It is clear that both cable theory and single axon preparations were essential to the experimental determination of passive nerve membrane properties. Once this was accomplished, it became important to avoid the complications of cable properties in order to pursue the details of active membrane properties. Marmont (120) and Cole (23, 24) introduced the techniques now known as space clamping and current clamping by using a long axial electrode inside a squid axon; together with concentric extracellular electrodes (including a guard ring arrangement), this permitted control of membrane current density. Then Cole (23, 24), followed by Hodgkin, Huxley, and Katz (78), combined voltage clamping with space clamping; the space clamp prevents cable complications while the voltage clamp prevents complication by capacitive current; then ionic current is revealed. This powerful technique, combined with the crucial concept of distinguishing the sodium ion current from the potassium ion current (79), provided the basis for the great achievement of Hodgkin & Huxley (77) in characterizing the voltage dependence and the kinetics of these ionic currents. It is now widely appreciated that the resulting Hodgkin-Huxley equations for ionic current, when combined with an unclamped membrane capacity, can account very well for the space-clamped

TABLE 2. *Parameters for Frog Myelinated Axon*

Parameter	Value
Outer diameter	14 μm
Myelin thickness	2 μm
Core diameter	10 μm
Myelin sheath properties	
Capacity per unit length	10-16 pF/cm
Capacity per unit area	0.003-0.005 μF/cm²
Dielectric constant	5-10
Specific resistance	500-800 MΩ cm
Resistance for unit area	0.1-0.16 MΩ cm²
Resistance for unit length	25-40 MΩ cm
Core resistance per unit length	140 MΩ/cm
Specific resistance of axoplasm	110 Ω cm
Distance between nodes	2 mm
Properties of node	
Capacity	0.6-1.5 pF
Resting resistance	40-80 MΩ
Area (assumed)	22 μm²
Capacity per unit area	3-7 μF/cm²
Resistance for unit area	10-20 Ω cm²
Action potential	116 mV
Resting membrane potential	−71 mV
Peak inward current density	20 mA/cm²
Conduction velocity	23 mm/ms

Values based on Huxley & Stämpfli (84, 85), Stämpfli (176), and Tasaki (180), as assembled by Hodgkin (24, 76).

action potential (77). Also, when introduced into the partial differential equation (cable equation) for an axon that is not space clamped, these ionic currents can account for action potential propagation (77).

DENDRITIC ASPECTS OF NEURONS

Axon-Dendrite Contrast

Interesting correlations of structure to function are apparent when dendrites are contrasted with axons. Before going into those details, it is noteworthy that the dendritic trees of neurons are unlikely candidates for space-clamping techniques. (Try to imagine the difficulties in threading a branched intracellular electrode throughout the branched core of a dendritic tree!) It would seem that cable properties must be regarded as an unavoidable complication in experiments made with the soma-dendritic portions of most neurons.

The morphological distinction between axon and dendrites arose about 80 years ago and thus antedates the neuron theory [see (154) for references]. The extensiveness of dendritic branching was established about 60 years ago by Ramón y Cajal (155) and confirmed by many followers. Pioneering quantitative studies of dendritic trees in cerebral cortex were made as early as 1936 by Bok (11) and in the 1950's by Sholl (173). These quantitative methods were extended to spinal cord neurons in 1961 by Aitken & Bridger (1) and later by Gelfan et al. [(56); see (56) also for other references]. The variety of dendritic patterns in different neuron types has recently been emphasized and illustrated by Ramón-Moliner (153, 154) and by the Scheibels (165); contributions of many other anatomists are reviewed in those papers. Very briefly, it can be said that the dendritic trees of vertebrate central nervous system (CNS) provide a very extensive surface area (about 20 times that of the soma, for motoneurons) over which tens of thousands of synapses are distributed to provide a synaptic surface density that is at least approximately the same at distal branch locations as at the soma and dendritic trunks (158, 188). But the functional distance from the soma of a distal dendritic synapse cannot be assessed in terms of anatomy alone.

Although we now know that dendritic branch lengths can be significantly less than λ and that an entire dendritic tree of a motoneuron usually corresponds at least approximately to an equivalent cylinder whose length is between one and two times λ, this knowledge is quite recent. In 1938, at a time when Lorente de Nó made many pioneering contributions to neuroscience, his analysis of "synaptic stimulation as a local process" (112) convinced him that the dendrites were very long compared with λ and that, even at the soma surface, synapses would need to be near each other to sum effectively; these opinions were rather widely accepted for many years. In 1959 Lor-ente de Nó & Condouris (116) still regarded dendritic lengths to be large compared with λ and therefore emphasized that active decremental conduction could compensate for otherwise severe passive electrotonic decrement with distance. Eccles also believed the dendrites to be much longer than λ. As recently as 1964 [(40), p. 111] he asserted that synapses on dendrites are virtually ineffective if situated on the more remote regions of the dendrites; his low estimates of dendritic λ values were based on a low estimate of membrane resistivity (R_m approx. 500 Ω cm²), which was interrelated with an underestimate of the dendritic contribution to input conductance measured at a motoneuron soma [(4a, 37–40, 46b, 119, 138–145); see subsections *Motoneuron Membrane Resistivity* and *Dendritic Dominance* and *Dendritic Electrotonic Length* for additional references and comment].

Both the evidence and the early biophysical interpretations of junctional membrane potentials and membrane properties were provided in 1951 by Fatt & Katz (47, 48) for the neuromuscular junction; corresponding results and interpretations were provided for synaptic transmission to spinal motoneurons by Eccles and his colleagues (14, 28, 29) and subsequently by many others. These junctional potentials could be graded in amplitude, and the synaptic membrane model had ionic permeability changes that differed from those of active membrane in not being voltage dependent. The problem of combining cable theory with localized synaptic membrane was treated by Fatt & Katz (47); the problem for a distributed density of synaptic input over a portion of a finite dendritic cable length was treated by Rall [(141, 143, 144); see also Eq. 2.36–2.49 in section ASSUMPTIONS AND DERIVATION OF CABLE THEORY].

In the late 1950's Bishop (10), Bullock (15), Grundfest (64), and others [e.g., (37, 38, 44, 46, 116, 139, 140)] reviewed and discussed what was being learned about synaptic and dendritic properties and functions and contrasted them with those of axons. On the one hand, the active (nonlinear) membrane properties of an axon can account for all-or-nothing impulse propagation from one end to the other; this enables an axon to fulfill its functional role of providing reliable signal transmission over long distances, for example from one region of the nervous system to another. Different properties and different functional roles were recognized for dendrites and synapses; the emphasis here was on graded response to different amounts of synaptic input. Such grading of synaptic potentials seemed to have more in common with passive membrane properties than with the all-or-nothing impulse of axonal membrane. It became important to consider whether passive dendritic membrane properties (i.e., passive cable properties of dendritic branches) would be sufficient to account for effective spatiotemporal integration of many synaptic inputs delivered to various portions of a neuronal soma-

dendritic surface. This required not only an extension of cable theory to such branching systems, but also required a theoretical basis for using both anatomic and electrophysiological data to estimate important geometric and membrane parameters of such neurons (139–145).

Very briefly, for motoneurons of cat spinal cord, the combination of theoretical and experimental effort has led to the conclusion that these dendritic branches differ from axons in being relatively short and in normally not generating action potentials; the synapses on distal dendritic branches are not too remote to be effective, and altogether the dendritic synapses can dominate the integrative behavior of the neuron. Nevertheless, if some other neuron type should correspond to different theoretical parameters, such that synapses at distal dendritic locations were at greater electrotonic distance (more than 3 times λ) from the soma, this would provide a basis for suspecting at least some active membrane properties at some locations in the dendritic tree.

Microelectrodes in Motoneurons

Direct electrical measurements on individual neurons of mammalian CNS depended on the introduction of glass micropipettes for intracellular stimulation and recording. This technique was introduced with muscle, by Graham & Gerard (62a) and Ling & Gerard (108), followed by Nastuk & Hodgkin (126) and by Fatt & Katz (47), and then by many others (53); the application to motoneurons of cat spinal cord was pioneered by Woodbury & Patton (187) and by Brock, Coombs, and Eccles (14), as reported in the 1952 Cold Spring Harbor Symposium for Quantitative Biology. By the mid-1950's there was a wealth of new electrophysiological data on motoneuron properties (2, 28, 29, 37, 54). Some of the early interpretations of these data and the resulting early estimates of motoneuron parameters proved to be erroneous because the cable properties of motoneuron dendritic trees were either neglected or underestimated; the recognition and early discussion of these misinterpretations began in 1957 [(46b, 138–140); see also (39), 174)].

It has usually been assumed that a microelectrode has penetrated either the soma or one of the larger dendritic trunks, when stable intracellular recordings are obtained; occasionally there is evidence for more distal dendritic locations. However, even if we know that the microelectrode is in the soma, it is important to emphasize that we do not measure properties of the soma membrane alone, uncomplicated by the cable properties of the dendrites. Figure 2 illustrates that when such an electrode is used to apply electric current between the soma interior and a distant extracellular electrode (not shown in Fig. 2) some of this current flows directly across the soma membrane and some of it flows into the several dendritic trees (and the axon) for varying distance before
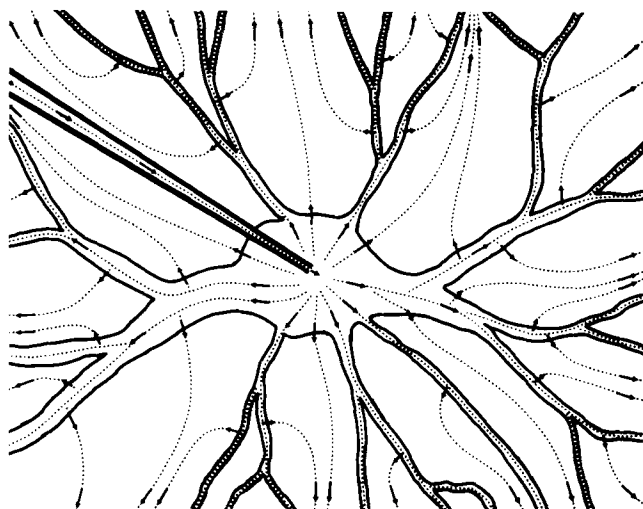
FIG. 2. Flow of electric current from a microelectrode whose tip penetrates the cell body (soma) of a neuron. Full extent of dendrites is not shown. External electrode to which the current flows is at a distance far beyond the limits of this diagram. [From Rall (139).]

crossing the membrane. How the applied current divides between these different paths depends on a combination of geometric and electrical considerations (139). The geometric considerations include the size of the neuron soma, the diameters of the several dendritic trunks, as well as their length and taper, and at least some measure of the amount and extent of dendritic branching in each tree. The electrical considerations include the membrane resistivity and capacity, as well as the volume resistivity of the intracellular and extracellular conducting media; the membrane resistivity is not necessarily the same for the soma and all the dendritic branches.

For a better understanding of the interrelation of these many factors, and to make effective use of available anatomic and electrophysiological data, it became desirable (and even necessary) to formulate explicit theoretical models of neurons having extensive dendritic trees (139–144).

Theoretical Neuron Models and Parameters

It should be emphasized that there is a family of dendritic neuron models. This is composed of particular models that differ in their suitability for different applications because of different choices in simplifying assumptions. The most simplified cases have the advantage of simpler mathematical treatment and simpler biophysical insights. More complicated examples include geometric or membrane complications judged important for particular applications.

It may avoid confusion to distinguish between the conceptual model and the mathematical model. The conceptual model consists of the various simplifying assumptions, some of which can be represented diagrammatically (i.e., one diagram may provide a shorthand symbol for the geometric assumptions and

some of the boundary conditions, while other diagrams represent the membrane models). Nevertheless the working model is a mathematical model consisting of several equations that incorporate the simplifying assumptions and express the interdependence of the primary variables and the theoretical parameters. For some problems, these equations can be solved explicitly; for other problems, the solutions can only be computed numerically. In either case, one often uses graphical methods (or numerical curve fitting) to test the agreement between experiment and theoretical predictions for different values of the parameters. In this way one can obtain estimates of the values of the parameters that provide best agreement with experimental data and one can judge the adequacy of the particular theoretical model for the experiments in question.

Equations have been deferred to the latter portions of this chapter. Here the major simplifying assumptions are noted briefly; a detailed exposition and discussion of these assumptions was provided in 1959 [(139); see also (91, 141, 143)].

A dendritic tree was idealized to consist of a cylindrical trunk and cylindrical branch components. The membrane was assumed to be uniform. The extracellular surface of the entire neuron was assumed isopotential, at least for most purposes. The interior of the soma was assumed isopotential; together with the preceding assumption, this means that the entire soma membrane was assumed to be space clamped; this lumped soma membrane provided a common point of origin for the dendritic trees. At this origin and at all dendritic branch points, the internal potential was assumed continuous and the current conserved (i.e., Kirchhoff's law). The electric current and potential in each trunk and branch cylinder were assumed to obey the one-dimensional cable theory idealization of a core conductor (see section ASSUMPTIONS AND DERIVATION OF CABLE THEORY). The dendritic terminals were assumed to have sealed ends. The membrane was assumed to have simple passive prop-

erties except where synaptic properties were specified (141).

With these assumptions, Rall showed (139) how one can solve the steady-state distribution of current and membrane potential in a neuron model where dendritic branches could be of any arbitrary lengths and diameters, as indicated in Figure 3; how this solution provides a basis for estimating some motoneuron parameters from the experimental data was also shown.

Commentary on the estimation of motoneuron parameters is provided in subsequent sections. A current set of parameter estimates for cat spinal motoneurons is listed in Table 3, which includes a representative value together with a range of values for each parameter, as well as references to the literature. Definitions of these parameters are given in the section entitled LIST OF SYMBOLS. The mathematical relations between these parameters are dealt with in later sections of this chapter and in the references cited.

With regard to variety in neuron models, it should be noted that some models have made use of the class of dendritic trees that can be represented as an equiv-
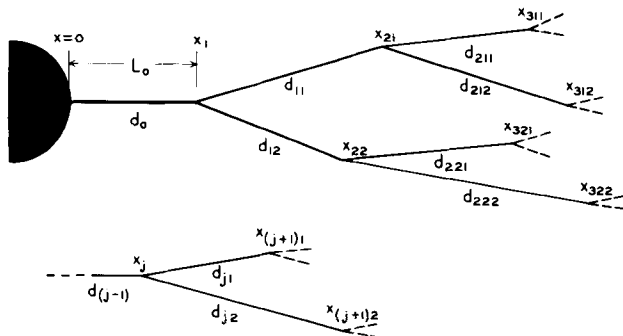
FIG. 3. Arbitrary dendritic branching to illustrate the subscript notation used to treat this problem. Originally L_0 represented actual trunk length; subsequently, I have preferred to use ℓ_0 for actual length and $L_0 = \ell_0/\lambda_0$ as the dimensionless electrotonic length of a dendritic trunk. [From Rall (139).]

TABLE 3. *Parameter Estimates for Cat Spinal Motoneurons*

Parameter	Symbol	Representative Value and Range	References
Neuron input resistance	R_N	1.5 MΩ (0.3–6)	5, 6, 16, 18, 28, 54, 102, 119, 150
Membrane resistivity	R_m	2,500 Ω cm^2 (10^3–10^4)	5, 6, 87, 102, 119, 139
Membrane time constant	τ	5 ms (3–12)	6, 16, 18, 87, 119, 138, 140, 142, 145
Membrane capacitance	C_m	2 μF cm^{-2} (1–4)	6, 142
Time constant ratio	τ_0/τ_1	5 (3–11)	6, 18, 88, 119, 130, 145, 146, 148
Neuron electrotonic length, soma plus dendritic trees	L_N	1.5 (1–2)	5, 6, 18, 87, 119, 130, 141, 145, 148
Conductance ratio, dendrites/soma	ρ	10 (3–25)	5, 6, 87, 102, 119, 130, 139, 140
Intracellular resistivity	R_i	70 Ω cm (50–100)	6
Combined dendritic $d^{3/2}$*	$\Sigma d^{3/2}$	200 × 10^{-6} cm$^{3/2}$ (10^{-4} to 10^{-3})	5, 6, 102, 119, 139
Dendritic surface area*	$A_{\Sigma D}$	28 × 10^{-4} cm^2 (10^{-4} to 10^{-2})	1, 56
Soma surface area*·†	A_S	1 × 10^{-4} cm^2 (10^{-5} to 10^{-3})	1, 56, 119, 139
Neuron surface area*·†	A_N	29 × 10^{-4} cm^2 (10^{-4} to 10^{-2})	1, 5, 6, 56

* Representative values chosen to be consistent with those above, on the simplifying assumption that these dendritic trees can be represented as equivalent cylinders.   † Representative values agree with $\rho = 10$, according to Eq. 5.15, provided either that $R_{mS} = R_{mD}$, with $G_{inj} = 0.7 A_S/R_{mS}$, or that $R_{mS} = 0.6 R_{mD}$, with $G_{inj} = 0$.

alent cylinder [(92, 93, 141–145, 150, 161); see also subsection *Class of Trees Equivalent to Cylinders*]. Some have dispensed with an explicitly lumped soma (150, 161) because of the advantage gained for explicit solutions in the dendritic branches; some models have treated dendritic trees as cylinders of semi-infinite length (4, 28, 92, 93, 138, 140). Still other computations have been done with compartmental models (143, 144, 151). [Each compartment represents a lumping of the membrane parameters for some region of membrane surface; with coarse lumping a compartment may correspond to several dendritic branches, while with fine lumping it could correspond to only a portion of a branch. Such a compartmental model can accommodate as much detail in branching pattern, and as much detail in the spatiotemporal pattern of synaptic excitation and inhibition, as one wishes to specify. This compartmental model corresponds mathematically to a system of ordinary differential equations; see (143) for further details and references].

Class of Trees Equivalent to Cylinders

Although it was implicit in reference (139), it was made explicit in references 141–143 that a particular class of dendritic branching permits an entire dendritic tree to be reduced to an equivalent cylinder. In Figure 4 a symmetrical example of a dendritic tree belonging to this class is illustrated. It should be noted that the high degree of branching symmetry shown in this example is convenient but not necessary for this class. Given the usual simplifying assumptions (already noted above), the essential additional condition is a constraint on branch diameters: the diameters $(d_1$ and $d_2)$ of two daughter branches arising at any branch point can be unequal, but they must satisfy a particular constraint $(d^{3/2}$ constraint), namely, that the sum of their 3/2 power values $(d_1^{3/2} + d_2^{3/2})$ equals the 3/2 power of the parent cylinder diameter. Branch lengths can be unequal, provided that all terminal branches end with the same boundary condition and at the same electrotonic distance (sum of ℓ/λ values from soma to terminal). This class of dendritic branching has been valuable both as an aid to intuitive understanding of cable properties in dendrites and as an aid to the formulation of explicit mathematical solutions, including both steady-state and transient solutions in the separate dendritic branches [see (150, 161)]. Another useful property of such dendritic trees is the fact that equal increments of electrotonic distance $(\Delta x/\lambda)$ in the whole tree (e.g., increments of 0.2 are indicated by dashed lines in Fig. 4) correspond to equal amounts of dendritic surface area (141); this property is helpful when thinking about various dendritic distributions of synaptic excitation and inhibition in terms of synaptic density and intensity.

This class of dendritic trees was developed and used as a very convenient idealization. It was not
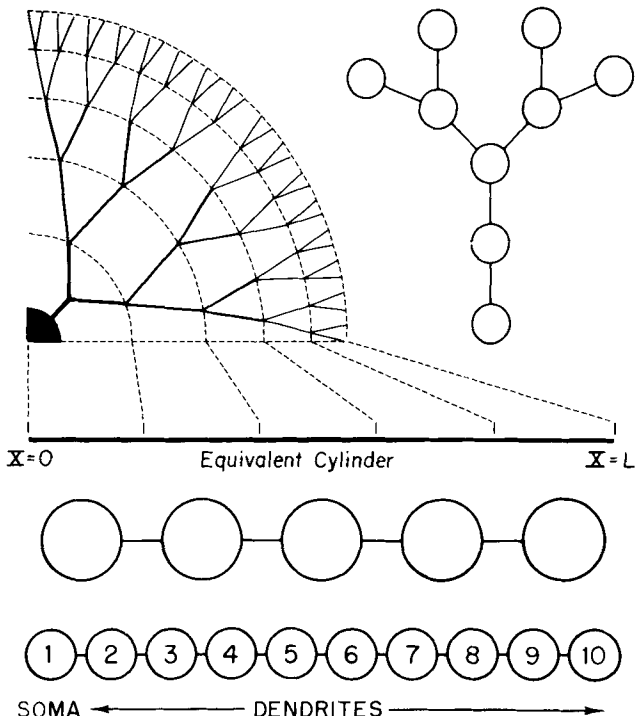
FIG. 4. Symmetrical dendritic tree, illustrative of a class of trees that can be mathematically transformed into an equivalent cylinder (141–144) and into approximately equivalent chains of equal compartments. *Dashed lines* divide both the tree and the cylinder into 5 equal increments of electrotonic distance, having equal membrane surface area. In one specific example (141, 143), the dendritic trunk diameter was 10 μm, and successive branch diameters were 6.3, 4.0, 2.5, 1.6, and 1.0 μm, which satisfy both symmetry and the constraint on $d^{3/2}$ values. Chain of 5 compartments corresponds to the 5 increments of electrotonic distance above. Chain of 10 compartments, used for Fig. 7, 8, and 10, represents the soma as compartment 1, and progressive electrotonic distance out into the dendrites is represented by compartments 2–10.

proposed as a law of nature, but it was noticed that preliminary data on branch diameters in motoneurons did not deviate drastically from such a constraint, and it was suggested that future data be examined in terms of the sum of the $d^{3/2}$ values (139). Thus it is noteworthy that Lux et al. (119) examined 50 bifurcations in motoneuron dendritic trees of their carefully studied sample and found that the ratio of summed daughter $d^{3/2}$ to parent $d^{3/2}$ ranged between 0.8 and 1.2, with a mean value of 1.02 ± 0.12 SD; this provides surprisingly strong support for using this idealization with motoneurons. The measurements of Barrett & Crill (5, 6), however, indicated a steady decrease of the summed $d^{3/2}$ value with increasing distance from the soma; some of this was due to taper and some was due to early termination of certain branches. While this taper provides a warning, it does not invalidate the notion that the equivalent cylinder concept provides a very useful idealization. Also, even when there is a small amount of taper, the concept of the electrotonic length of the most nearly equivalent cylinder is still a very useful one and

provides a good approximation to the more exact estimate that can be obtained when taper is taken into account (unpublished results of S. S. Goldstein and W. Rall, and personal communication with J. N. Barrett).

Motoneuron Membrane Resistivity and Dendritic Dominance

In 1957 both Fatt (46b) and Rall (138) emphasized the importance of giving sufficient weight to the cable properties of the dendrites when one interprets the microelectrode experiments. In 1959 Rall (139) also emphasized the importance of ranges of values, both because there is a range of motoneuron sizes and because of the uncertainties in matching one range of values (0.5-2.5 MΩ) for neuron input resistance (R_N), measured by electrophysiologists on their experimental sample of motoneurons, with another range of values for soma and dendritic dimensions, obtained by anatomists from their different sample of spinal cord neurons. It was found, on the basis of published data then available, that if the membrane resistivity (R_m) is assumed to be uniform over the soma and dendrites, its theoretically estimated value could range from 1,000 to 8,000 Ω cm^2, with midrange around 4,000-5,000 Ω cm^2. Then the factor of dendritic dominance (ρ), defined as the ratio of combined dendritic input conductance to soma membrane conductance, was estimated to be 10 or more, with midrange values from 21 to 35, or about 10 times the value of 2.3 used by Eccles and his collaborators. It was pointed out that large values of ρ provide a measure of the dominance of dendritic properties over somatic properties in determining various whole neuron properties of motoneurons. Rall [(139), p. 520] also pointed out that this leads naturally to a possible functional distinction between dendritic and somatic synaptic excitation: the slower dendritic contribution would be well suited for fine adjustment of central excitatory states, while the relatively small number of somatic synaptic knobs would be well suited for rapid control of reflex discharge.

Because of the functional implications and because of the uncertainties in matching the anatomic and physiological samples, this paper (139) drew attention to a number of questions and problems, including the desirability of making histological measurements on the same individual neuron that physiological measurements have been made on. This difficult feat was accomplished about 10 years later by Lux et al. (119) and by Barrett & Crill (5-7); thus, improved estimates of these motoneuron parameters were provided. For R_m, Lux et al. (119) obtained an average estimate of 2,750 Ω cm^2 $\pm$ 1,010 SD; Barrett and Crill obtained a lower bound of about 1,800 Ω cm^2 and pointed out that the dendritic value could exceed 8,000 Ω cm^2 if the somatic value were much lower. Discussion of the various sources of uncertainty can be found in these papers.

Even recent estimates of the dendritic dominance factor (ρ) have exhibited considerable variability and uncertainty. Nelson & Lux (130) estimated a range between 5 and 10. Lux et al. (119) regard $\rho = 7$ as a midvalue, while Barrett & Crill (5-7) have tabulated estimates ranging from 4.6 to 16 (mean 9.3). Jack & Redman (93) and subsequently Iansek & Redman (86) also provided estimates of ρ (and of ρ_∞, which corresponds to dendrites extended to infinite length) from analysis of transients; their estimates are usually greater than 4 and often greater than 20. However, it should be added that there is general agreement among all who have recently studied both the estimation of ρ and dendritic electrotonic length (L) that a) the values of L can be estimated more reliably than the values of ρ and b) the concept of dendritic dominance is not only supported by the values of ρ, but also enhanced by L values around 1.5, which means that distal dendritic synapses are not functionally remote from the soma.

Dendritic Electrotonic Length

The idea that the dimensionless electrotonic length of a dendritic tree (sum of $\Delta x/\lambda$ values from trunk origin to a representative dendritic terminal) could have a value as small as 1 or 2 can be found in the early numerical examples of explicit dendritic branching [see (139), Table 1 and (141), Table 1]. However, because such low values conflicted with the opinions of Lorente de Nó (112, 116), Eccles (37-40), and others, it was important to consider the best available measurements of actual dendritic branching, including both branch lengths and diameters. These were provided by Aitken [(1) and personal communication] for 10 neurons in the lumbosacral region of cat spinal cord. A computational analysis of these data was carried out for a wide range of R_m values. The resulting ranges of calculated input resistances and dendritic electrotonic lengths were studied, and the midrange (corresponding to the experimental range of motoneuron input resistance values) was found to correspond to a dendritic electrotonic length range of approximately 1-2; this conclusion was stated explicitly (143), but the full details of the computation remain unpublished.

This knowledge was important for computations of theoretical synaptic potentials designed to demonstrate the effect of different dendritic input locations (143, 144), especially when the theoretical range of results was to be compared with the experimental range found for miniature excitatory postsynaptic potentials (EPSP's) in cat spinal cord (17, 149). The kind of agreement found between these experimental and theoretical results (149) had several implications. Not only did it demonstrate that different dendritic synaptic input locations could account for most of the observed variety, but it also provided indirect support for the estimated range of dendritic electro-

tonic length. It may be noted that this indirect support came from a study of membrane potential transients; it did not depend on measurements of dendritic branches.

A theoretical basis for estimating dendritic electrotonic length from the multiple time constants contained in membrane potential transients was provided in 1962 (141), and this was made more explicit some years later [(145); see Eqs. 4.1–4.6 below, with the associated discussion of passive decay transients, time constant ratios, and electrotonic length]. The point to be emphasized here is that this new method of estimating dendritic electrotonic length is independent of the older method. The older method depended on the details of branch lengths and diameters and on estimates of R_m and R_i leading to estimates of λ values in the branches. The new method depends on an analysis of transients; it depends on branch dimensions only in the general sense that dendritic trees are approximated by their most nearly equivalent cylinder, and it depends on the assumption of uniform passive membrane properties, but not on any particular estimated range of values for R_m and R_i.

The agreement between these two methods of estimating dendritic electrotonic length for cat spinal motoneurons has been very encouraging. In several laboratories, the analysis of transients alone has confirmed the earlier estimate of L values ranging approximately from 1 to 2 (18, 86, 90, 130). Furthermore both methods have been applied to individual motoneurons in the remarkable experiments of Lux et al. (119) and of Barrett & Crill (6, 7); they found good agreement between the two methods and with the range of L values already noted.

Such confirmation in several laboratories has contributed to a growing recognition that these theoretical models do provide a means of combining anatomic and electrophysiological information into a useful representation of dendritic cable properties. Also calculations of passive electrotonic spread from dendritic synaptic locations to the soma have now been carried out by several research groups (4, 7, 87, 90, 93, 141–144, 149, 159, 161, 183); their conclusion has been that for L values between 1 and 2, even distally located dendritic synapses should not be dismissed as ineffective.

When people ask me questions about the functions of dendritic branches in other neuron types, both vertebrate and invertebrate, my response is to ask them for experimental data needed to estimate the electrotonic distances involved. It seems timely to explore the feasibility of both methods of estimating dendritic electrotonic lengths in several different neuron types. Both tissue culture and those invertebrate preparations that permit visual control of electrode locations provide the possibility of more complete experimental testing of both methods and of the assumptions that underlie them.

Membrane Potential Transients and Time Constants

Except in the simplest cases, it is necessary to use the mathematical results of cable theory to define the relation of a membrane potential transient to the passive membrane time constant. Many of those mathematical results are presented in a later section (PASSIVE MEMBRANE POTENTIAL TRANSIENTS AND TIME CONSTANTS).

In 1957 it was recognized (138, 140) that erroneously low estimates of motoneuron membrane time constants had resulted from a neglect of dendritic cable properties. At issue was not merely the correction of a low estimate of τ, but also some complicated arguments about the duration of synaptic potentials (54) and whether prolonged residual synaptic currents need be postulated to account for the observation that monosynaptic EPSP's usually had longer durations than monosynaptic inhibitory postsynaptic potentials (IPSP's) (32, 37–40). These issues have been carefully discussed elsewhere (140), and the details are not repeated here. Already then it was pointed out that the difference in time course between the brief IPSP and the usually longer EPSP could be understood if these inhibitory synapses were located near the soma and these excitatory synapses were distributed over the dendrites, as well as the soma [(140), p. 521; cf. (32, 39, 149, 174)]. The central idea was that once the erroneously low membrane time constant was corrected, the decay of these synaptic potentials could be regarded as a passive decay of membrane potential, following a brief flow of synaptic current; thus for brief synaptic input (or brief applied current) at the soma, the passive decay must be initially more rapid because of electrotonic spread from the soma out into the dendrites.

Although these transient dendritic cable properties were analyzed first for dendritic trees approximated as cylinders of semi-infinite length, solutions for equivalent cylinders of finite length were derived, illustrated, and discussed by 1962 (141–153). The mathematical results (141) were used to calculate the spatiotemporal distributions of membrane potential illustrated here in Figures 5 and 6, for the case where steady synaptic excitation is applied uniformly to half the length of the equivalent cylinder. Figure 5 shows the membrane depolarization as a function of dimensionless electrotonic distance at several different times during sustained synaptic excitation; it can be seen that for this example (with $L = 1.0$) the "hot" end is about 10% more depolarized than the midpoint and the "cool" end is about 10% less depolarized than the midpoint (for $T = 1.0$ or more); however, at early times the differences are relatively greater. The time course at these three locations is illustrated by Figure 6A, and the effect of suddenly turning off the synaptic excitation after a duration $\Delta T = 0.2$ is shown by the inset (Fig. 6B). The three transients of
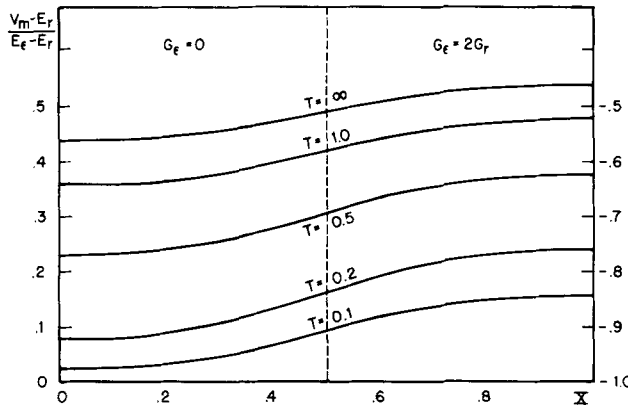
FIG. 5. Distributions of membrane depolarization for an excitatory conductance step in the peripheral half of a dendritic tree, for several values of $T = t/\tau$. In the central half of the dendritic tree (i.e., $X = 0$ to $X = 0.5$) the conductances are assumed to remain at their resting values. Over the peripheral half of the dendritic tree (i.e., $X = 0.5$ to $X = 1.0$) the conductance (G_ϵ) is assumed to step from zero to a value of $2G_r$ at $T = 0$. [Calculations are based on equations in (141).]
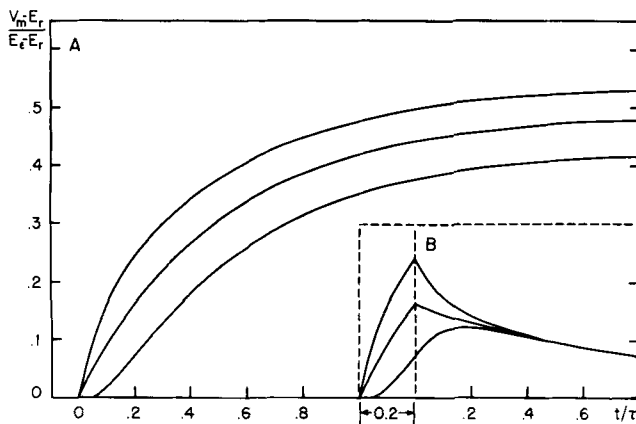

FIG. 6. Transients of membrane depolarization at the central end, the peripheral end, and at the middle of a dendritic tree. A: 3 curves at left illustrate the same problem as in Fig. 5; uppermost curve corresponds to the peripheral end $(X = 1)$; intermediate curve corresponds to $X = 0.5$; lowest curve corresponds to the central end $(X = 0)$. B: 3 curves at right illustrate the response to a square conductance pulse. On step is the same as in A; off step occurs 0.2 units of T later; the duration of the square conductance pulse is indicated by vertical dashed lines. [For equations used to calculate the off transients, see (141).]

Figure 6B can be regarded as theoretical synaptic potentials when the synaptic conductance is approximated as a square step on followed by a square step off after $\Delta T = 0.2$, over half the length of the equivalent cylinder. At the hot end, the transient rises more rapidly to a higher peak and then falls more rapidly during its early decay. At the cool end, there is a delayed rise, but the rise continues after the conductance pulse is over; the latter can be understood as the result of an equalizing spread of membrane depolarization from the hot half to the cool half of the equivalent cylinder. This equalizing spread is governed by a time constant that is shorter than the passive mem-

brane time constant (see Eq. 4.3); this corresponds to the fact that the early decay at the hot end is more rapid than the later decay; the later decay is essentially the same at all locations because by this time the remaining membrane depolarization has become essentially uniform.

This simple example illustrates two aspects of dendritic cable properties that have been explored extensively in subsequent research. One aspect, how the shape of a synaptic potential depends on the location of the synaptic input, in relation to that of the recording electrode, has been examined by means of computations with compartmental models (143, 144, 149) and also by computations with series solutions (90–93, 146, 161). Another aspect, how the differences in shape can be understood in terms of equalizing electrotonic spread, has been made explicit in the analysis of transients to separate out the time constants (145), thus providing estimates for both the passive membrane time constant and the dendritic electrotonic length (see Table 3 and the discussion of Eqs. 4.1–4.6).

Spatiotemporal Effects with Dendritic Synapses

At a time when dendritic synapses were usually ignored or treated as equivalent to somatic synapses, it was important to demonstrate both the effect of different dendritic input locations on the resulting EPSP to be expected at the soma and the effect of contrasting spatiotemporal patterns constructed from such input locations. In Figures 7 and 8 the results of computations with the 10-compartment model are summarized; this model was included earlier in Figure 4 and has been mathematically defined and discussed (143). The four cases in Figure 7 show the EPSP time course computed for the soma (compartment no. 1) when an equal amount of synaptic conductance (step on, with step off after $\Delta T = 0.25$) was assumed to be located as shown in the four inset diagrams. In case A, the proximal dendritic input location resulted in the EPSP with the steepest rise to the earliest and largest peak. In cases B–D, as the input location was shifted to more distal dendritic compartments, the EPSP shape was progressively delayed, with a slower rise to a lower peak amplitude. In Figure 8, the same four inputs have been applied in opposite spatiotemporal sequences, A→B→C→D and D→C→B→A. It can be seen that the two results were quite different, although the amount of synaptic conductance was the same in both cases; only the spatiotemporal pattern of the two inputs was different. Furthermore, when the same total amount of synaptic conductance was distributed uniformly over compartments 2–9 for $T = 0$–1.0, the intermediate (dashed) curve was obtained. At least three conclusions can be drawn: 1) a temporal sequence of synaptic inputs does not result in a unique EPSP unless the soma-dendritic locations of these
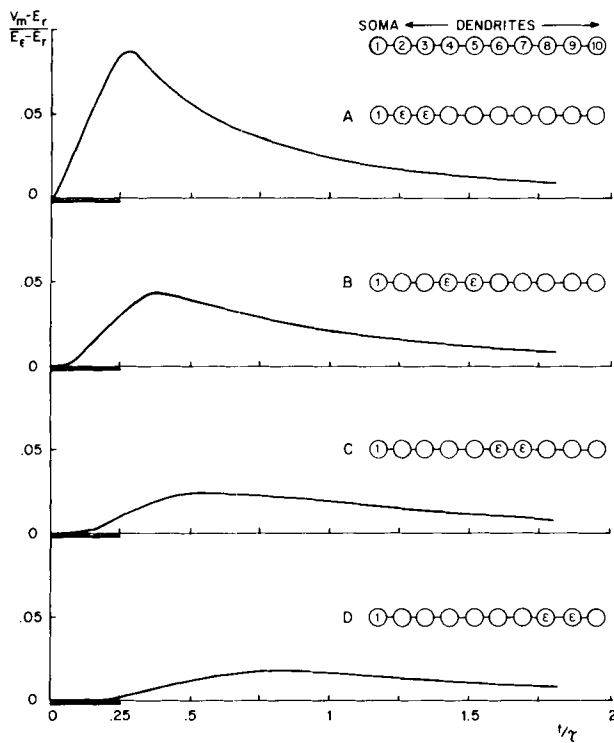
FIG. 7. Computed transients at the soma (compartment 1) for 4 synaptic inputs that differ only in their input locations. In each case, the synaptic input consisted of $G_\epsilon = G_r$ in 2 compartments for a time interval, $T = 0$ to $T = 0.25$, indicated by *heavy black bar*. In A, the input was applied to compartments 2 and 3, in B to 4 and 5, in C to 6 and 7, and in D to 8 and 9. [See Fig. 4 for the relation of such compartments to the dendritic branches; see (143) for equations and discussion of compartmental modeling.]

inputs are specified; *2*) for a maximal peak depolarization at the soma, the distal dendritic synaptic input should occur earlier than the somatic and proximal dendritic synaptic input; and *3*) for rapid achievement and maintenance of a steady soma depolarization level, a brief somatic input followed by a prolonged sequence of distal dendritic inputs would be more effective.

In addition to these conclusions, it has also been demonstrated and discussed (143, 144, 149, 150, 161) that, when synaptic inputs are localized to particular dendritic branches, both the effectiveness of synaptic inhibition and the departure from simple summation of two synaptic excitations depend on large local membrane depolarizations and especially on how much of the depolarization generated at one location has spread to the other location by the time the synaptic conductance transient occurs there, because this influences the amount of synaptic current generated; a large membrane depolarization at the second synaptic site will decrease both the driving potential and the resulting synaptic current for an excitatory synapse, but, for an inhibitory synapse, its driving potential and the resulting inhibitory synaptic current would be increased. Because of this, one can easily distinguish the effects of simultaneous distal dendritic synaptic excitation and inhibition for two extreme cases: when these inputs occur in different dendritic trees they do not influence each others' driving potentials and their EPSP and IPSP amplitudes combine linearly at the soma; however, when they occur in the same or sister branches of one tree,
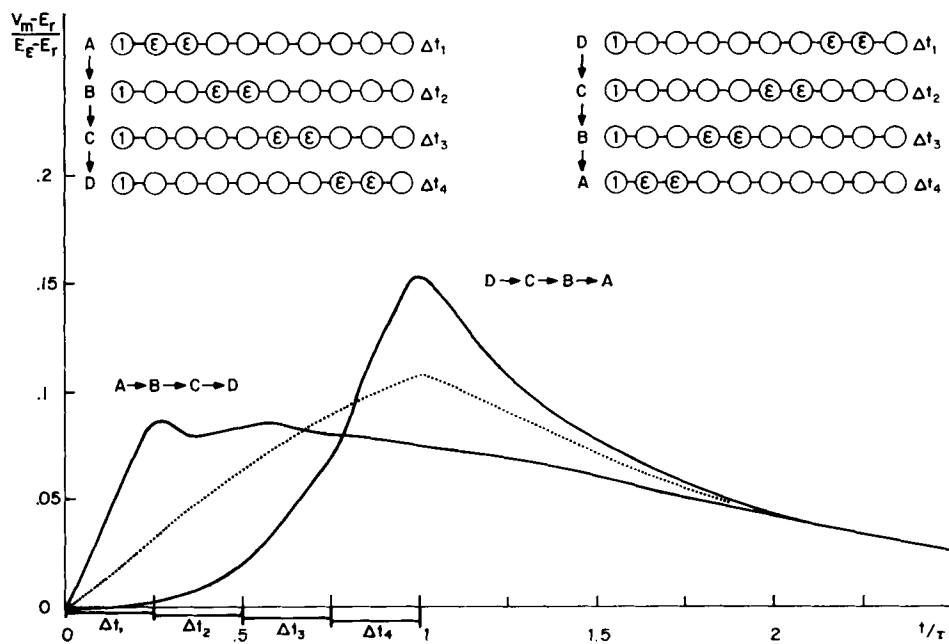
FIG. 8. Effect of two spatiotemporal sequences on transient soma-membrane depolarization. Two input sequences, A → B → C → D and D → C → B → A, are indicated at *upper left* and *upper right*, respectively; component input locations are the same as in Fig. 7. Time sequence is indicated by means of the 4 successive time intervals, Δt_1, Δt_2, Δt_3, and Δt_4, each equal to 0.25 τ. *Dotted curve* shows the computed effect of $G_\epsilon = 0.25\,G_r$ in compartments 2–9 for the period $\tau = 0$ to $t = \tau$. [For further details, see (143).]

there is local interaction (caused by changes in synaptic driving potentials) with the result that the EPSP at the soma is reduced by more than the amplitude of the separate IPSP.

It may be noted that an early treatment of nonlinear summation of muscle end-plate potentials was provided by Martin (121). Calculations for brief transients and for dendritic locations have been reviewed recently (7, 150, 159, 161).

Excitatory Postsynaptic Potential Shape Index Loci

Because the experimental variety of EPSP shapes is discussed later in this Handbook (see the chapter by Burke and Rudomin), and the detailed comparison between theory and experiment can be found in several papers (87, 90, 149), the objective here is to focus briefly on two contrasting theoretical shape index loci. These loci were obtained because of a need to compare experimental variety with theoretical variety, when the source of the variety was not under full control. We wish to contrast the variation in EPSP shape that would be caused by varying the time course of synaptic input alone with the variation that would be caused by changing only the input location. By choosing two shape indices, the time to peak (or rise time) and the half-width, the shape of each EPSP could be represented as a point on a two-dimensional graph of half-width versus time to peak. Figure 9 shows a plot of three shape index pairs, at left, for the three EPSP shapes at right; these EPSP shapes were computed for the three synaptic current time courses shown as dotted curves, on the assumption that the synaptic input was spatially uniform over the entire soma-dendritic surface; thus no cable properties were involved. The straight line drawn through the three points at left can be regarded as the theoretical locus
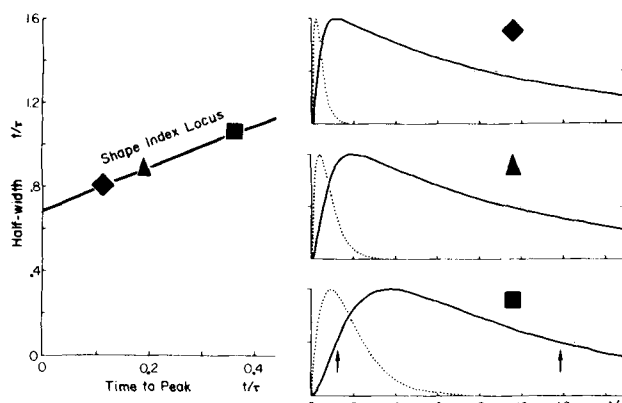
FIG. 9. *Right*: computed EPSP's (*solid traces*) generated by synaptic currents of different time courses (*dotted traces*). Synaptic currents are assumed to be uniformly distributed over entire soma-dendritic surface. *Arrows* on the lowermost EPSP indicate its half-width. *Left*: plot of paired shape index values for EPSP's generated by uniformly distributed synaptic input with coordinates as labeled. The ◆, ▲, and ■ on the plot represent the shapes of corresponding EPSP's on the *right* side of the figure. |See (149).|

of shape index pairs for this family of EPSP shapes. What makes this locus interesting is that it is quite different from that obtained when a single input time course is applied at different dendritic locations (Fig. 10). Similar loci were computed also for a faster input time course and a slower input time course (144, 149). The effect of combining two or three input locations was also explored (149). When experimental EPSP shapes are plotted in the same way, it is possible to compare the pattern of their scatter with these loci. The original sample of Burke (17, 149), despite scatter caused by the unknown variation in membrane time constant, permitted us to conclude that the locus (Fig. 9) resulting from variation of input time course alone could be ruled out and that single input locations could account for more than half of the EPSP shapes, while two or more input locations were needed to account for the longer half-widths. The later experimental sample of Jack et al. (89, 90) had a reduced scatter (see Fig. 11) because the membrane time constants had been determined and also any shapes that were obviously due to two or more locations were excluded; these data, and also the average EPSP shapes of Mendell & Henneman (123), have shown good agreement with shape index loci, like that in Figure 10, based on single input locations.

In Figure 12 an additional test of our interpretations is shown. Here a shape index plot was used to display the EPSP's studied earlier by Smith et al. (174) using impedance bridge techniques at the soma. The filled circles represent those EPSP's for which an impedance transient was detected, while the open circles represent those for which an impedance transient was not detected. The correlation of the slower EPSP shapes with failure to detect impedance transients is theoretically expected for distal dendritic input locations (144, 149, 174). In contrast, the correlation of the faster EPSP shapes with detection of impedance transients is theoretically expected for proximal dendritic synaptic input locations.

This section is concluded with the cautionary remark that such an analysis must not be applied uncritically to other experimental situations where there may be little reason to believe that the several synaptic inputs have the same brief time course.

Comments on Extracellular Potentials

Early insights into the relation of extracellular potential distributions to dendritic orientation include those of Bishop and colleagues (10a, 21a), and of Lorente de Nó (114, 115), who made a distinction between open and closed fields, the latter being characterized by radial (spherical) symmetry. A computation of the time course of extracellular potential in such a closed field, generated by a somatic action potential with passive electrotonic spread into dendritic trees (assumed to extend symmetrically in all directions from the soma) has been reported (142) and is illustrated in Figure 13. These computed results were in good agreement with experimental results
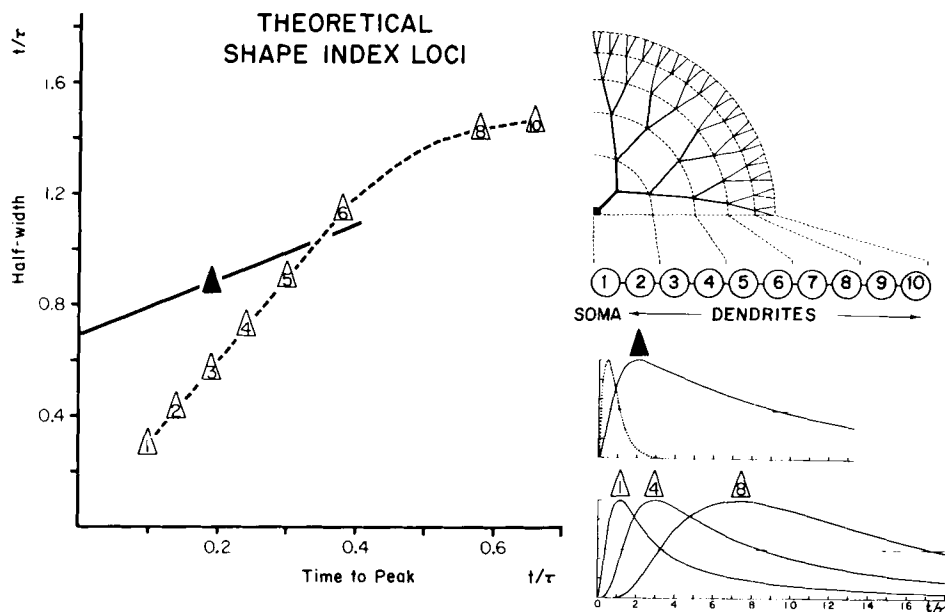
FIG. 10. *Right*: diagrammatic representation of the transformation of soma-dendritic receptive surface of a neuron into a chain of 10 equal compartments. Below are graphs of computed EPSP's occurring in compartment 1, obtained with the compartmental model for the medium synaptic current time course (*upper graph, dotted line*). Synaptic current introduced equally to all compartments gave the upper computed EPSP (▲). Synaptic current localized to a single compartment gave the lower 3 computed EPSP's: compartment 1 (△), compartment 4 (▲), or compartment 8 (▲). *Left*: EPSP shape index values for computed EPSP's shown at *right*. *Dashed line*, locus of EPSP shapes generated when synaptic input is limited to the numbered compartment. *Solid line*, locus for spatially uniform depolarization of the cell. Note that scales are in units of dimensionless ratio t/τ. |See (149).|
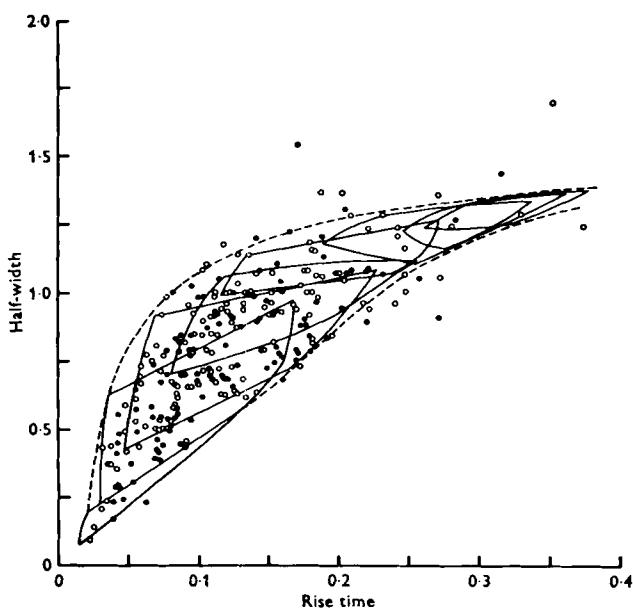
FIG. 11. Scatter diagram of normalized shape indices of the EPSP's from the motoneurons for which a time constant was obtained. ●, EPSP's recorded from knee flexor motoneurons; ○, EPSP's recorded from ankle extensor motoneurons. Two *dashed lines* show theoretical boundaries for the shape indices with the assumed values of parameters (α = 12–100; ρ_λ = 4–25; L = 0.75–1.5). The set of areas, each bounded by a *continuous line*, show the theoretical boundaries for particular distances. |See (90).|

(46a, 128) from cat spinal motoneurons; this agreement was timely in demonstrating the error of a belief that a diphasic extracellular record in the dendritic region could result only from active propagation of an impulse along the dendritic branches. Here (142), and in the closed field portion of the computations for the olfactory bulb (147, 151), it was shown that extracellular negativity (relative to a distance reference electrode) throughout the closed field correlates with centripetal extracellular current flow from dendrites to the actively depolarizing soma; the current flows inward across the soma membrane and then returns as centrifugal intracellular current inside the dendritic trunks and branches. The subsequent (diphasic) reversal from extracellular negativity to extracellular positivity correlates with active repolarization of the somatic membrane; then the extracellular current flows centrifugally from the soma out into the volume between the dendrites, then across the dendritic membrane, and finally returns as centripetal intracellular current.

Because intuition based on axonology had led to a belief that extracellular positivity should always be expected just outside a membrane source (where current flows outward into the extracellular medium), it is important to emphasize that this is not true for multipolar dendritic neurons or for closed fields (142). This can be understood in two different ways. For an

idealized closed field, when the dendritic membrane is a (passive) source of extracellular current that flows (centripetally) to the somatic sink, the potential near dendritic membrane (source) is negative relative to a distant electrode; however, it is less negative than the potential near the soma sink. Furthermore, in the reversed phase, when the dendritic membrane is a (passive) sink for extracellular current that flows (centrifugally) from the repolarizing somatic source, the potential near dendritic membrane (sink) is positive, but less positive than that near the soma source. Even without the assumption of an idealized closed field, for a multipolar neuron (Fig. 14) one can gain understanding by considering this as the superposition of two separate fields: a soma sink field for current flowing from infinity, and a separate dendritic source field for equal total current flowing to infinity (142). The dendritic surface area is large and widely distributed and must have a low source current density; the much smaller soma surface must have a relatively large sink current density. The separate dendritic source field does generate a positive potential relative to a sink at infinity, but this positive potential is small (+50 μV at R = 4 of Fig. 14). The separate somatic sink field generates negative potentials of larger magnitude, especially near the soma and proximal dendrites, because of the high current density converging toward the soma (about −900 μV at the soma surface and −150 μV at R = 4 of Fig. 14). When these two fields are superimposed, the negativity outweighs the positivity except at locations close to distal dendritic branches (−150 μV + 50 μV yields −100 μV at R = 4

FIG. 13. Theoretically calculated relation between intracellularly and extracellularly recorded action potentials. *Uppermost curve*, experimental "AB spike" followed by an "A spike" as recorded intracellularly from a cat motoneuron by Nelson & Frank (128). The other intracellular curve represents the theoretically calculated passive electrotonic spread into a dendritic cylinder of infinite length; it corresponds to a radial distance, R = 18 [i.e., an electrotonic distance, x/λ, of $(R$ − 1$)/40$ = 0.425; this would correspond to about 600 μm in the examples considered]. Extracellular curves were calculated on the assumption of radial symmetry. Curve for R = 18 has been multiplied by 10 to aid the comparison of shape. Curve at R = 3 has a shape extremely similar to that at R = 1, except that the peak at R = 1 has an amplitude about 5 times that at R = 3. [See (128, 142).]

FIG. 12. Shape index plot for evoked EPSP's for which impedance measurements were available. Time to peak as abscissa; half-width as ordinate; scales in milliseconds. ●, EPSP's accompanied by a measurable impedance change; ○, EPSP's not accompanied by a detectable impedance change. *Dotted outline*, scatter of shape index values for observed miniature EPSP (for reference). [See (149, 174).]

in Fig. 14). With superposition the source and sink at infinity are cancelled and the distributed dendritic source matches the concentrated somatic sink current; the resultant extracellular potential near the dendritic sources is negative, yet the current does flow away from these sources (it flows from −100 μV at R = 4 to ca. −800 μV at the soma in Fig. 14). These quantitative details are included here to help convince readers that insights gained from axonology should not be applied uncritically to the dendritic regions of a multipolar neuron.

When a population of neurons is arranged as a cortex, with complete spherical symmetry, and the neurons are activated synchronously, this also generates a closed field of extracellular potential (114, 115, 147, 151). By using cable theory to compute the spati-
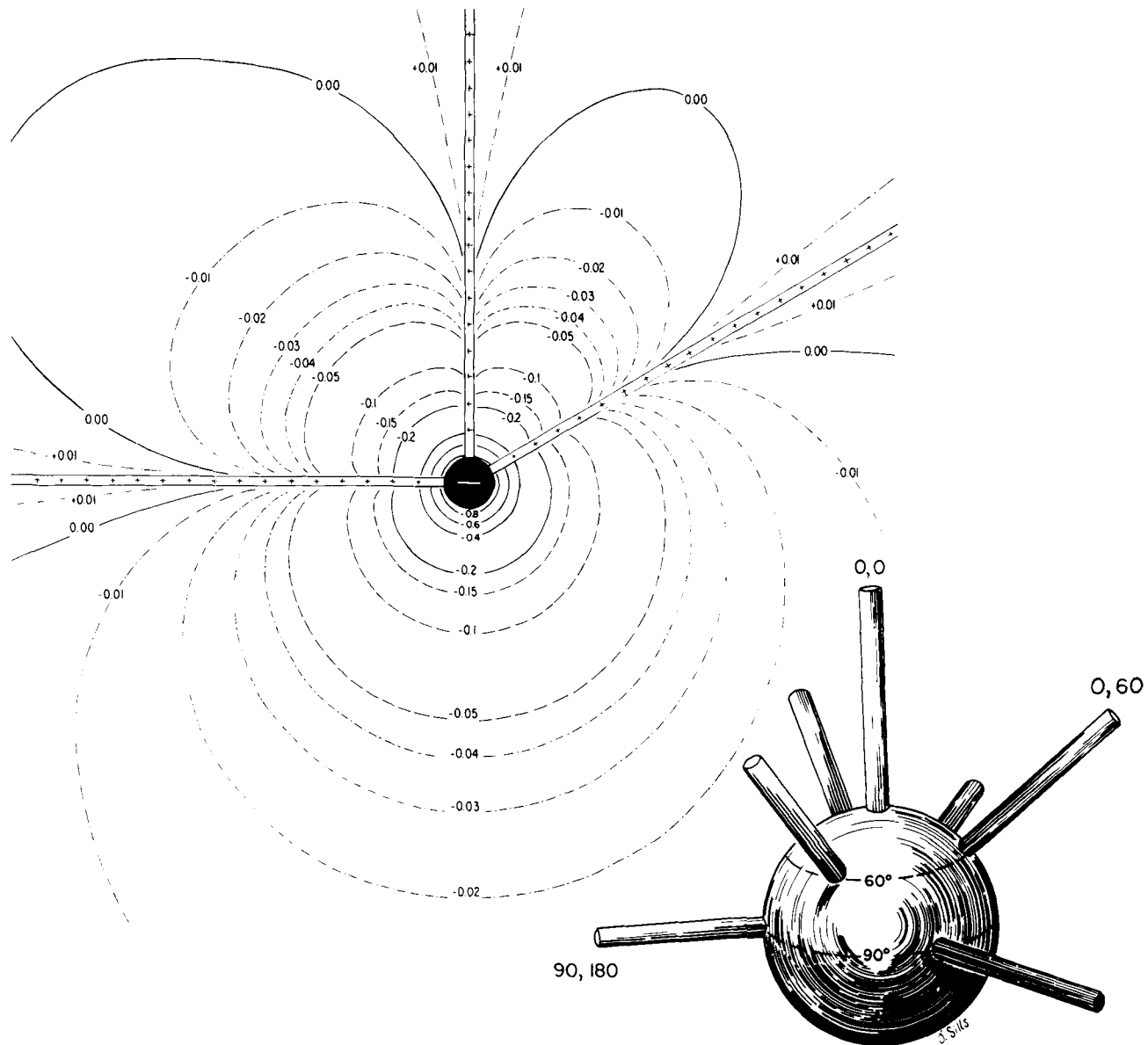
FIG. 14. Computed isopotential contours for a spherical soma with 7 cylindrical dendrites, of which only 3 can be seen in the plane shown here. Relative to 1 dendrite shown on the vertical (polar) axis, 3 dendrites were equally spaced at 60° from the polar axis, and 3 more dendrites were equally spaced at the equator (see *inset*). The soma was the sink for extracellular current; the dendritic cylinders were sources of extracellular current corresponding to passive electrotonic spread at the time of the peak of an antidromic action potential. For this calculation, dendritic λ was set equal to 40 times the somatic radius. Numbers labeling the contours correspond to the quantity $V_c/(I_N R_c/4\pi b)$, where I_N is the total current flowing from dendrites to soma, R_c represents extracellular volume resistivity, and b represents the soma radius. For the particular case of the peak somatic action potential in a cat motoneuron, this numerical quantity expresses the value of V_c approximately in millivolts. This is because of the following order of magnitude consideration: I_N is of the order 10^{-7} A, because the peak intracellular action potential is of the order 10^{-1} V, and the whole neuron instantaneous conductance is of the order 10^{-6} Ω^{-1}; $R_c/4\pi b$ is of the order 10^4 Ω, because the soma radius, b, lies between 25 and 50 μm, and the effective value of R_c probably lies between 250 and 500 Ω cm. [See (142).]

otemporal distribution of membrane potential and current in each neuron and by assuming perfect spherical symmetry and synchrony in the population, the resulting spatiotemporal distribution of extracellular potential can be computed (147, 151). Furthermore, if the spherical symmetry is punctured, either by incompleteness of the spherical shell or by incomplete activation, the resulting field of extracellular potential is no longer closed, but important aspects of the resulting open field can be usefully approximated by the considerations summarized diagrammatically in Figure 15; these considerations have been pre-
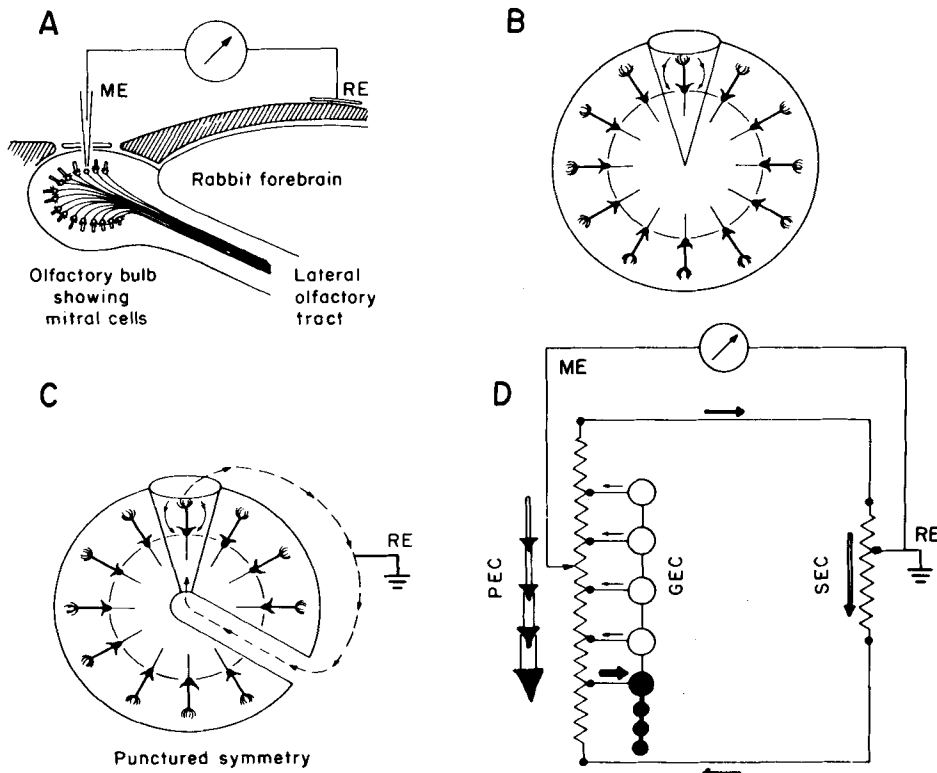
FIG. 15. Cortical symmetry and synchronous activation of the mitral cell population. *A*: schematic diagram of experimental recording situation. Microelectrode (*ME*) penetrates the olfactory bulb; reference electrode (*RE*) is distant. Mitral cells are arranged in an almost spherical cortical shell; their axons all project into the lateral olfactory tract. Single-shock stimulation to the lateral olfactory tract results in synchronous antidromic activation of the mitral cell population. *B*: complete spherical symmetry of a cortical arrangement of mitral cells. *Cone* indicates a volume element associated with one mitral cell; *arrows* indicate extracellular current generated by this mitral cell; current is as though confined within its cone when activation is synchronous for the population. *C*: punctured spherical symmetry. *Arrows* inside the *cone* represent the primary extracellular current generated per mitral cell; *dashed line* (with *arrows*) represents the secondary extracellular current per mitral cell. Location of the reference electrode along the resistance of this secondary pathway serves as a potential divider. *D*: the potential divider aspect (*C*) combined with a compartmental model. Relations of both the microelectrode (*ME*) and the reference electrode (*RE*) to the primary extracellular current (*PEC*) and the secondary extracellular current (*SEC*) are shown. Generator of extracellular current (*GEC*) is a compartmental model representing the synchronously active mitral cell population. *Solid arrows* adjacent to the compartmental model represent the direction of membrane current flow at the moment of active, inward, soma-membrane current (*heavy black arrow*); dendritic membrane current is outward. *Open arrows* represent the direction of extracellular current flow (both PEC and SEC) at this same moment. [See (147, 151).]

sented and discussed in some detail by Rall and Shepherd (147, 151) who were concerned with an application to field potentials in the olfactory bulb of rabbit. The concept is most easily understood for a small puncture that offers a relatively large resistance to the secondary extracellular current (SEC) that flows from the outer surface of this cortex, around, and through the puncture to the inner surface of this cortex. For complete, unpunctured spherical symmetry, there is no such secondary extracellular current; there is only the primary extracellular current (PEC), which, because of the symmetry and synchrony, flows as though it were confined within conical volumes, each cone being associated with one neuron of the synchronously active population. With

a small puncture of high resistance, most of the extracellular current still flows as primary extracellular current in such conical volumes (except for edge effects near the puncture), and only a small fraction of the total extracellular current flows as secondary extracellular current; this means that the gradient of extracellular potential within the cones is almost unchanged from the unpunctured case, but the values of extracellular potential, relative to a distant reference electrode, can be significantly shifted by what we have called a "potential divider" effect. As explained more fully by Rall and Shepherd (151), the outer arm of the potential divider can be thought of as the resistance along which the secondary extracellular current flows from the dendritic terminals out-

ward to a zero potential surface that is isopotential with ground and the distant reference electrode; the inner arm of the potential divider corresponds to the resistance from the zero potential surface, through the puncture, to the inner spherical boundary of the primary region. In the application to the mitral cell population of olfactory bulb, the ratio of these two resistances (outer/inner) was taken to be about 1/4; this was consistent with a peak extracellular potential of $+0.5$ mV at the bulb surface, coincident with a peak extracellular potential of -2.0 mV at the inner boundary of the mitral body layer.

The agreement betwen theory and experiment for the mitral cell population led to the recognition that subsequent activity (in period III) must be mainly in the granule cell population (147, 151); additional considerations of polarity and timing led to the postulation of dendrodendritic interactions between mitral cells and granule cells, and these theoretical considerations were reinforced by independent electron-microscopic observations of reciprocal synapses between the dendrites of mitral and granule cells [(152); see (147, 151, 170-171) for details and additional references]. It was recognized then (152) that these results and interpretations contained wider implications for neurophysiology: neurons having dendrites but no axon could perform locally, possibly without an action potential; they might contribute to lateral inhibition and enhancement of contrast; they could also provide a recurrent inhibition that might contribute to adaptive damping and possibly also to rhythmic activation of a population. The possibilities of such dendrodendritic pathways are now beginning to be explored in many regions of the CNS (171).

With regard to the potential divider concept, it was conjectured that this might provide a useful approximation also in cases of larger puncture or of less complete cortical activation (151). This conjecture had already found experimental support (172). Recent extensive computations carried out with very large punctures (more than hemispheric) have shown that the potential divider concept (together with increasing secondary current shunting of the primary current) can provide quite good approximations even in such cases [see M. Klee & W. Rall, (103b)].The application to cerebellum has been discussed and illustrated by Zucker (190); additional computations for cerebellum have been carried out by Llinás & Nicholson (110).

Additional Comments and References

A number of topics are mentioned only briefly to draw attention to references where details can be found.

With regard to the application of dendritic models, the emphasis here has been on motoneurons of cat spinal cord. Applications to pyramidal cells (83, 94, 118, 175, 177) have been reviewed briefly [(150), p.

671-673; see (183, 183a) for application to neurons of the red nucleus].

In a detailed study of the input resistance at one dendritic branch, Rall & Rinzel (150) showed explicitly that this input resistance (R_{BI}) exceeds that at the soma (R_N) by less than the series sum of the core resistances along the direct line from the input point to the soma. Also they showed that the steady attenuation factor (voltage at branch input point/voltage at soma) is always greater than the input resistance ratio (R_{BI}/R_N). Furthermore, for equal synaptic conductance inputs to a branch or to a soma, although the local depolarization is greater at the branch input site than at a soma input site, the attenuation factor is even greater, and less depolarization reaches the soma; for the steady-state problem, the voltage ratio at the two input sites is less than R_{BI}/R_N [(150), p. 673-675]; for the transient problem, the ratio of peak voltages at the two input sites is greater than R_{BI}/R_N [(161), p. 777-779], but the attenuation factor is much larger still; numerical illustrations, as well as analytical expressions, are provided for both cases (150, 161). Despite very large attenuation of peak voltages, a consideration of charge dissipation ratios shows that a very significant portion of the dendritic input charge does reach the soma (4a, 7, 87, 159, 161).

With regard to the size principle relating to synaptic excitation thresholds in motoneuron populations (66), considerations involving synaptic densities on dendrites and soma have been discussed by Burke [(16, 18); see the chapter by Burke and Rudomin in this *Handbook*] and by Zucker (191).

Some aspects of repetitive firing of motoneurons have been explored with soma-dendritic modeling (63, 103, 168a). Recent useful analog models have been described (48a, 107a, 137). Detailed modeling of antidromic activation, from axon, to hillock, to soma and dendrites, has been reported and described (35, 151). Changes of action potential shape and velocity have been studied in regions of changing core conductor geometry [(62, 152a); see also (103a) for additional references].

The idea that action potentials in dendritic branches could provide a basis for logical operations relating to success or failure at branch points has been noted by many researchers [(3, 62, 116, 148); R. FitzHugh, personal communication; Y. Y. Zeevi, Ph.D. thesis and personal communication]. Such a phenomenon may well prove important to the understanding of activity in the dendritic trees, or axonal branches, of some neuron types. However, the dendritic membrane of cat spinal motoneurons does seem to be essentially passive [(150), p. 671], except perhaps under the abnormal conditions associated with chromatolized motoneurons (106).

The effect of an extracellular potential gradient on the excitability of a dendritic neuron depends on how the dendritic trees are aligned with respect to the potential gradient (127, 142, 151). If dendritic trees

extend equally in both directions (from a central soma) along a constant gradient, one set of dendritic terminals will be depolarized while the other set is hyperpolarized, and the soma remains unaffected. However, with a radial gradient (127), or with dendrites extending only in one direction (142, 151), it is possible for a neuron soma or a spike trigger zone to receive either hyperpolarization or depolarization sufficient to change the threshold or the frequency of firing.

A very generalized treatment of dendritic branching has recently been provided by Butz & Cowan (19), utilizing Laplace transforms and special symbols. A method of solving cable problems with Laplace transformed boundary conditions, by a computational inversion procedure, has recently been described by Norman (131). Voltage clamping has recently been explored numerically by Moore et al. (125a).

CABLE EQUATIONS DEFINED

Usual Cable Equation

The cable equation of neurophysiology is a partial differential equation that is usually expressed

$$\lambda^2 \partial^2 V/\partial x^2 - V - \tau \partial V/\partial t = 0 \qquad (1.1)$$

where the variable, V, depends on two independent variables, x and t; λ and τ are constants depending on the materials. As explained in the derivation below, V represents the departure of membrane potential from its resting value, x represents distance along the length of the core conductor, and t represents time; also τ is known as the time constant of the membrane and is sometimes designated τ_m, while λ is the length constant of the core conductor and is sometimes called the space constant. The way in which λ and τ depend on the electrical properties of the core conductor materials (the membrane and the intracellular and extracellular media) is shown in the LIST OF SYMBOLS and explained below (see section ASSUMPTIONS AND DERIVATION OF CABLE THEORY).

Sometimes this cable equation is reexpressed in terms of the dimensionless variables $X = x/\lambda$ and $T = t/\tau$,

$$\partial^2 V/\partial X^2 - V - \partial V/\partial T = 0 \qquad (1.2)$$

This can be useful in simplifying certain manipulations and in simplifying the mathematical expressions for solutions. Also tabulating and plotting solutions in terms of X and T means that a single set of numerical values can be applied equally well to different core conductors having different λ and τ values.

Steady-state Cable Equations

We distinguish between DC and AC steady states. For the DC steady state, V depends on x, but not on t;

then $\partial V/\partial t = 0$, and the cable equation (Eq. 1.1) reduces to an ordinary differential equation

$$\lambda^2 d^2 V/dx^2 - V = 0 \qquad (1.3)$$

Many useful results, such as cable input resistance and steady-state attenuation with distance, can be obtained most simply by studying the solutions of Equation 1.3 for various boundary conditions.

For an AC steady state, we consider the variable $V = U \exp(j\omega t)$, where V and U are both complex variables and U is independent of t. Then the cable equation (Eq. 1.1) reduces to the expression

$$\lambda^2 d^2 U/dx^2 - (1 + j\omega\tau)U = 0$$

or to the expression

$$d^2 U/dX^2 - q^2 U = 0 \qquad (1.4)$$

where $q = (1 + j\omega\tau)^{\frac{1}{2}}$ and U is a complex function of X and ω. Solutions of this equation can be used to obtain expressions for AC admittance, impedance, and transfer functions [e.g., (6, 117, 140, 150)].

Augmented Cable Equations

For situations where applied electric fields, synaptic excitation, or active membrane properties are present, it becomes necessary to consider a more general cable equation

$$\partial^2 V/\partial X^2 - V - \partial V/\partial T = F \qquad (1.5)$$

which includes a function F on the right-hand side. When $F = 0$, one recovers the homogeneous partial differential equation (Eq. 1.2) considered before. When current or voltage is applied only at a few discrete points along a passive cable, then $F = 0$ for lengths of cable that lie between these points. When an extended electrode or complex electrode array is applied along the length of the cable, we obtain Equation 1.5 with F as a function of X, and if this applied field varies with time, we have F as a function of X and T, but still not of V (e.g., see Eq. 2.31). But, when the input disturbance is a synaptic conductance change, the resultant synaptic current depends on V, as well as on the spatiotemporal distribution of synaptic input; in this case, F is a function of V, as well as X and T, as illustrated in Equation 2.43. Furthermore, when consideration is extended to cables having active membrane properties, F in Equation 1.5 becomes not only a function of V, X, and T, but also a function of one or more auxiliary variables, and Equation 1.5 must be supplemented by equations governing these auxiliary variables; the BVP model of FitzHugh (49, 51) has one auxiliary variable, while the well-known model of Hodgkin & Huxley (77) has three auxiliary variables, m, n, and h [see (51, 52) for discussion of the mathematical properties of such systems; see also (43, 160) for further results and references].

Comment: Cable Versus Wave Equation

The cable equation, heat conduction equation, and diffusion equation are all partial differential equations of the same parabolic type. Such equations, and their solutions, differ significantly from those of the elliptic type (e.g., Laplace's equation of potential theory) and from those of the hyperbolic type (e.g., electromagnetic wave equation). When electromagnetic inductance is added to a telegraph cable or transmission line, the partial differential equation gains a term that is proportional to $LC\ \partial^2V/\partial t^2$, and this changes the equation from the parabolic type to the hyperbolic type; engineers have long known that this can enhance telegraph signal propagation. However important this is for engineering, a recent attempt (109) to account for nerve impulse propagation as a wave solution of such a differential equation can be dismissed for two important reasons: not only did this involve a misunderstanding of the importance of the nonlinear membrane properties elucidated by Hodgkin and Huxley, it tacitly assumed an amount of electromagnetic inductance that far exceeds the negligible amount present in nerve (95, 169). Many have recognized that nerve impulse propagation has much more in common with the traveling chain reaction of a lighted fuse than with electromagnetic wave propagation.

Modified Cable Equation for Tapering Core

Previous equations (Eqs. 1.1-1.5) all apply to a uniform cable, corresponding to a core conductor of constant cross section. If the cross section changes continuously with distance, a partial differential equation more complicated than Equation 1.1 results. However, for a particular class of exponential flare or taper, this equation can be transformed to the relatively simple form

$$\partial^2V/\partial Z^2 + K\partial V/\partial Z - V - \partial V/\partial T = 0 \quad (1.6)$$

where K is a constant that determines the amount of exponential flare or taper, and Z represents a generalization of $X = x/\lambda$, for changing λ [see (62, 141)]. For the special case of zero taper or flare, $K = 0$, and Z becomes equivalent to X, with the result that Equation 1.6 then is reduced back to Equation 1.2.

General Solution of Steady-state Cable Equation

The ordinary differential equation (Eq. 1.3) is homogeneous, linear, and of second order, with constant coefficients. It can have only two linearly independent solutions; its general solution is composed of two such (linearly independent) solutions, with two arbitrary constants. For any specific problem, two boundary conditions are needed to determine the two arbitrary constants and thus provide a unique solution of that problem.

The general solution of Equation 1.3 can be expressed in many alternative (but equivalent) forms. The most familiar form is

$$V = A_1 \exp(x/\lambda) + A_2 \exp(-x/\lambda) \quad (1.7)$$

where the two exponential functions are linearly independent solutions, while A_1 and A_2 represent the two arbitrary constants. It can be verified by differentiation twice with respect to x, that Equation 1.7 is a solution of Equation 1.3 for any values of A_1 and A_2.

Particularly useful alternative forms of this general solution can be expressed in terms of hyperbolic sines and cosines

$$V = B_1 \cosh(x/\lambda) + B_2 \sinh(x/\lambda) \quad (1.8)$$

and

$$V = C_1 \cosh(L - X) + C_2 \sinh(L - X), \quad (1.9)$$

where the hyperbolic functions (available in standard mathematical tables and standard computer subroutines) are defined by

$$2 \cosh(x/\lambda) = \exp(x/\lambda) + \exp(-x/\lambda)$$

$$2 \sinh(x/\lambda) = \exp(x/\lambda) - \exp(-x/\lambda)$$

also, in Equation 1.9, X is the dimensionless distance variable (x/λ) and $L = l/\lambda$ is a constant relevant to a cylinder of finite length.

The equivalence of general solutions (Eqs. 1.7-1.9) implies the following relations between the different pairs of arbitrary constants.

$$2A_1 = B_1 + B_2 = (C_1 - C_2) \exp(-L)$$

$$2A_2 = B_1 - B_2 = (C_1 + C_2) \exp(+L).$$

The advantage of these alternative forms of the general solution is the simplification achieved when one selects the form best suited to particular boundary conditions. Equation 1.7 is best for infinite lengths because regularity at $+\infty$ requires that $A_1 = 0$ when x ranges from $x = 0$ to $x = +\infty$; regularity at $-\infty$ requires that $A_2 = 0$ when x ranges from $x = 0$ to $x = -\infty$. Equations 1.8 and 1.9 are useful for finite lengths, especially for the sealed-end boundary condition, $dV/dx = 0$ at $x = 0$ or at $X = L$, or for the clamped-end boundary condition, $V = 0$ at $x = 0$ or at $X = L$. Specifically, $V = 0$ at $x = 0$ requires that $B_1 = 0$ in Equation 1.8, while $V = 0$ at $X = L$ requires that $C_1 = 0$ in Equation 1.9; on the other hand, $dV/dx = 0$ at $x = 0$ would require that $B_2 = 0$ in Equation 1.8, while $dV/dx = 0$ at $X = L$ would require that $C_2 = 0$ in Equation 1.9 [see (34, 139, 185)].

Basic Transient Solutions of Cable Equation

Both Fourier and Kelvin knew that for partial differential equations of the general form

$$\partial^2V/\partial X^2 - V - \partial V/\partial T = 0 \quad (1.10)$$

solutions can be expressed in the form

$$V = U \exp(-T) \quad (1.11)$$

where V and U are both functions of X and T, and U is a solution of the simpler heat conduction equation

$$\partial^2 U/\partial X^2 - \partial U/\partial T = 0 \qquad (1.12)$$

This means that Fourier's methods and the many specific solutions that he and later workers elaborated for the simple heat equation (Eq. 1.12) can be applied also to the cable equation (Eqs. 1.2 and 1.10) through the transformation defined by Equation 1.11, when care is given to changed boundary conditions.

Solutions Using Separation of Variables

One type of solution is called separable because it can be expressed as the product of two functions, of which one is a function of X but not of T, while the other is a function of T but not of X. An example of such a solution of Equation 1.12 can be expressed

$$U = \cos(\alpha X) \exp(-\alpha^2 T) \qquad (1.13)$$

where α can be any constant; it is easily verified that this is a solution of Equation 1.12 because $\partial^2 U/\partial X^2$ and $\partial U/\partial T$ both equal $-\alpha^2 U$. It follows from Equation 1.11 that the corresponding solution of the cable equation (Eq. 1.10) can be expressed

$$V = \cos(\alpha X) \exp(-T - \alpha^2 T) \qquad (1.14)$$

If $\cos(\alpha X)$ is replaced by $\sin(\alpha X)$, this also provides a solution. Furthermore, because the differential equation is both linear and homogeneous, such solutions can be combined into a more general solution

$$V = [A \sin(\alpha X) + B \cos(\alpha X)] \exp(-T - \alpha^2 T) \qquad (1.15)$$

where we now have three arbitrary constants, A, B, and α. It may be noted that dependence on X and T are still separated in this more general solution of the cable equation. For any specific problem, the values of A, B, and α must be determined from the boundary conditions and the initial condition. For finite lengths with simple boundary conditions at both ends, Fourier first showed how to construct the specific solution that satisfies an arbitrary initial condition. This solution has been applied to nerve (141, 145, 150, 161); for a finite length of passive cable with sealed ends $(\partial V/\partial X = 0$ at $X = 0$ and $X = L)$ the solution can be expressed as the infinite series

$$V(X, T) = \sum_{n=0}^{\infty} B_n \cos(n\pi X/L) \qquad (1.16)$$

$$\exp[-T - (n\pi/L)^2 T]$$

where the coefficients (B_n) are known as the Fourier coefficients

$$B_0 = (1/L) \int_0^L W(X) \, dX \qquad (1.17)$$

and, for positive integer values of n,

$$B_n = (2/L) \int_0^L W(X) \cos(n\pi X/L) \, dX \qquad (1.18)$$

where $W(X)$ represents the initial condition $V(X, 0)$. For the particular initial condition of a point charge, Q_0, at $X = 0$ and $T = 0$, these Fourier coefficients reduce simply to

$$B_0 = Q_0/(L\lambda c_m) \qquad (1.19)$$

$$B_n = 2B_0 \qquad (1.20)$$

where λc_m represents the membrane capacity per λ length of cylinder. Thus B_0 represents the voltage expected if the charge (Q_0) were distributed uniformly over the membrane capacity along its finite electrotonic length (L).

Related solutions for different boundary conditions are available elsewhere (145), as are superposition solutions for certain dendritic trees [(150, 161); see also (6, 7, 90–93)].

Fundamental Solution for Instantaneous Point Charge

Useful solutions of a different mathematical form can be constructed from what is sometimes called the fundamental solution, or the Green's function, or the instantaneous point source solution. For the one-dimensional heat conduction equation (Eq. 1.12), this solution can be expressed

$$U(X, T) = C_0 T^{-\frac{1}{2}} \exp(-X^2/4T) \qquad (1.21)$$

where C_0 is a proportionality constant related to the amount of the instantaneous point charge located at $X = 0$, $T = 0$. One can confirm that this is a solution of Equation 1.12 by verifying that both $\partial^2 U/\partial X^2$ and $\partial U/\partial T$ are equal to the same expression, namely

$$C_0(-\tfrac{1}{2} T^{-3/2} + \tfrac{1}{4} X^2 T^{-5/2}) \exp(-X^2/4T)$$

From Equations 1.11 and 1.21, the corresponding fundamental solution for the cable equation (Eq. 1.10) can be expressed

$$V(X, T) = C_0 T^{-\frac{1}{2}} \exp(-X^2/4T - T) \qquad (1.22)$$

It may be noted that where X extends to $\pm\infty$,

$$C_0 = Q_0/(2\lambda c_m \pi^{\frac{1}{2}}) \qquad (1.23)$$

for an instantaneous point charge of Q_0 coulombs applied at $X = 0$, $T = 0$ in agreement with Hodgkin [(47), Appendix I]; for the semi-infinite case, where X extends only from 0 to $+\infty$, C_0 is twice as large. Because λc_m is the capacity per λ length, integration of $\lambda c_m V$ over X yields an overall charge equal to $Q_0 \exp(-T)$.

This fundamental solution underlies many more complicated solutions constructed to fit particular initial conditions and boundary conditions. Some of these can be obtained by superpositions based on the method of images (21, 92, 93, 161). Other solutions involving error functions and closely related functions are usually obtained by "operational methods" that were pioneered by Heaviside and are now usually carried out by means of Laplace transforms (21, 33, 80, 92, 93, 117, 131, 140, 161).

Because solutions 1.21 and 1.22 do not have their dependence on X and T separable (in contrast to solutions 1.13 and 1.14), it is of interest to point out that already in 1822 Fourier demonstrated and discussed the fact that such solutions are related by an integral

$$\int_{-\infty}^{+\infty} \cos{(\alpha X)} \exp{(-\alpha^2 T)}d\alpha = (\pi/T)^{\frac{1}{2}} \exp{(-X^2/4T)}$$

[see articles 374 and 375, (55)]. This underlies all passive membrane transients and explains why they can be decomposed either into sums of exponentials or into sums of response functions (to instantaneous point charge) [see (91, 145, 161) and (21), p. 274–275; see also section PASSIVE MEMBRANE POTENTIAL TRANSIENTS AND TIME CONSTANTS].

LIST OF SYMBOLS

For Membrane Cylinders

V_i	Electric potential on intracellular side of membrane (V)
V_e	Electric potential on extracellular side of membrane (V)
$V_m = V_i - V_e$	Membrane potential difference, intracellular minus extracellular (V)
E_r	Resting membrane emf; resting value of V_m (V)
$V = V_m - E_r$	Electrotonic potential, as deviation of membrane potential from its resting value (V)
V_0	Value of V at $x = 0$ or $t = 0$ (V)
R_i	Volume resistivity of intracellular medium (Ω cm)
R_e	Volume resistivity of extracellular medium (Ω cm)
R_m	Resistance across a unit area of passive membrane (Ω cm²)
C_m	Capacitance per unit area of membrane (F cm⁻²)
d	Diameter of membrane cylinder (cm)
$r_i = 4R_i/\pi\, d^2$	Core resistance per unit length (Ω cm⁻¹)
$r_e = R_e/\pi\, h\, d$	Resistance per unit length of a thin external cylindrical layer of thickness h (Ω cm⁻¹)
$r_m = R_m/\pi\, d$	Resistance across a unit length of passive membrane cylinder (Ω cm)
$c_m = C_m\, \pi\, d$	Membrane capacity per unit length of cylinder (F cm⁻¹)
$\tau = r_m c_m = R_m C_m$	Passive membrane time constant (s)
t	Time (s)
$T = t/\tau$	Dimensionless time variable
$\lambda = [r_m/(r_i + r_e)]^{1/2}$	Length constant of core conductor, where r_e is usually set equal to zero for large external volume (cm)

$\lambda = [(R_m/R_i)(d/4)]^{1/2}$	Length constant of cylindrical core conductor, when extracellular resistance is neglected (cm)
x	Actual distance along the core conductor axis (cm)
$X = x/\lambda$	Electrotonic distance (dimensionless)
i_i	Intracellular core current along axis, positive toward increasing x (A)
i_e	Extracellular current parallel to axis, positive toward increasing x (A)
i_m	Membrane current per unit length, positive outward (A cm⁻¹)
$I_m = i_m/\pi\, d$	Membrane current density, positive outward (A cm⁻²)
i_{Ai}	Internally applied current per unit length, positive outward (A cm⁻¹)
i_{Ae}	Externally applied current per unit length, positive outward (A cm⁻¹)
I_0	Input current applied intracellularly at $X = 0$ (A)
$R_\infty = r_m/\lambda = \lambda r_i = (r_m r_i)^{1/2}$ $= (2/\pi)(R_m R_i)^{1/2} (d)^{-3/2}$	Input resistance for a semi-infinite length, when $r_e = 0$ (Ω)
$R_{\pm\infty} = R_\infty/2$	Input resistance when x extends to both $+ \infty$ and $- \infty$ away from the input point, and $r_e = 0$ (Ω)
$G_\infty = 1/R_\infty$	Input conductance for semi-infinite length, when $r_e = 0$ (mho $= \Omega^{-1}$)

For Finite Length of Uniform Cylinder

ℓ	Actual length of core conductor (cm)
$L = \ell/\lambda$	Electrotonic length of core conductor (dimensionless)
$R_{CL,\, ins} = R_\infty \coth L$	Input resistance at one end of cylinder of length L, when the other end is insulated $(\partial V/\partial X = 0)$ (Ω)
$R_{CL,\, clp} = R_\infty \tanh L$	Input resistance at one end of cylinder of length L, when the other end is clamped $(V = 0)$ (Ω)
$Z_{CL,\, ins} = (R_\infty/q) \coth (qL)$	Input impedance at one end of cylinder of electrotonic length L, when the other end is insulated $(\partial V/\partial X = 0)$ [see (150)]
$Z_{CL,\, clp} = (R_\infty/q) \tanh (qL)$	Input impedance at one end of cylinder of electrotonic length L, when the other end is clamped $(V = 0)$ [see (150)]
$q = (1 + j\omega\tau)^{1/2}$	For an AC steady state
$\tau_1, \tau_2, \ldots, \tau_n$	Equalizing time constants for cable of finite length
$C_0, C_1, C_2, \ldots, C_n$	Coefficients (independent of t) used to form a linear com-

$K_{\text{ins}} (X, L, T)$ bination of exponential decays

$K_{\text{ins}} (X, L, T)$ Response at time T and location X in a cylinder of length L, insulated $(\partial V/\partial X = 0)$ at the origin for instantaneous point charge placed at the end $X = L$ [see (161), both for the Laplace transform of this response function and for two representations in the time domain]

$K_{\text{cip}} (X, L, T)$ Response at time T and location X in a cylinder of length L, clamped $(V = 0)$ at the origin for instantaneous point charge placed at the end $X = L$ [see (161), both for the Laplace transform and for two representations in the time domain]

For Synaptic Membrane

E_r Resting membrane emf (V)
E_ϵ Synaptic excitatory emf (V)
E_j Synaptic inhibitory emf (V)
$V = V_m - E_r$ Deviation of membrane potential from rest (V)
$V_\epsilon = E_\epsilon - E_r$ Synaptic excitatory equilibrium value of V (V)
$V_j = E_j - E_r$ Synaptic inhibitory equilibrium value of V (V)
$G_r = 1/R_m$ Resting membrane conductance per unit area $(\Omega^{-1}\ \text{cm}^{-2})$
G_ϵ Synaptic excitatory conductance per unit area $(\Omega^{-1}\ \text{cm}^{-2})$
G_j Synaptic inhibitory conductance per unit area $(\Omega^{-1}\ \text{cm}^{-2})$
$\mathscr{E} = G_\epsilon/G_r$ Dimensionless synaptic excitatory intensity; also excitatory variable in Eqs. 2.50–2.52
$\mathscr{J} = G_j/G_r$ Dimensionless synaptic inhibitory intensity; also quenching auxiliary variable in Eqs. 2.50–2.52
$\mathscr{V} = V/V_\epsilon$ Normalized membrane depolarization (dimensionless)
$\mu = (1 + \mathscr{E} + \mathscr{J})/\tau$ Rate constant in Eqs. 2.39 and 2.42 (s^{-1})
$\tau_{\epsilon j} = \tau/(1 + \mathscr{E} + \mathscr{J})$ Effective membrane time constant for an area receiving uniform and constant synaptic input; see Eqs. 2.43–2.49 (s)
$\lambda_{\epsilon j} = \lambda/(1 + \mathscr{E} + \mathscr{J})^{1/2}$ Effective length constant over a length receiving uniform and steady synaptic input; see Eqs. 2.43–2.49 (cm)

For Dendritic Neuron Model

R_N Whole neuron input resistance
$G_N = 1/R_N$ Whole neuron input conductance

G_S Soma conductance
$\sum_j G_{Dj}$ Combined dendritic input conductance
$\rho = \sum_j G_{Dj}/G_S$ Dendritic to soma conductance ratio
$G_{Dj} = B_{0j}G_{xj}$ Input conductance of jth dendritic tree
G_{xj} Input conductance of jth dendritic trunk cylinder when extended for infinite length away from soma
B_{0j} Weighting factor for jth dendritic tree at origin, $X = 0$; see Eq. 3.37
G_A Input conductance of axon
G_{inj} Injury conductance
A_S Soma surface area
A_D Surface area of dendritic tree or equivalent cylinder
$A_{\Sigma D}$ Summed surface area of all dendritic trees belonging to one neuron
$A_N = A_S + A_{\Sigma D}$ Surface area of soma and dendrites, and of most nearly equivalent cylinder
R_m Membrane resistivity when uniform everywhere
R_{mS} Membrane resistivity of soma membrane
R_{mD} Membrane resistivity of dendritic membrane
$X_1 = \int_0^{x_1} (1/\lambda)dx$ Electrotonic distance from the origin in a dendritic tree, where λ changes at every branch point
$L = \int_0^{x_m} (1/\lambda)dx$ Electrotonic length of a dendritic tree where all terminal branches terminate at the same electrotonic distance from the origin
L_j Electrotonic length of jth dendritic tree or equivalent cylinder
L_D Dendritic electrotonic length when all trees have same value $(L_D = L_j$ for all j$)$
L_N Electrotonic length of that cylinder most nearly equivalent to soma plus dendrites

For Idealized Neuron Model [see (150, 161)]

N Number of equivalent dendritic trees (or their equivalent cylinders) that are coupled at $X = 0$
L Electrotonic length of each of those trees or equivalent cylinders
M Number of orders of symmetrical branching, specifically in the dendritic tree that receives the input
X_1 Electrotonic distance from the origin to the first point of

branching

X_k Electrotonic distance from the origin to the kth-order branch points

R_{Tz} Value of R_z for the trunk cylinder of one dendritic tree

R_N Whole neuron input resistance at the point ($X = 0$) of common origin of the N trees or equivalent cylinders

R_{BL} Input resistance at the end ($X = L$) of one terminal branch of the neuron model

V_{BL} Steady value of V at input branch terminal

V_0 Steady value of V at the origin of the neuron model

$AF_{BL,0} = V_{BL}/V_0$ Attenuation factor from input branch terminal to soma

ASSUMPTIONS AND DERIVATION OF CABLE THEORY

The assumptions and derivation have been presented variously by many authors [e.g., (24, 33, 52, 69, 80, 101, 136, 141, 162, 179, 181, 182)]. In the following presentation the simplest case is explained first; the effects of complicating assumptions are explained later.

One Dimensional in Space

The basic simplifying assumption of cable theory is to reduce the spatial dependence of V to one dimension, namely, distance along the length of the cable or core conductor. Thus it is assumed that any radial or angular dependence of V within the core, or outside the membrane, can be neglected. Support for this has been obtained in two different ways. Experiments with single nonmyelinated axons have yielded reasonably good agreement with cable theory predictions (24, 27, 73, 80, 98, 157, 181, 182). Also errors resulting from this simplification have been assessed in theoretical studies that explicitly include all three dimensions of a cylindrical coordinate system (22, 41, 132, 134-136, 146); such errors are found to be negligible for many problems of interest.

Intracellular Core Resistance

It is assumed that the intracellular medium provides a simple ohmic resistance to electric current flow. Together with the preceding assumption, this implies that the long, thin core can be characterized by a core resistance per unit length, symbolized r_i. For a simple, uniform core conductor, the value of r_i is constant for all x; however, core conductors of different cross section, or of different material, will have different r_i values. If R_i (Ω cm) represents the specific resistance, or volume resistivity (i.e., resistance across a unit cube) of homogeneous intracellular material and if A_i (cm²) represents the area of

cross section of the core, then $r_i = R_i/A_i$ (Ω/cm). Because the core is usually assumed to have a circular cross section, this is usually expressed

$$r_i = R_i/(\pi a^2), \quad [\Omega/cm] \tag{2.1}$$

where a represents the core radius.

Ohm's Law for Core Current

For a length increment, $\Delta x = x_2 - x_1$, illustrated in Figure 16A, the core resistance equals $r_i \Delta x$ Ω; this resistance has been assigned to the lumped resistance element shown in Figure 16B. If Δx is small enough that the core current, i_i, does not change along this length increment, Ohm's law implies that

$$i_i r_i \Delta x = -\Delta V_i, \quad [V] \tag{2.2}$$

where V_i represents the intracellular potential, and $-\Delta V_i$ represents the potential difference, $V_{i1} - V_{i2}$, as shown in Figure 16, A and B. The minus sign in Equation 2.2 satisfies the physical requirement that positive core current (flowing in the direction of increasing x) corresponds to negative ΔV_i (i.e., decreasing V_i with increasing x). For continuously varying V_i and i_i, we divide both sides of Equation 2.2 by Δx and then take the limit as $\Delta x \to 0$. This limit, for $\Delta V_i/\Delta x$, can be expressed as the ordinary derivative dV_i/dx, if V_i depends only on x and not on t; however, when V_i is a function of both x and t, but t is held constant during the limiting process, this limit is known as the partial derivative, $\partial V_i/\partial x$. The resulting version of Ohm's law for the core current can be expressed

$$i_i r_i = -\partial V_i/\partial x, \quad [V/cm] \tag{2.3}$$

Conservation of Current

Because the core has been assumed purely resistive and one-dimensional, conservation of current implies that whenever the core current flowing into a small length increment, Δx, exceeds the amount of core current flowing onward from that region, this excess of current must be accounted for. As indicated in Figure 16, C and D, this excess current must escape from the core as membrane current, provided that no intracellular electrodes are present. If i_m represents outward membrane current per unit length, and, if Δx is small enough that i_m does not change along this length, then $i_m \Delta x$ equals the amount of current escaping outward across this Δx length of the membrane cylinder. Then current conservation can be expressed

$$i_m \Delta x = -\Delta i_i, \quad [A]$$

as can be verified in Figure 16, C and D. Dividing through by Δx, and taking the limit as $\Delta x \to 0$, yields the expression

$$i_m = -\partial i_i/\partial x, \quad [A/cm] \tag{2.4}$$
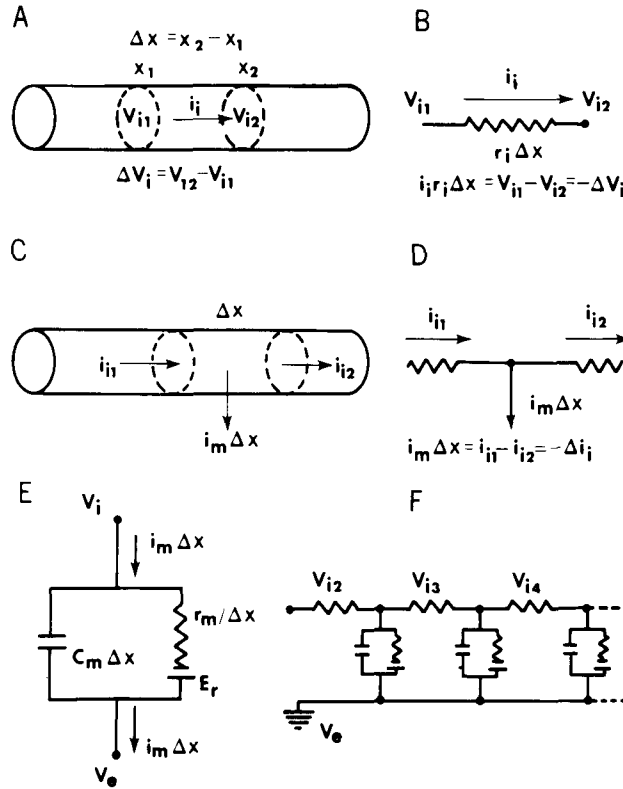
FIG. 16. Derivation of cable equation. Relation between cylindrical core conductor length increments and the lumped elements of the electric equivalent circuit are shown. *A* and *B*: relation of core current to the increment in voltage and in length (see Eq. 2.1-2.3). *C* and *D*: relation between membrane current and change in core current (see Eq. 2.4). *E*: membrane current divided into 2 parallel components, one capacitive and one resistive (see Eq. 2.10). *F*: lumped circuit approximation to a continuous cable, sometimes called a ladder network.

where i_m and i_i can be functions of both x and t. Before introducing complications caused by applied current electrodes (see Eqs. 2.28-2.30), we continue the cable equation derivation for the least complicated case.

Relation of Membrane Current to V_i

The relation of core current to V_i is already given by Equation 2.3. For a uniform core conductor, r_i is independent of x, and differentiation of Equation 2.3 with respect to x yields

$$r_i \partial i_i / \partial x = -\partial^2 V_i / \partial x^2, \; [\text{V/cm}^2]$$

which, when substituted into Equation 2.4, yields

$$i_m r_i = \partial^2 V_i / \partial x^2, \; [\text{V/cm}^2] \qquad (2.5)$$

It is important to note that this equation is valid, regardless of the detailed membrane model chosen and regardless of the extracellular potential distribution; it depends only on the one-dimensional core with constant r_i and on conservation of current with no intracellular electrodes applying current.

Effect of Assuming Extracellular Isopotentiality

In many problems of interest, the extracellular potential is nearly isopotential over a large extracellular volume, and the value of $\partial V_e / \partial x$ along the outside surface of the membrane is very much smaller than $\partial V_i / \partial x$ along the inside. This provides a partial justification for assuming extracellular isopotentiality, implying $\partial V_e / \partial x = 0$; additional incentive is provided by the fact that this simplification is especially useful when there is taper or branching of the core conductor (139, 141).

The membrane potential difference is defined, $V_m = V_i - V_e$, in agreement with what has become the usual convention since 1958 (24, 37, 75, 99, 139). (The older convention of using $V_e - V_i$ arose long before intracellular electrodes made it usual to record V_i relative to V_e, experimentally.) The departure of V_m from its resting value is defined $V = V_m - E_r$, or

$$V = V_i - V_e - E_r, \; [\text{V}] \qquad (2.6)$$

where E_r is the resting emf of the membrane.

For a uniform membrane, E_r must be independent of x, implying $\partial E_r / \partial x = 0$. This together with $\partial V_e / \partial x = 0$ (for extracellular isopotentiality) means that differentiation of Equation 2.6 implies $\partial V / \partial x = \partial V_i / \partial x$, and further that

$$\partial^2 V / \partial x^2 = \partial^2 V_i / \partial x^2, \; [\text{V/cm}^2]$$

Using this, Equation 2.5 can be reexpressed as

$$i_m = (1/r_i)\partial^2 V / \partial x^2, \; [\text{A/cm}] \qquad (2.7)$$

which relates i_m to V without yet having specified any particular membrane model. It should be noted that this rather simple equation becomes supplanted by a more complicated equation (Eq. 2.30) when extracellular isopotentiality is not assumed and when electrodes apply current inside the region of interest. Before treating these complications, we introduce the passive membrane model that is needed to complete the simpler cable equation derivation.

Passive Membrane Model

In Figure 16*E* the equivalent circuit that is generally used to represent passive membrane properties is shown; a membrane capacity is regarded as electrically in parallel with a membrane resistance, and there is a resting emf or battery (E_r) placed in series with the resistance. The membrane capacitance per unit length, c_m (F/cm), and the passive membrane resistance for unit length, r_m (Ω cm) are related to the membrane capacitance per unit area, C_m (F/cm²), and the passive membrane resistance for unit area, R_m (Ω cm²), by the expressions

$$c_m = 2\pi a C_m, \; [\text{F/cm}] \qquad (2.8)$$

and

$$r_m = R_m / (2\pi a), \; [\Omega \; \text{cm}] \qquad (2.9)$$

where $2\pi a$ represents the circumference of the membrane cylinder; if there is significant departure from circular cross section, $2\pi a$ should be replaced by an expression for the noncircular circumference. For the length increment, Δx, Figure 16E indicates a capacity of $c_m \Delta x$ F, and a resistance of $r_m/\Delta x$ Ω. The fact that the total outward membrane current, $i_m \Delta x$, is the sum of the resistive and capacitative currents can be expressed

$$i_m \Delta x = (V_m - E_r)\left(\frac{\Delta x}{r_m}\right) + (c_m \Delta x)\left(\frac{\partial V_m}{\partial t}\right), [A]$$

This equation can be simplified because Δx can be factored out of every term and because $V = V_m - E_r$ and $\partial V/\partial t = \partial V_m/\partial t$ on the assumption that E_r is independent of time; the result is

$$i_m = V/r_m + c_m \partial V/\partial t, [A/cm] \qquad (2.10)$$

for outward membrane current per unit length. It may be noted that this also implies

$$I_m = V/R_m + C_m \partial V/\partial t, [A/cm^2] \qquad (2.11)$$

where I_m represents outward membrane current density (A/cm^2) and in agreement with previous expressions (Eqs. 2.8 and 2.9)

$$i_m = 2\pi a I_m, [A/cm] \qquad (2.12)$$

Resulting Cable Equation for Simple Case

Now the expression for i_m provided by Equation 2.10, for the passive membrane model, can be equated with that provided by Equation 2.7, from a consideration of core current; the result can be multiplied through by r_m to obtain the expression

$$V + r_m c_m \partial V/\partial t = (r_m/r_i)\partial^2 V/\partial x^2, [V] \qquad (2.13)$$

By defining $\tau = r_m c_m$ and $\lambda^2 = r_m/r_i$, we can rewrite this partial differential equation in the form

$$\lambda^2 \partial^2 V/\partial x^2 - V - \tau \partial V/\partial t = 0, [V] \qquad (2.14)$$

which agrees with the cable equation shown earlier (Eq. 1.1).

Physical Meaning of Cable Equation Terms

By reviewing how Equation 2.14 was obtained, one can check the physical meaning of each term in the cable equation: V is proportional to the resistive (or leakage) component of the outward membrane current, as it varies with x and t; $\partial V/\partial t$ is proportional to the capacitive component of the outward membrane current, as it varies with x and t; $\partial^2 V/\partial x^2$, traced back through Equations 2.7–2.4, is proportional to the excess of core current (excess of that which enters over that which leaves a small length increment of core) as it varies with x and t; this excess escapes the core as outward membrane current, when no intracellular current electrode is present.

Physical Meaning of τ

The left-hand side of Equation 2.13 and the resulting definition of $\tau = r_m c_m$ depend on the passive membrane model (Fig. 16E and Eqs. 2.8–2.12); they do not depend on assuming extracellular isopotentiality or absence of current electrodes. From Equations 2.10 and 2.11, it can be seen that dependence on membrane surface area becomes cancelled in forming the product $r_m c_m$ or $R_m C_m$. This product has electrical units of ohm times farad [the fact that this product has the physical dimension of time can be verified as follows: a capacity has the physical dimensions of Q/V or of $I/(dV/dt)$, in A/(V/s), which is equivalent to s/Ω; therefore the RC product reduces simply to s]. Thus the passive membrane time constant

$$\tau = R_m C_m = r_m c_m, [s] \qquad (2.15)$$

is a membrane parameter that has the dimension of time and does not depend on membrane area.

The physical significance of τ as a natural decay constant for uniform membrane potential decay is seen most easily by considering a patch of membrane that is assumed to have a spatially uniform membrane potential and to be electrically isolated in the sense that its total membrane current is held to zero (i.e., space clamp, with current clamp set to zero). Then Equations 2.10 and 2.11 simplify to

$$dV/dt = -V/\tau, [V/s] \qquad (2.16)$$

This ordinary differential equation is of a form that is very well known for simple first-order decay; it implies that the rate of change of V is proportional to $-V$ and that the constant of proportionality is $1/\tau$; its solution can be expressed

$$V = V_0 \exp(-t/\tau), [V] \qquad (2.17)$$

where V_0 represents the initial value of V, when $t = 0$. This implies that when $t = \tau$, the value of V will have decayed to 1/e of V_0, or about 0.37 V_0; also, when the natural log of V is plotted against t, this results in a straight line whose slope is $-1/\tau$. This provides the basis for an experimental estimate of τ for a membrane that can be space clamped. However, when $V(x, t)$ is not spatially uniform, its passive decay is more complicated than Equation 2.17; the mathematical expressions for such passive decay are solutions of the cable equation for particular initial boundary conditions (e.g. see Eqs. 4.1 and 4.8). It is interesting to add, as pointed out by Hodgkin & Rushton (80), that even when $V(x, t)$ is not spatially uniform the total charge on the membrane still undergoes a simple exponential decay with τ as the time constant; this does assume absence of any short circuit or voltage clamp across the membrane.

Physical Meaning of λ

The right-hand side of Equation 2.13 and the resulting definition of $\lambda^2 = r_m/r_i$ do not depend on the

membrane capacity, but they do depend on passive membrane resistance and on the assumption of extracellular isopotentiality. As shown in the next section, the definition of λ becomes generalized to

$$\lambda^2 = r_m/(r_i + r_e), \text{ [cm}^2\text{]} \qquad (2.18)$$

when one assumes an extracellular resistance per unit length, r_e (Ω/cm). Because r_m is expressed in ohms centimeters and $(r_i + r_e)$ in ohms per centimeter, the expression for λ^2 corresponds to square centimeters. Also, because rearrangement yields

$$\lambda(r_i + r_e) = r_m/\lambda, \text{ [}\Omega\text{]} \qquad (2.19)$$

it can be seen that (for $r_e = 0$) the length constant (λ) corresponds to that length of core conductor for which the core resistance (λr_i) exactly equals the resistance (r_m/λ) across the membrane for the same length of membrane cylinder; such characterization of the length constant was noted long ago by Rushton (162) and by others.

When $r_e = 0$, one consequence is extracellular isopotentiality. Also then Equations 2.1, 2.9, and 2.18 can be used to express the length constant as a simple function of the cylinder radius (a) or diameter (d) and the more general resistivities, R_m and R_i. Thus, for $r_e = 0$

$$\lambda^2 = \left(\frac{R_m}{2\pi a}\right)\left(\frac{\pi a^2}{R_i}\right)$$

$$= (R_m/R_i)(a/2), \text{ [cm}^2\text{]}$$

This provides the basis for the expression

$$\lambda = \sqrt{(R_m/R_i)(d/4)}, \text{ [cm]} \qquad (2.20)$$

which shows that λ is proportional to the square root of the cylinder diameter (d) when R_m/R_i is constant and extracellular isopotentiality ($r_e = 0$) is assumed. If, for example, $R_m/R_i = 40$ cm, or 4×10^5 μm, then $d = 10$ μm implies $\lambda = 10^3$ μm, or 1 mm, while $d = 90$ μm implies $\lambda = 3$ mm. It may be noted that, when the core does not have a circular cross section, one should use the more general expressions, $r_m = R_m/P_m$ and $r_i = R_i/A_i$, where A_i is the area of core cross section and P_m is the perimeter described by the membrane in this cross section; then one obtains

$$\lambda = \sqrt{(R_m/R_i)(A_i/P_m)}, \text{ [cm]}$$

as has been pointed out by Mirolli & Talbott (124); this also depends on extracellular isopotentiality.

The physical significance of λ as a natural length constant is illustrated most easily by considering the special case of a steady-state distribution of V along a semi-infinite cable, extending from $x = 0$ to $x = \infty$. Assume that a steady value, $V = V_0$, is maintained at $x = 0$ and that no voltage is applied elsewhere (i.e., V is continuous and bounded out to $x = \infty$). The solution of the steady-state cable equation (Eq. 1.3) for these boundary conditions is simply

$$V = V_0 \exp{(-x/\lambda)}, \text{ [V]} \qquad (2.21)$$

For this special case, Equation 2.21 defines a simple exponential decrement with distance, where the length constant (λ) plays a role similar to that of the time constant (τ) in Equation 2.17. Clearly Equation 2.21 provides a basis for an experimental estimate of λ, but it is important to add the warning that steady-state decrement with distance can be very different from this for different boundary conditions (see Eq. 3.24 and Fig. 21).

Electrotonic Distance, Length, and Decrement

Because electrotonus and electrotonic spread with distance were central to the early history of core conductor theory and because actual distances (x) become more meaningful when expressed in terms of the natural length constant (λ) it has been found convenient to refer to the dimensionless distance ($X = x/\lambda$) as electrotonic distance; also a core conductor of finite length (ℓ) can be characterized as having an electrotonic length ($L = \ell/\lambda$). An axon usually has a large electrotonic length of at least 10, but more often of the order of 100 or even 1,000. Individual dendritic branches can correspond to electrotonic distance increments ranging from about 0.1 to 1 or 2, while the entire dendritic tree of a spinal motoneuron corresponds to an electrotonic length usually ranging between 1 and 2. For such finite lengths, it is important to emphasize that electrotonic decrement with distance depends as much on the boundary conditions at both ends as on the electrotonic distance (see Fig. 21). Also, under transient conditions, electrotonic decrement with distance can differ very significantly from that under steady-state conditions. Thus it should be understood that electrotonic decrement cannot, in general, be characterized by Equation 2.21.

Effect of Placing Axon in Oil

When a nonmyelinated axon is removed from a large volume of ionic solution and placed in air or in oil, a thin layer of ionic solution remains on the outside surface of the membrane. For convenience, this thin layer is assumed to be uniform and to provide an extracellular resistance per unit length (r_e). In air, r_e changes with time as evaporation takes place, or as isotonic solution is dripped on to prevent membrane injury caused by drying; in oil, r_e is much more nearly constant with time.

For one-dimensional flow of extracellular current (i_e), Ohm's law can be expressed

$$i_e r_e = -\partial V_e/\partial x, \text{ [V/cm]} \qquad (2.22)$$

where V_e now depends on x and t, and this equation may be compared with the corresponding equation (i.e., Eq. 2.3) for the intracellular core current. Because $V = V_i - V_e - E_r$ and because E_r is assumed to be independent of x, differentiation yields

$$\partial V/\partial x = \partial V_i/\partial x - \partial V_e/\partial x$$
$$= -i_i r_i + i_e r_e, \ [V/cm] \qquad (2.23)$$

where the last expression makes use of Equations 2.3 and 2.22. When r_i and r_e are both independent of x

$$\partial^2 V/\partial x^2 = r_i(-\partial i_i/\partial x) + r_e \partial i_e/\partial x, \ [V/cm^2] \quad (2.24)$$

At this point of the derivation, expressions for $\partial i_i/\partial x$ and $\partial i_e/\partial x$ are needed and the presence of applied current (intracellular or extracellular) within the region of interest becomes important; that complication is dealt with later in Equations 2.28 and 2.29. For regions containing no current electrodes, conservation of current implies

$$i_m = -\partial i_i/\partial x = \partial i_e/\partial x, \ [A/cm] \qquad (2.25)$$

where the first two terms restate Equation 2.4 (see Fig. 16, C and D) and the third term extends the same principle to the (one-dimensional) extracellular current. When this is substituted into Equation 2.24, the result is

$$\partial^2 V/\partial x^2 = (r_i + r_e)i_m, \ [V/cm^2] \qquad (2.26)$$

and when this is combined with Equation 2.10, Equation 2.13 becomes supplanted by

$$V + r_m c_m \partial V/\partial t = [r_m/(r_i + r_e)]\partial^2 V/\partial x^2, \ [V] \quad (2.27)$$

This corresponds to the same cable equation (i.e., Eqs. 1.1 and 2.14) as before, provided that the definition of λ^2 is generalized to $r_m/(r_i + r_e)$, as in Equation 2.18.

Such a core conductor is illustrated diagrammatically in Figure 17A in which both the intracellular core and the extracellular conducting layer, as well as both intracellular and extracellular electrodes that apply current, are shown.

Effect of Applied Current

First suppose that one or more intracellular electrodes (one of which could be a long axial electrode, as used with squid axons) apply current in the core. Let i_{Ai} represent this intracellularly applied current per unit length of core. If i_{Ai} is constant along a length (Δx), then $i_{Ai}\Delta x$ is the amount of this current introduced into this increment of core. Then, as illustrated in the upper half of the lumped circuit diagram (Fig. 17B), conservation of current can be conveniently expressed as Kirchhoff's law; namely, that the algebraic sum of all currents flowing into a circuit node must be zero; for the upper half of Figure 17B, this requirement is

$$i_{i1} - i_{i2} + i_{Ai}\Delta x - i_m \Delta x = 0$$

Because $i_{i1} - i_{i2} = -\Delta i_i$, one can divide through by Δx, and take the limit as $\Delta x \to 0$, obtaining

$$\partial i_i/\partial x = i_{Ai} - i_m, \ [A/cm] \qquad (2.28)$$

Similarly extracellularly, let $i_{Ae}\Delta x$ represent the
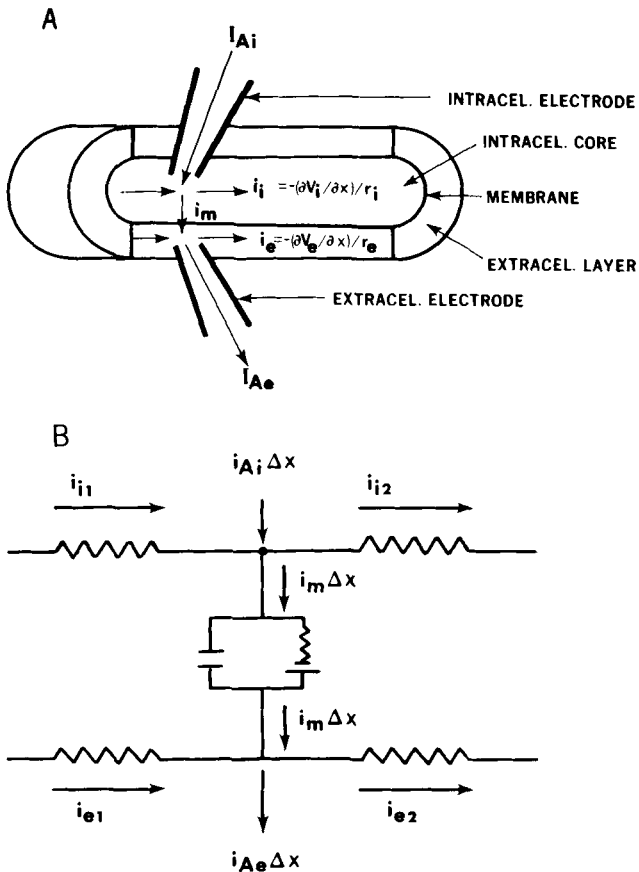
FIG. 17. Relation of applied current (at both intracellular and extracellular points) to membrane current and to longitudinal current (both intracellular core current and extracellular longitudinal current). *A*: 2 microelectrodes with a core conductor diagram somewhat similar to that used by Taylor (182). *Intracel.*, intracellular; *extracel.*, extracellular. *B*: lumped parameter circuit diagram used for an application of Kirchoff's law for conservation of current (see Eq. 2.28-2.33).

current flowing from Δx of the exterior layer to external applied current electrodes (see subsection *Comment on Sign Conventions*); then, as illustrated in the lower half of Figure 17B, conservation of current requires that

$$i_{e1} - i_{e2} - i_{Ae}\Delta x + i_m\Delta x = 0$$

which implies

$$\partial i_e/\partial x = i_m - i_{Ae}, \ [A/cm] \qquad (2.29)$$

When Equations 2.28 and 2.29 are used instead of Equation 2.25 for substitution into Equation 2.24, the result is

$$\partial^2 V/\partial x^2 = (r_i + r_e)i_m - r_i i_{Ai} - r_e i_{Ae}, \ [V/cm^2] \quad (2.30)$$

When this is combined with Equation 2.10 and use is made of $\tau = r_m c_m$ and $\lambda^2 = r_m/(r_i + r_e)$, the result can be expressed

$$\lambda^2 \partial^2 V/\partial x^2 - V - \tau \partial V/\partial t$$
$$= -\lambda^2(r_i i_{Ai} + r_e i_{Ae}), \ [V] \qquad (2.31)$$

which is an example of the augmented cable equa-

tion (Eq. 1.5), where the forcing function on the right-hand side can be a function of both x and t.

A particularly interesting special case results when

$$i_{Ai} = i_{Ae} \equiv i_{Aie}, \text{ [A/cm]} \qquad (2.32)$$

Then Equation 2.31 simplifies to

$$\lambda^2 \partial^2 V/\partial x^2 - V - \tau \partial V/\partial t = -r_m i_{Aie}, \text{ [V]} \quad (2.33)$$

On the other hand, if $r_i i_{Ai} = -r_e i_{Ae}$, the right-hand side of Equation 2.31 is reduced to zero.

Comment on Sign Conventions

The contribution of applied current in Equations 2.30 and 2.31 is consistent with that exhibited by earlier derivations in the literature [e.g., (33, 80, 182)] if one is careful to note the sign convention for V_m and i_m. [According to the earlier (i.e., pre 1958) convention, i_m was regarded as positive inward and $V_m = V_e - V_i$ had a positive resting value; also applied current, designated i_p for "polarizing" current, was positive inward and was applied only by extracellular electrodes; with this older convention, positive i_p contributes to positive i_m and tends to increase V_m, which represents a hyperpolarizing change from resting conditions; however, excitatory depolarizations and action potentials appear as negative deflections.] With the present sign convention [e.g., (24, 37, 75, 99, 139)] $V_m = V_i - V_e$ has a negative resting value, and i_m is taken as positive outward; to be consistent, intracellularly applied current (i_{Ai}) is regarded positive outward and extracellularly applied current (i_{Ae}) is also regarded as positive outward (see Fig. 17B); with this convention, positive applied current contributes to positive i_m and tends to increase V_m as before, but such increasing V_m (e.g., from -70 to -60 mV) represents a depolarizing change from resting conditions; thus excitatory depolarizations and action potentials appear as positive deflections.

It may also be noted that the older derivations defined total longitudinal current as

$$I_l = i_i + i_e, \text{ [A]} \qquad (2.34)$$

which is also adopted here. However, because the older derivations treated only extracellularly applied current, they obtained the expression $\partial I_l/\partial x = i_p$ and then substituted $\partial I_l/\partial x$ for i_p in some of their equations. Today, it seems preferable to restore their i_p for their $\partial I_l/\partial x$ in their equations before comparing them with the present results, because here Equations 2.28 and 2.29 imply that

$$\partial I_l/\partial x = i_{Ai} - i_{Ae}, \text{ [A/cm]} \qquad (2.35)$$

which is more general than in the older papers. It is interesting to note that the special case of Equations 2.32 and 2.33 corresponds to $\partial I_l/\partial x = 0$. This case is valuable for superposition purposes because it provides for an applied current arrangement that depolarizes the membrane without disturbing $\partial I_l/\partial x$.

Effect of Synaptic Membrane Conductance

The idea that synaptic current is generated by a change in postsynaptic membrane conductance came from the experiments and interpretations by Fatt & Katz (47, 48) with neuromuscular junctions and by Coombs, Eccles, and Fatt (29) with spinal motoneurons of cat. When such a conductance change is localized to a few discrete points (or very small areas) along a core conductor, the cable equation remains unchanged along lengths between these points, and both the synaptic conductance and the resulting synaptic current can be incorporated into boundary conditions at these points. On the other hand, when the synaptic conductance change is distributed over the entire membrane surface by a very large number of widely distributed synapses, the cable equation itself becomes modified.

In Figure 18 an equivalent circuit used to represent synaptic membrane is shown where both synaptic excitation and synaptic inhibition can be present (141–144). Based on diagrams of Fatt & Katz (47, 48) and Coombs et al. (29), it shows four parallel pathways for current flow across the membrane; one pathway is capacitive and three are conductive. Each conductive pathway contains a different emf that is assumed to remain constant. The resting emf (E_r) is in series with the resting membrane conductance, $G_r = (1/R_m)$ (mho/cm^2). The synaptic excitatory emf (E_ϵ) is in series with its associated synaptic conductance, G_ϵ (mho/cm^2). Also the synaptic inhibitory emf (E_j) is in series with its associated synaptic conductance, G_j (mho/cm^2). Both G_ϵ and G_j are zero under resting conditions ($V_m = E_r$) and also under conditions where there is passive electrotonic spread in the absence of distributed synaptic input. When G_ϵ is very much larger than G_r and G_j and I_m is very small, then V_m tends very close to E_ϵ; thus E_ϵ can also be called the synaptic excitatory equilibrium potential. Similarly, when G_j is dominant, V_m
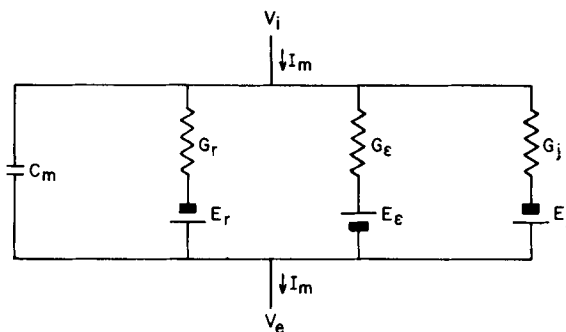
FIG. 18. Electric equivalent circuit model of synaptic membrane. Per unit area, C_m is the membrane capacity, G_r is the resting membrane conductance in series with battery E_r representing the resting emf, G_ϵ is the synaptic excitatory conductance in series with battery E_ϵ representing the synaptic excitatory emf, and G_j is the synaptic inhibitory conductance in series with battery E_j representing the synaptic inhibitory emf (see Eq. 2.36 and 2.37). [This model was based on those of Fatt & Katz (47, 48) and of Coombs, Eccles, and Fatt (29); see also Hodgkin & Katz (79).]

tends very close to E_j, which can be called the synaptic inhibitory equilibrium potential.

Under all conditions, the outward membrane current density, I_m (A/cm^2), in Figure 18 can be expressed mathematically as the sum of four components

$$I_m = C_m \partial V_m/\partial t + G_r(V_m - E_r) \\ + G_\epsilon(V_m - E_\epsilon) + G_j(V_m - E_j) \quad (2.36)$$

where C_m is expressed in farads per square centimeter, as elsewhere, G_r, G_ϵ, and G_j are all expressed in mho per square centimeter, and V_m, E_r, E_ϵ, and E_j are all expressed in volts (with signs taken as interior minus exterior). It is useful to multiply every term of this equation by R_m (or the equivalent of dividing by G_r) and to define the synaptic intensity variables ($\mathscr{E}$ and $\mathscr{J}$) as the conductance ratios, $\mathscr{E} = G_\epsilon/G_r$ and $\mathscr{J} = G_j/G_r$. Then this equation becomes

$$I_m R_m = \tau \partial V/\partial t + V + \\ \mathscr{E}(V - V_\epsilon) + \mathscr{J}(V - V_j) \quad (2.37)$$

where not only $V = V_m - E_r$, with $\partial V/\partial t = \partial V_m/\partial t$ because E_r is constant, but also $V_\epsilon = E_\epsilon - E_r$ and $V_j = E_j - E_r$, which constants are consistent with a convention adopted by Hodgkin & Huxley (77).

Before considering cable effects, we consider an isolated uniform patch of membrane, where I_m, $\mathscr{E}$, and $\mathscr{J}$ are all assumed to be uniform. Equation 2.37 can be rearranged to the form

$$\tau dV/dt + (1 + \mathscr{E} + \mathscr{J})V \\ = I_m R_m + \mathscr{E}V_\epsilon + \mathscr{J}V_j \quad (2.38)$$

Also, for periods of time during which the synaptic intensities $\mathscr{E}$ and $\mathscr{J}$ remain constant, this can be reduced to a simpler form

$$dV/dt = -\mu(V - V_s) \quad (2.39)$$

where the rate constant, μ, is defined

$$\mu = (1 + \mathscr{E} + \mathscr{J})/\tau = (G_r + G_\epsilon + G_j)/C_m \quad (2.40)$$

also

$$V_s = (I_m R_m + \mathscr{E}V_\epsilon + \mathscr{J}V_j)/(1 + \mathscr{E} + \mathscr{J}) \quad (2.41)$$

represents the steady-state value of V for this patch when I_m, as well as $\mathscr{E}$ and $\mathscr{J}$, remains constant. It may be noted that with μ and V_s constant, Equation 2.39 has the well-known solution for $t > 0$

$$V - V_s = (V_0 - V_s) \exp(-\mu t) \quad (2.42)$$

where V_0 represents the value of V when $t = 0$. It may be remarked that this is an example of exponential decay to a nonresting steady state with a time constant, $\tau/(1 + \mathscr{E} + \mathscr{J})$, which is smaller than the passive membrane time constant.

Next, to find the cable effects, we refer back to Equations 2.7, 2.10, and 2.11 and, noting that $i_m r_m = I_m R_m$, we use Equation 2.37 in place of Equation 2.10 to obtain the following partial differential equation instead of Equation 2.14

$$\lambda^2 \partial^2 V/\partial x^2 - V - \tau \partial V/\partial t \\ = \mathscr{E}(V - V_\epsilon) + \mathscr{J}(V - V_j) \quad (2.43)$$

This corresponds to the augmented cable equation (Eq. 1.5), where the forcing function

$$F = \mathscr{E}(V - V_\epsilon) + \mathscr{J}(V - V_j) \quad (2.44)$$

is a function of V, as well as the synaptic intensities $\mathscr{E}$ and $\mathscr{J}$, which may depend on X and T; this expression for F can be normalized by dividing through by $V_\epsilon = E_\epsilon - E_r$ (143, 151).

Furthermore, when $\mathscr{E}$ and $\mathscr{J}$ are uniform over the length in question and constant over the time in question, it is then useful to transpose $\mathscr{E}V$ and $\mathscr{J}V$ from the right to the left side of Equation 2.43 to obtain

$$\lambda^2 \partial^2 V/\partial x^2 - (1 + \mathscr{E} + \mathscr{J})V \\ - \tau \partial V/\partial t = - \mathscr{E}V_\epsilon - \mathscr{J}V_j \quad (2.45)$$

which no longer has V on the right side but now differs from the augmented cable equation (Eq. 1.5) on the left side. This complication can be handled as it was by Rall [(141), p. 1082–1085], but an equivalent, and perhaps more illuminating, way of expressing the same approach is to divide both sides of Equation 2.45 by the factor $(1 + \mathscr{E} + \mathscr{J})$ and to reexpress the result in terms of modified λ and τ values

$$(\lambda_{\epsilon j})^2 \partial^2 V/\partial x^2 - (V - V_{\epsilon j}) - \tau_{\epsilon j} \partial V/\partial t = 0 \quad (2.46)$$

where

$$\tau_{\epsilon j} = \tau/(1 + \mathscr{E} + \mathscr{J}) \quad (2.47)$$

$$\lambda_{\epsilon j} = \lambda/(1 + \mathscr{E} + \mathscr{J})^{1/2} \quad (2.48)$$

$$V_{\epsilon j} = (\mathscr{E}V_\epsilon + \mathscr{J}V_j)/(1 + \mathscr{E} + \mathscr{J}) \quad (2.49)$$

For a time and distance over which $\mathscr{E}$ and $\mathscr{J}$ remain constant, Equations 2.47–2.49 define constants, and the partial differential equation (Eq. 2.46) becomes a homogeneous cable equation with modified constant coefficients. The new variable $V - V_{\epsilon j}$ has the same derivatives as V because $V_{\epsilon j}$ is a constant that can be regarded as a combined synaptic equilibrium value (for V, and not V_m) obtained when both $\partial V/\partial t = 0$ and $\partial^2 V/\partial x^2 = 0$; it is almost a weighted mean of $V_\epsilon = E_\epsilon - E_r$ and $V_j = E_j - E_r$, with $\mathscr{E} = G_\epsilon/G_r$ and $\mathscr{J} = G_j/G_r$ used as weights; it is also equal to V_s of Equation 2.41 when $I_m = 0$ for the isolated patch. It may be noted that $\tau_{\epsilon j}$ and $\lambda_{\epsilon j}$ are both smaller than normal, but not by the same factor. A method and examples for treating a cylinder composed of two regions with different constant $\mathscr{E}$ and $\mathscr{J}$ values have been illustrated (141). A compartmental treatment of such problems is also available (143, 144).

Effect of Active Membrane Properties

Both the Hodgkin-Huxley model (77) and Fitz-Hugh's BVP model (49, 51) have been fully presented elsewhere. The purpose here is to indicate

very briefly how the circuit diagram (Fig. 18) and the notation of the preceding section can be reinterpreted and extended to provide a useful model of active membrane. Here we reinterpret G_ϵ as the excitatory conductance of the active process; it can be thought of as corresponding to Hodgkin-Huxley sodium conductance, less its resting value. Similarly we reinterpret G_j as the conductance of the quenching or restorative component of the active process; it can be thought of as corresponding to Hodgkin-Huxley potassium conductance, less its resting value. The resting conductance (G_r) is regarded as incorporating both the resting values of sodium and potassium conductances, as well as the leakage conductance of Hodgkin and Huxley. If we also introduce the normalized, dimensionless variable $\mathscr{V} = V/V_\epsilon$, Equation 2.43 can be reexpressed

$$\partial\mathscr{V}/\partial T + \mathscr{V} - \partial^2\mathscr{V}/\partial X^2$$
$$= (1 - \mathscr{V})\mathscr{E} - (\mathscr{V} - \beta)\mathscr{J} \qquad (2.50)$$

where $\beta = V_j/V_\epsilon$ is a dimensionless constant; the left side of Equation 2.50 represents passive membrane cable properties, while the right side represents the contribution of active membrane properties. The dimensionless variables $\mathscr{V}$, $\mathscr{E}$, and $\mathscr{J}$ all vary with X and T. To generate and propagate an action potential, one needs auxiliary equations that govern the early rise and fall of $\mathscr{E}$ together with a slower but overlapping rise and fall of $\mathscr{J}$. A particular pair of auxiliary equations has been used (62, 151)

$$\partial\mathscr{E}/\partial T = k_1\mathscr{V}^2 + k_2\mathscr{V}^4 - k_3\mathscr{E} - k_4\mathscr{E}\mathscr{J} \qquad (2.51)$$

$$\partial\mathscr{J}/\partial T = k_5\mathscr{E} + k_6\mathscr{E}\mathscr{J} - k_7\mathscr{J} \qquad (2.52)$$

where $k_1 \ldots k_7$ are constant coefficients whose values must be chosen to obtain suitable behavior. Suitable sets of values of these coefficients have been previously reported (62, 151). It may be noted that the system composed of Equations 2.50–2.52 has the merit of being an autonomous system of differential equations because all the coefficients (β and $k_1 \ldots k_7$) are independent of X and T and also independent of $\mathscr{V}$.

INPUT RESISTANCE AND STEADY DECREMENT WITH DISTANCE

Both input resistance and steady decrement with distance are steady-state concepts associated with a constant current or voltage applied across the membrane at some point, together with the assumption of constant membrane properties. Usually passive membrane properties are assumed and solutions of the steady-state cable equation (Eq. 1.3) are needed; the boundary conditions are used to determine the arbitrary constants of the general solution (Eqs. 1.7–1.9). Occasionally one may assume constant synaptic activity; then steady-state solutions of Equation 2.45 or 2.46 are required.

Note on Correspondence with Experiment

The results below are for one-dimensional cable theory with idealized boundary conditions. For any given experiment, one should consider what discrepancies may result from mismatch between the reality and the idealized assumptions. A fine-tipped micropipette can have an electrical resistance of as much as 10 or 100 MΩ, which must not be confused with the input resistance of the neuron. This high resistance results from the constricted channel for ionic current flow inside the pipette tip taper. Just outside the tip, an additional "convergence resistance" of the order of 10^5–10^6 Ω results from the convergence of the three-dimensional current flow very close to the pipette orifice; this convergence resistance becomes further increased when the pipette orifice is very close to the membrane. Significant complication can occur when current and voltage electrode tips are very close to each other and to the membrane. Such problems have been emphasized by Eisenberg and his colleagues [(41, 42); see also (91, 132, 134a, 146, 183b)]. Because such three-dimensional effects, both in the volume and at the membrane, have extremely short time constants (132, 146), they can be separated from the primary one-dimensional cable effects by examining transients when applied current has been turned off or by careful comparison between the effects of low-frequency and high-frequency sinusoids (183b).

Cable of Semi-infinite Length

It is important to distinguish the semi-infinite case (Fig. 19, A and B), extending from $x = 0$ to $x = +\infty$, from the doubly infinite case (Fig. 19, C and D), extending from $x = -\infty$ to $x = +\infty$. By realizing that twice as much steady current applied across the membrane at $x = 0$ is required to maintain $V = V_0$ at $x = 0$ in the doubly infinite case, one can understand that its input conductance ($G_{\pm x}$) is twice as large as that (G_x) for the semi-infinite case and that its input resistance ($R_{\pm x}$) is half as large as that (R_x) for the semi-infinite case.

In the semi-infinite case (Fig. 19, A and B), the boundary conditions can be stated as

$$V = V_0 \text{ at } x = 0, \qquad (3.1)$$

and

$$V \text{ remains bounded as } X \to \infty \qquad (3.2)$$

Physical intuition suggests an even stronger second boundary condition, such as V being smaller than V_0 for all $x > 0$, on the assumption that the membrane is everywhere passive and that no current or voltage is applied anywhere except at $x = 0$. However, the weaker boundary condition (Eq. 3.2) is sufficient because $\exp(x/\lambda)$ in general solution (Eq. 1.7) becomes unbounded as $x \to \infty$, and this requires setting $A_1 = 0$. Then because $\exp(-x/\lambda) = 1$ when $x = 0$, the
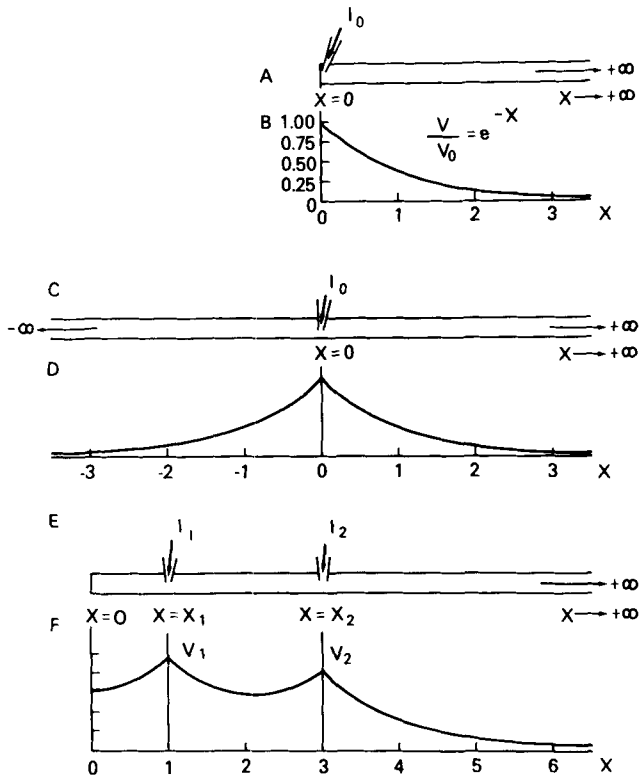
FIG. 19. Steady states for infinite and semi-infinite lengths. A and B: semi-infinite length extending from a sealed end (at $X = 0$) out toward $X = \infty$; an intracellular electrode applies I_0 at $X = 0$; placement of the extracellular electrode is not critical because extracellular isopotentiality is assumed. C and D: doubly infinite length, with symmetry about intracellular electrode that introduces I_0 at $X = 0$. E and F: intracellular electrodes at $X = X_1$ and $X = X_2$; I_1 and I_2 are those currents needed to clamp V to V_1 at $X = X_1$, and V to V_2 at $X = X_2$; the core conductor is sealed at $X = 0$.

first boundary condition (Eq. 3.1) requires that we select $A_2 = V_0$. Thus the boundary value problem defined by Equation 1.3 over the range from $x = 0$ to $x = \infty$, with the two boundary conditions (Eqs. 3.1 and 3.2), has the solution

$$V = V_0 \exp(-x/\lambda), \text{ for } x \geq 0 \qquad (3.3)$$

This exponential decrement with distance is illustrated graphically as curve B in Figure 19. It has the following simple properties: the slope, dV/dx, equals $-V/\lambda$ for every $x \geq 0$; also, when the natural log of V is plotted against t, the result is a straight line whose slope is $-1/\lambda$. The steady voltage decrement (attenuation) from the value at $x = x_1$ to that at $x = x_2$ can be expressed

$$\frac{V_1}{V_2} = \exp\left(\frac{x_2 - x_1}{\lambda}\right) \qquad (3.4)$$

If $x_2 - x_1$ happens to equal λ, then the attenuation factor, V_1/V_2, is 2.718, corresponding to the base e of the natural logarithms.

For this semi-infinite case (Fig. 19, A and B) the steady applied current, I_0, flowing out of the intracellular electrode at $x = 0$, must equal the core

current flowing to the right from $x = 0$, on the usual assumption that no current can leak out to the left through the sealed end. Referring to Equation 2.3 for core current, this means that

$$I_0 = \left(\frac{1}{r_i}\right)\left[-\frac{dV_i}{dx}\right]_{x=0} \qquad (3.5)$$

When extracellular isopotentiality is assumed, $dV_i/dx = dV/dx$; then differentiation of Equation 3.3 and substitution in Equation 3.5 yields

$$I_0 = V_0/(\lambda r_i)$$

The input resistance (R_∞) is simply the steady ratio, V_0/I_0; this equals λr_i. This result for the semi-infinite case, with extracellular isopotentiality, can be expressed in several alternate forms

$$R_\infty = \lambda r_i = (r_m r_i)^{1/2} = r_m/\lambda$$
$$= (2/\pi)(R_m R_i)^{1/2}(d)^{3/2} \qquad (3.6)$$

The fact that λr_i also happens to equal the resistance of a λ length of core and the fact that r_m/λ happens to equal the resistance to a current of uniform density across the membrane of a λ length of cylinder have often been noted before. It should be added, however, that in this steady state, the core current and the membrane current density both decrease exponentially with distance.

[It may be noted that for a cable corresponding to a nonmyelinated axon placed in oil, the input resistance for a pair of electrodes (inside and outside at $x = 0$) would equal

$$\lambda(r_i + r_e) = [r_m(r_i + r_e)]^{1/2} = r_m/\lambda$$

where $\lambda^2 = r_m/(r_i + r_e)$; see Eq. 2.22-2.27.]

Comments about R_x, G_x, Core Current, and Input Current

The fact that R_x is proportional to the $-3/2$ power of diameter and that the corresponding input conductance (G_x) is proportional to the $+3/2$ power of diameter has proved important in the consideration of dendritic branching. Thus it is relevant to note explicitly that these proportionalities depend on the assumption of extracellular isopotentiality and on the assumption of constant resistivities of core and membrane materials. It is easy to understand why a smaller diameter should give a larger input resistance, because both the core resistance per unit length and the membrane resistance for unit length are increased by the smaller diameter, but the 3/2 power is not quite as obvious. For anyone who already knows that λ is proportional to $d^{1/2}$, one need only point out that r_i is proportional to d^{-2}, and thus the product λr_i is proportional to $d^{-3/2}$. Alternatively, one can note that r_m is proportional to d^{-1} and that the product $r_m r_i$ is proportional to d^{-3}.

Although R_x and G_x have been defined in terms of the semi-infinite length, one finds that they prove to be useful core conductor parameters also when deal-

ing with finite lengths and with branching boundary conditions. For example, a very useful expression for core current is

$$i_i = G_x(-\partial V/\partial X)   (3.7)$$

This follows from the original expression (Eq. 2.3) because the definition of $X = x/\lambda$ means that $\partial V/\partial X = (1/\lambda)(\partial V/dx)$ and because the assumption of extracellular isopotentiality means that $\partial V_i/\partial x = \partial V/\partial x$. In Equation 3.7, the voltage gradient is with respect to dimensionless X; both the physical resistivities and the diameter of the core conductor are contained in the value of G_x.

Similarly, when an intracellular micropipette introduces input current (I_i) at $X = X_1$ of a core conductor (see Fig. 19, E and F and Fig. 1B), this input current divides into two core currents; the core current flowing to the right at $X = X_1$ can be expressed

$$i_{i(X=X_1+)} = G_x[-\partial V/\partial X]_{X=X_1+}$$

while the core current flowing to the left is negative, with its absolute value given by

$$|i_{i(X=X_1-)}| = -i_{i(X=X_1-)} = G_\infty[+\partial V/\partial X]_{X=X_1-}$$

Conservation of current (in the core at the point $X = X_1$) requires that the input current (I_i) be equal to the sum of these two core currents; thus

$$I_1 = G_x \{[+\partial V/\partial X]_{X=X_1-} + [-\partial V/\partial X]_{X=X_1+}\}   (3.8)$$

provides an expression for the input current that is valid for any boundary conditions assumed to the left and to the right of $X = X_1$. For steady-state conditions, this provides a means of solving for input conductance or input resistance in problems with complicated boundary conditions (e.g., see Eqs. 3.11–3.14).

Doubly Infinite Length

For the doubly infinite case (Fig. 19, C and D), V must remain bounded for $x = \pm\infty$. Does this mean that A_2, as well as A_1, in Equation 1.7 must be set equal to zero, implying that $V = 0$ for all x? If no current is applied across the membrane and the membrane is passive everywhere; then $V_m = E_r$ everywhere, implying $V = 0$ everywhere. However, when current is applied across the membrane at one point, we can choose that point as the origin $(x = 0)$; relative to this origin, we can now distinguish two semi-infinite regions. The solution of this problem consists of two solutions, one for each region; this means that four boundary conditions are needed. Two are provided by boundedness at $x = +\infty$ and at $x = -\infty$. A third boundary condition can be expressed as $V = V_0$ at $x = 0$. The fourth condition can be expressed as continuity of V at $x = 0$, where the two regions are joined; this is equivalent to using the third condition twice, once for each region. For the region $x = 0$ to $x = +\infty$, Equations 3.1–3.4 apply as before; but for the region $x = 0$ to $x = -\infty$, bounded-

ness requires $A_2 = 0$ in Equation 1.7 while the boundary condition at the origin requires that $A_1 = V_0$, which yields

$$V = V_0 \exp(x/\lambda), \text{ for } x \leq 0.   (3.9)$$

This, together with Equation 3.3, provides the solution for the doubly infinite length, with steady current or voltage applied across the membrane at $x = 0$. Curve D in Figure 19 illustrates this solution; it can be seen that, while V is continuous at $x = 0$, the slope (dV/dx) is discontinuous at $x = 0$; that is, this slope jumps from $+V_0/\lambda$ to $-V_0/\lambda$ at $x = 0$. The fact that these slopes are of equal absolute magnitude is consistent with a physical intuitive understanding that for such a symmetrical situation, equal amounts of oppositely directed core current must flow away from the intracellular electrode. Thus, for the same $V = V_0$ at $X = 0$, the input current is twice that of Equation 3.5 and the input conductance (I_0/V_0) can be expressed

$$G_{\pm x} = 2G_x$$

while the input resistance (V_0/I_0) can be expressed

$$\begin{aligned} R_{\pm x} &= R_x/2 \\ &= r_m/2\lambda = \lambda r_i/2 \\ &= (1/\pi) (R_m R_i)^{1/2}(d)^{-3/2} \end{aligned}   (3.10)$$

which may be compared with Equation 3.6. The same result can be obtained from Equation 3.8 for input at $X = X_1$, provided that one assumes doubly infinite extension of the cylinder from $X = X_1$ to $\pm\infty$ without any other complicating inputs or boundary conditions. Then the steady-state slopes (dV/dX) at $X = X_1$ are equal to $+V_1$ at left, and $-V_1$ at right, with the result that $I_1 = 2G_x V_1$, implying $I_1/V_1 = 2G_x$.

Case of Voltage Clamps at X_1 and X_2

The case of voltage clamps at X_1 and X_2 (Fig. 19, E and F) serves several purposes. Input currents divide nonsymmetrically, and a semi-infinite length is divided into three regions, $0 \leq X \leq X_1$, $X_1 \leq X \leq X_2$, $X_2 \leq X \leq \infty$. Thus it is useful to display and briefly to discuss the steady-state solution for this case, especially since some experiments may resemble this case much more closely than the simpler previous cases.

For the region $0 \leq X \leq X_1$, we assume a sealed end $(dV/dX = 0)$ at $X = 0$ and $V = V_1$ at $X = X_1$. With these two boundary conditions, it is advantageous to use the form of general solution given by Equation 1.8 because the boundary condition at $X = 0$ requires that we set $B_2 = 0$. Then the boundary condition at $X = X_1$ requires that $B_1 = V_1/\cosh(X_1)$, and the solution for this region can be expressed

$$V = V_1 \frac{\cosh(X)}{\cosh(X_1)}, \text{ for } 0 \leq X \leq X_1   (3.11)$$

For the region between the two voltage clamps, the

steady-state solution can be expressed

$$V = \frac{V_1 \sinh (X_2 - X) + V_2 \sinh (X - X_1)}{\sinh (X_2 - X_1)}$$

   (3.12)

$$\text{for } X_1 \leq X \leq X_2$$

where it can be seen that setting $X = X_1$ makes $V = V_1$, and setting $X = X_2$ makes $V = V_2$. It may be noted that the two voltage clamps need not be set at the same voltage.

For the semi-infinite region from $X = X_2$ to $+\infty$, the steady-state solution can be expressed

$$V = V_2 \exp (X_2 - X), \text{ for } X \geq X_2 \quad (3.13)$$

By examining the slopes (dV/dX) at $X = X_1$ and $X = X_2$, we can find the input currents I_1 and I_2, required to maintain the steady voltage clamps (refer back to discussion associated with Eq. 3.8). Then we find that the input conductance at $X = X_1$ can be expressed

$$\frac{I_1}{V_1} = G_x \left\{ \tanh (X_1) \right.$$

$$\left. + \frac{\cosh (X_2 - X_1) - V_2/V_1}{\sinh (X_2 - X_1)} \right\} \quad (3.14a)$$

while that at $X = X_2$ can be expressed

$$\frac{I_2}{V_2} = G_x \left\{ \frac{-V_1/V_2 + \cosh (X_2 - X_1)}{\sinh (X_2 - X_1)} + 1 \right\} \quad (3.14b)$$

It is noteworthy that the solution (Eq. 3.12) between X_1 and X_2 is completely independent of conditions outside this region, when V_1 and V_2 are specified. This would not be true if I_1 and I_2 were specified instead of V_1 and V_2, because then the two input conductances (which do depend on the boundary conditions and solutions in the other regions) become unavoidably involved.

|If either voltage clamp is set at $V = 0$, this means $V_m - E_r = 0$, and hence that V_m is clamped to its resting value at that point. On the other hand, a complete short circuit of the membrane means $V_m = 0$, which implies that $V = -E_r$ at that point; for example, when $E_r = -70$ mV (interior minus exterior) a membrane short circuit implies clamping $V = +70$ mV at the point.|

Relations Between Axon Parameters

At this point it seems useful to summarize the relations between axon parameters, such as those tabulated in Table 1. Although extracellular electrodes with axons placed in oil were used in the earlier experiments, ever since the 1951 paper of Fatt & Katz (47) it has seemed both simpler and more useful to give primary emphasis to intracellular electrodes with extracellular isopotentiality ($r_e = 0$). Then, supposing that experimental measurements have provided estimates of λ and of input

resistance (either R_x or $R_{\pm x}$), one wishes to obtain estimates of r_m and r_i and then of R_m and R_i and, from transients, also τ and C_m. The following equations summarize these relations

$$(r_m/r_i)^{1/2} = \lambda \quad (3.15)$$

$$(r_m r_i)^{1/2} = R_x = 2R_{\pm x} \quad (3.16)$$

From these two relations, it follows that

$$r_m = \lambda R_x = 2\lambda R_{\pm x} \quad (3.17)$$

$$r_i = R_x/\lambda = 2R_{\pm x}/\lambda \quad (3.18)$$

Given these estimates, one needs the axon diameter to calculate estimates of R_m and R_i

$$R_m = r_m \pi d \quad (3.19)$$

$$R_i = r_i \pi d^2/4 \quad (3.20)$$

However, the axon diameter may be neither uniform nor easily determined. As good direct estimates of R_i become available (20a, 57a), these provide an indirect means of estimating an effective diameter value from r_i as

$$d = 2 \left(\frac{R_i}{\pi r_i} \right)^{1/2} \quad (3.21)$$

If τ is correctly estimated from an analysis of transients, then the estimates of r_m and R_m lead to corresponding estimates of c_m and C_m. In other words, cable experiments can be used to estimate λ, $R_{\pm x}$, and τ, from which one can deduce r_i, r_m, and c_m; then one must have an experimental estimate of either d or R_i in order to obtain estimates of R_m, C_m, and either R_i or d. With very complete and accurate experimental results, computational best estimates of all parameter values could be solved for simultaneously.

In order to facilitate understanding of the relation between the earlier extracellular experiments (27, 80) and the more recent experiments with intracellular electrodes (13, 47, 59), the following brief comments are included. The purpose of placing the axon in oil was to restrict the extracellular electrolyte to a thin layer whose resistance per unit length (r_e) exceeded r_i. This forced a significant fraction of the applied current to cross the membrane; it also increased the amplitude of the electrotonic component of the extracellularly recorded potential difference. With the two extracellular electrodes placed far apart (many λ lengths), the fraction of the applied current that penetrated the axon was equal to $r_e/(r_e + r_i)$; furthermore the ratio of the extracellular component to the total steady electrotonic potential generated across the membrane was also $r_e/(r_e + r_i)$. The compounding of these two effects can be seen to account for the fact that the apparent extracellular input resistance, which was designated y by Hodgkin & Rushton (80), is smaller than the transmembrane input resistance, $\lambda(r_e + r_i)/2$, by exactly the

square of the above factor; that is

$$y = \left(\frac{r_e}{r_e + r_i}\right)^2 \frac{\lambda(r_e + r_i)}{2}$$

$$= \frac{\lambda r_e^2}{2(r_e + r_i)} \qquad (3.22)$$

This has also been expressed

$$y = m\lambda \, r_e/2r_i$$

where m represents the resultant, $r_i \, r_e/(r_e + r_i)$, for r_e and r_i considered in parallel (24, 27, 80).

Finite Length: Effect of Boundary Condition at $X = X_1$

Here attention is focussed on a finite length of core conductor, extending from $X = 0$ to $X = X_1$, with steady voltage applied at the origin (see Fig. 20). The boundary condition at $X = X_1$ is left adjustable to facilitate comparisons between several possibilities: *a*) termination of the core conductor, possibly by a sealed end, by a voltage-clamp condition, or by a synaptic input or an injury condition and *b*) continuation of the core conductor, by means of daughter branches (see Fig. 20 *B*) or by an unbranched extension that may have a different diameter or different membrane properties.

For this purpose, a particularly useful form of the general solution is

$$V/V_1 = \cosh (X_1 - X) + B_1 \sinh (X_1 - X) \quad (3.23)$$

which differs from Equation 1.8 only by substituting the constant X_1 for L and by relabeling the two arbitrary constants. The values of V_1 and B_1 still need to be determined from a pair of boundary conditions. If we choose $V = V_0$ at $X = 0$ as one boundary condition, then setting $X = 0$ in Equation 3.23 pro-

A

B
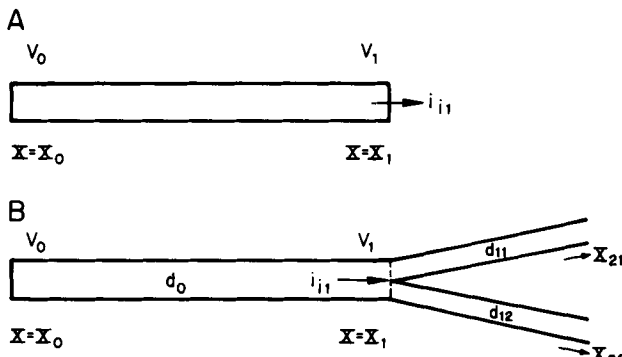
FIG. 20. Finite length of core conductor, from $X = 0$ to $X = X_1$. Core conductor is sealed at $X = 0$, but the boundary condition at $X = X_1$ is adjustable. Core current, i_{i1} at $X = X_1$ depends on the conditions there: whether a sealed or leaky termination, or whether a branch point. In B, the parent branch (trunk) has a diameter d_0; one daughter branch has a diameter d_{11} and extends from $X = X_1$ to $X = X_{21}$; the other daughter branch has a diameter d_{12} and extends to X_{22}.

vides the expression

$$V_0/V_1 = \cosh (X_1) + B_1 \sinh (X_1) \quad (3.24)$$

This defines the attenuation factor for the steady attenuation of V from $X = 0$ to $X = X_1$ as a function of X_1 and B_1. Using this relation to eliminate V_1 from Equation 3.23 provides the useful solution

$$V = V_0 \left(\frac{\cosh (X_1 - X) + B_1 \sinh (X_1 - X)}{\cosh X_1 + B_1 \sinh X_1}\right) \quad (3.25)$$

This solution still contains the constant B_1, which provides for different boundary conditions at $X = X_1$. An illustration of how this solution (and the attenuation defined by Eq. 3.24) can be quite different for different values of B_1 is provided by glancing briefly ahead at Figure 21, which is discussed more fully below; briefly, the upper three curves correspond to $B_1 = 0$ for three different values of X_1, while the lower three curves correspond to $B_1 = \infty$, the middle curve corresponds to $B_1 = 1$. Although B_1 can have other values, these few curves suggest the desirability of obtaining an understanding of what the value of B_1 means biophysically.

It is helpful to think of B_1 as a dimensionless ratio of conductances

$$B_1 = G_1/G_\infty \quad (3.26)$$

where G_1 can be regarded as a formal conductance such that the core current at $X = X_1$ can be expressed

$$i_i = V_1 G_1, \quad \text{at } X = X_1 \quad (3.27)$$

If the core conductor is terminated at $X = X_1$, then G_1 represents the terminal conductance. However, when the core conductor is not terminated at $X = X_1$, then G_1 corresponds to the input conductance into the continuation, whether branched or unbranched; for the special case where the original cylinder is extended to $+\infty$, one gets $G_1 = G_\infty$, implying $B_1 = 1$. When the continuation has an input conductance (G_1) that exceeds the G_∞ value of the original cylinder, then $B_1 > 1$ and the attenuation factor (V_0/V_1) is greater than for $B_1 = 1$; on the other hand; $G_1 < G_\infty$ implies $B_1 < 1$, and the attenuation factor is smaller than for $B_1 = 1$.

The advantage of leaving the value of B_1 adjustable was demonstrated in a systematic solution for arbitrary dendritic branching (139). However, useful insight can also be gained by explicitly noting the limiting special cases corresponding to values of 0, 1, and ∞ for B_1. Such limiting cases were noted also by Weidmann (185), in relation to Purkinje fibers.

Sealed End at $X = X_1$: Case of $B_1 = 0$.

Usually a sealed end is idealized by assuming that no current can leak out of the core conductor at $X = X_1$; this has also been called an "insulated" bound-

ary condition because it is equivalent to an insulating terminal membrane (150); it has also been called the "open-circuit" terminal boundary condition (92). This boundary condition can be expressed equivalently as $G_1 = 0$ or as $dV/dX = 0$ at $X = X_1$; each of these implies $B_1 = 0$. When $B_1 = 0$, Equation 3.25 reduces to the simpler solution

$$V = V_0 \frac{\cosh (X_1 - X)}{\cosh X_1}. \qquad (3.28)$$

This solution is illustrated by curves A, B, and C in Figure 21, for three different electrotonic lengths, $L = X_1$ of 0.5, 1.0, and 2.0; each of these three curves can be seen to have a zero slope at $X = X_1$, as required by the sealed end.

It follows (from Eqs. 3.7 and 3.28) that the input current can be expressed

$$I_0 = G_x V_0 \tanh X_1$$

provided that none of the input current can leak leftward at $X = 0$. Here the input conductance (I_0/V_0) is proportional to the tanh of X_1, while the input resistance (V_0/I_0) is proportional to the coth of X_1. If X_1 is replaced by L, this input resistance can be expressed

$$R_{\text{CL.ins}} = R_x \coth L \qquad (3.29)$$

where the subscript "CL" designates a cylinder of finite electrotonic length (L) and subscript "ins" designates a sealed or insulated boundary condition at the far end of the cylinder. These subscripts were introduced in an earlier context (150, 161) where they also designated corresponding AC input impedances and transient response functions, especially for use as components in superposition solutions of more complicated problems.
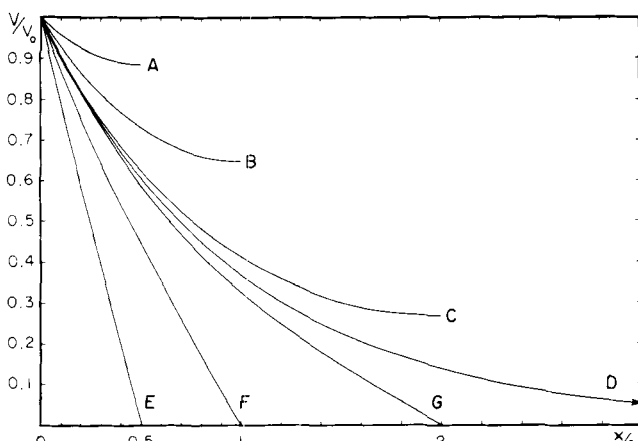

FIG. 21. Decrement of V with distance for different boundary conditions at the far end of a cylinder of finite length. Curves A, B, and C correspond to a sealed-end boundary condition ($dV/dX = 0$) at $X = 0.5$, 1.0, and 2.0, respectively (see Eq. 3.28 for $B_1 = 0$ in Eq. 3.25). Curves E, F, and G correspond to a voltage-clamped boundary condition ($V = 0$, meaning $V_m = E_r$) at $X = 0.5$, 1.0, and 2.0, respectively (see Eq. 3.31 for $B_1 = \infty$ in Eq. 3.25). Curve D is a simple exponential (Eq. 3.34) corresponding to $B_1 = 1$ in Eq. 3.25. [From Rall (139)]

[Corresponding to Equation 3.29, the input impedance for an AC steady state is a complex quantity that can be expressed

$$Z_{\text{CL.ins}} = (R_x/q) \coth (qL) \qquad (3.30)$$

where q represents the complex quantity

$$q = (Y_m/G_m)^{1/2} = (1 + j\omega\tau)^{1/2}$$

as in Equation 1.4; see (150) for additional impedance expressions, including separation into real and imaginary parts. The expression on the right side of Equation 3.30 also represents the Laplace transform of the corresponding transient response function (161), provided that $q = (1 + p)^{1/2}$, where p represents the Laplace transform variable.]

With regard to the sealed or insulated boundary condition, if the cylinder were sealed with a disk composed of resting membrane, this would strictly imply $G_1 = (\pi d^2)/(4R_m)$, giving $B_1 = G_1/G_x = [(d/4)(R_m/R_i)]^{1/2}$. For example, if $d = 4$ μm and $R_m/R_i = 25$ cm $= 25 \times 10^4$ μm, then $B_1 = 2 \times 10^{-3}$, which differs negligibly from $B_1 = 0$. If the terminal membrane is made more conductive than resting membrane, either by injury, synaptic input, or pharmacological agents, then B_1 can differ significantly from zero, (see Eqs. 3.46, 3.47 and 3.55).

Voltage Clamp ($V_1 = 0$) at $X = X_1$: Case of $B_1 = \infty$

Although this boundary condition has sometimes been referred to as a "short circuit," such a designation risks confusion and error. An actual physical short circuit of resting membrane must mean $V_m = 0$; this would imply $V = -E_r$, which differs from $V = 0$ except for a membrane that has a zero resting membrane potential. The present case of $B_1 = \infty$, or $V = 0$ at $X = X_1$, means that $V_m - E_r = 0$ and thus really implies that the membrane potential (V_m) is clamped to its resting value at $X = X_1$. This condition reduces Equation 3.25 to the simpler solution

$$V = V_0 \frac{\sinh (X_1 - X)}{\sinh X_1} \qquad (3.31)$$

which is illustrated graphically by curves E, F, and G in Figure 21 for the three electrotonic lengths, $L = X_1$ of 0.5, 1.0, and 2.0; each of these curves slopes more steeply than reference curve D.

It follows (from Eqs. 3.7 and 3.31) that the input current can be expressed

$$I_0 = G_x V_0 \coth X_1$$

provided that none of the input current can leak leftward at $X = 0$. Here the input conductance (I_0/V_0) is proportional to the coth of X_1, while the input resistance (V_0/I_0) is proportional to the tanh of X_1; exactly the reverse of the previous special case. If X_1 is replaced by L, this input resistance can be expressed as

$$R_{\text{CL,clp}} = R_\infty \tanh L \qquad (3.32)$$

where, as with Equation 3.29, subscript CL designates a cylinder of finite electrotonic length (L), but another subscript, clp, designates a voltage clamp ($V = 0$, meaning $V_m = E_r$) at the far end [see (150, 161)].

[The corresponding AC input impedance can be expressed

$$Z_{\text{CL,clp}} = (R_\infty/q) \tanh (qL) \qquad (3.33)$$

where q is the same complex quantity noted above with Equation 3.30. The expression on the right side of Equation 3.33 also represents the Laplace transform of the corresponding transient response function (161), provided that $q = (1 + p)^{1/2}$, where p represents the Laplace transform variable.]

Semi-infinite Extension at $X = X_1$:
Case of $B_1 = 1$

Semi-infinite extension of the original cylinder means $G_1 = G_\infty$, or $B_1 = 1$. We already know that the solution for semi-infinite length is given by Equation 3.3; however, it should also be noted that when $B_1 = 1$ in Equation 3.25, the definitions of the hyperbolic functions imply a simplification to

$$V = V_0 \exp (-X) \qquad (3.34)$$

This special case is included as curve D in Figure 21. The input conductance has already been defined as G_∞ and the input resistance as R_∞ (Eq. 3.6), provided that none of the input current can leak leftward at $X = 0$.

Input Conductance for Finite Length
General Case

For the general case of Equation 3.25, where B_1 is left unspecified, application of Equation 3.7 results in the following expression for the input current at $X = 0$

$$I_0 = V_0 G_\infty \left(\frac{\sinh X_1 + B_1 \cosh X_1}{\cosh X_1 + B_1 \sinh X_1}\right) \qquad (3.35)$$

provided that none of the input current can leak leftward at $X = 0$. Then we can express the input conductance at $X = 0$ as

$$G_0 = \frac{I_0}{V_0} = B_0 G_\infty \qquad (3.36)$$

where B_0 represents a dimensionless conductance ratio that can be expressed

$$B_0 = \frac{G_0}{G_\infty} = \frac{B_1 + \tanh X_1}{1 + B_1 \tanh X_1} \qquad (3.37)$$

This important relation shows explicitly how B_0 and G_0 depend on B_1 and X_1; it defines how the input

conductance at the origin depends on the still adjustable boundary condition at $X = X_1$. The next step is to see how the value of B_1 depends on the branches that arise at $X = X_1$, because this then provides the basis for a systematic solution of dendritic branching systems (139) or of core conductors composed of connected segments of finite length but possibly changing diameter (4a, 6, 62).

Branches at $X = X_1$

For the case where two branches arise at $X = X_1$ (e.g. Figs. 3 and 20B) we can begin with the basic idea that G_1 at X_1 equals the sum of input conductances into the two branches. We can write this

$$G_1 = G_{11} + G_{12} \qquad (3.38)$$

It is important to remember that G_∞ is proportional to $d^{3/2}$ (given constant materials plus extracellular isopotentiality); thus the branch with diameter d_{11} has a G_∞ value that is smaller than that of the parent cylinder by the ratio $(d_{11}/d_0)^{3/2}$, while the ratio $(d_{12}/d_0)^{3/2}$ applies to the other branch. Thus, when Equation 3.38 is divided through by the parent G_∞ value, one obtains

$$B_1 = (d_{11}/d_0)^{3/2} B_{11} + (d_{12}/d_0)^{3/2} B_{12} \qquad (3.39)$$

where B_{11} and B_{12} depend on the next boundary conditions (at X_{21} and X_{22} in Fig. 3) in the same way that B_0 was shown to depend on the boundary condition at X_1 in Equation 3.37; that is

$$B_{11} = \frac{B_{21} + \tanh (X_{21} - X_1)}{1 + B_{21} \tanh (X_{21} - X_1)} \qquad (3.40)$$

and

$$B_{12} = \frac{B_{22} + \tanh (X_{22} - X_1)}{1 + B_{22} \tanh (X_{22} - X_1)} \qquad (3.41)$$

It may be noted that if the first branch happens to have a sealed termination at $X = X_{21}$, this would imply $B_{21} = 0$ and $B_{11} = \tanh (X_{21} - X_1)$. However, if two or more branches arise at $X = X_{21}$, then the value of B_{21} depends on these branches and their boundary conditions, and this process can be continued stepwise until terminal branches are reached; the same must be done for B_{22}. [A completely worked out example can be found in Fig. 5 and Table 1, (139).]

Comment on Branching Equivalent
to a Cylinder

For simplicity, consider a tree composed only of the trunk and the two primary branches considered above. The two branches can be unequal in diameter and in length. If both branches have the same terminal boundary condition ($B_{21} = B_{22} = B_2$) and the same dimensionless electrotonic length

$$(X_{21} - X_1) = (X_{22} - X_1) = (X_2 - X_1)$$

then the solutions in the two branches, for $V = V_1$ at $X = X_1$ are identical with respect to X, and this means that

$$B_{11} = B_{12} = \frac{B_2 + \tanh (X_2 - X_1)}{1 + B_2 \tanh (X_2 - X_1)} \qquad (3.42)$$

as can be seen from Equations 3.40 and 3.41. If the branch diameters satisfy the constraint

$$d_{11}{}^{3/2} + d_{12}{}^{3/2} = d_0{}^{3/2} \qquad (3.43)$$

then Equations 3.39 and 3.42 together imply that $B_1 = B_{11} = B_{12}$. This means that the solution (Eq. 3.25) from $X = 0$ to $X = X_1$ is the same as it would be if this cylinder were simply extended to $X = X_2$, with a terminal boundary condition corresponding to B_2, and this characterizes the equivalent cylinder.

Once this example is understood, it can be seen that a dendritic tree with many orders of branching can be boiled down to an equivalent cylinder in the same way, provided that the $d^{3/2}$ constraint is satisfied at every point of branching and provided that all terminal branches end at the same electrotonic distance from the origin with the same terminal boundary condition. Some readers may prefer another route to the equivalent cylinder [see (141)].

For neurons whose dendritic trees at least approximate the equivalent cylinder constraints, this concept provides a useful basis for a simplified neuron model whose parameters can be estimated from experiment (see Eqs. 5.9–5.16).

Comment on Membrane Injury at $X = X_1$

When an injury does not completely short-circuit the membrane, one must consider a finite injury conductance (G_{inj}) through which an injury current is driven by the local value of V_m. At $X = X_1$, $V_m = V_1 + E_r$ and the injury current, positive outward, can be expressed

$$I_{inj} = E_r G_{inj} + G_{inj} V_1 \qquad (3.44)$$

It is important to distinguish between the two component currents on the right side of Equation 3.44 because one of them is proportional to the value of V_1, while the other is independent of V_1; recognition of this is essential to solution of the problem.

By conservation of current, this injury current is related to the core currents on either side of $X = X_1$; for an unbranched continuation, this can be expressed by Equation 3.8 when its input current (I_1) is replaced by minus the injury current. However, if two branches arise at $X = X_1$, the core current to the right consists of two components, one for each branch. Then, for constant G_{inj} at $X = X_1$, the above considerations yield a boundary condition that can be expressed

$$(-dV/dX)_{X_1} = E_r B_{inj} + B_1 V_1 \qquad (3.45)$$

where

$$B_{inj} = G_{inj}/G_\infty \qquad (3.46)$$

and the definition of B_1 is generalized from Equation 3.39 to the expression

$$B_1 = B_{inj} + (d_{11}/d_0)^{3/2} B_{11} + (d_{12}/d_0)^{3/2} B_{12} \qquad (3.47)$$

This boundary condition is satisfied by a solution that differs slightly from Equation 3.23, namely

$$\begin{aligned} V = {} & V_1 \cosh (X_1 - X) \\ & + (B_1 V_1 + E_r B_{inj}) \sinh (X_1 - X) \end{aligned} \qquad (3.48)$$

where the value of V_1 is still to be determined by the boundary condition at $X = 0$.

If one chooses $V = V_0$ at $X = 0$, then Equation 3.48 requires that

$$V_1 = \frac{V_0 - E_r B_{inj} \sinh (X_1)}{\cosh (X_1) + B_1 \sinh (X_1)} \qquad (3.49)$$

and substituting this expression into Equation 3.48 provides the required solution.

On the other hand, if one chooses $dV/dX = 0$ at $X = 0$, Equation 3.48 requires that

$$V_1 = \frac{-E_r B_{inj}}{B_1 + \tanh (X_1)} \qquad (3.50)$$

and substituting this expression into Equation 3.48 provides the solution for this case.

For a numerical illustration, consider that $E_r = -70$ mV, $B_{inj} = 0.5$, $X_1 = 0.25 \approx \tanh (X_1) \approx \sinh (X_1)$ with $\cosh (X_1) \approx 1.0$, and $B_{11} = B_{12} = 1$ with diameters that satisfy the contraint defined by Equation 3.43. Then $B_1 = 1.5$ and Equation 3.50 gives a membrane depolarization at $X = X_1$ that is $(+70)(0.5)/(1.5 + 0.25)$, or $V_1 = 20$ mV, for the zero slope boundary condition at $X = 0$. Then the solution between $X = 0$ and $X = X_1$ (Eq. 3.48) reduces to

$$V = 20 \cosh (0.25 - X) -5 \sinh (0.25 - X)$$

which equals 20 mV at $X = 0.25$ and 18.75 mV at $X = 0$, with a zero slope at $X = 0$. From this result, one can conjecture (and confirm by using Eq. 3.49) that setting $V_0 > 18.75$ mV will result in negative dV/dX at $X = 0$, implying positive I_0, while setting $V_0 < 18.75$ mV will result in positive dV/dX at $X = 0$, implying negative I_0. This means that for $0 < V_0 < 18.75$ mV, positive V_0 results in negative I_0. This does not mean that the injury at $X = X_1$ results in a negative input resistance at $X = 0$. (Note that passive membrane is assumed.) Rather, there is a shift of a linear I_0 vs. V_0 relation; that is, without injury, this straight line passes through the origin, but with the specific injury defined above, the shifted straight line intersects $I_0 = 0$ at $V_0 = 18.75$ mV. This suggests the importance of looking at the slope conductance, dI_0/dV_0.

To obtain an expression for the slope conductance, we make use of the fact that $dI_0/dV_0 = (dI_0/dV_1) (dV_1/dV_0)$. From Equation 3.48, one obtains

$$I_0 = G_\infty [V_1 \sinh X_1$$
$$+ (B_1 V_1 + E_r B_{\text{inj}})\cosh X_1] \quad (3.51)$$

and thus that

$$dI_0/dV_1 = G_\infty [\sinh X_1 + B_1 \cosh X_1]$$

From Equation 3.49 one obtains

$$dV_1/dV_0 = [\cosh X_1 + B_1 \sinh X_1]^{-1}$$

Combining the last two expressions yields the required result

$$\frac{dI_0}{dV_0} = G_\infty \left(\frac{B_1 + \tanh X_1}{1 + B_1 \tanh X_1} \right) \quad (3.52)$$

which is remarkably similar to Equations 3.36 and 3.37, but it must be remembered that here B_1 includes the injury, as in Equation 3.47. This result shows that the slope conductance at $X = 0$ is a positive quantity that is independent of V_0; it also defines how the value of this slope conductance depends on how much the injury changes the value of B_1 at $X = X_1$.

Comment on Steady Synaptic Input at $X = X_1$

The effect of localized but steady synaptic input at $X = X_1$ is formally similar to that shown for injury in the preceding section. Because G_ϵ and G_j were defined as synaptic conductances per unit area in Figure 18 and in Equations 2.36 and 2.37, it is helpful to specify a local synaptic surface area (A) at $X = X_1$. If there is only synaptic excitation, the steady synaptic current at $X = X_1$ equals

$$G_\epsilon A(V_m - E_\epsilon) = G_\epsilon A V_1 + G_\epsilon A(E_r - E_\epsilon) \quad (3.53)$$

and Equations 3.45–3.52 apply when B_{inj} is replaced by $B_\epsilon = G_\epsilon A/G_\infty$, and E_r is replaced by $(E_r - E_\epsilon)$. Similarly, if there is only synaptic inhibition, the steady synaptic current at $X = X_1$ equals

$$G_j A(V_m - E_j) = G_j A V_1 + G_j A(E_r - E_j) \quad (3.54)$$

and Equations 3.45–3.52 apply when B_{inj} is replaced by $B_j = G_j A/G_\infty$ and E_r is replaced by $(E_r - E_j)$. However, if both synaptic excitation and inhibition are present over area A at $X = X_1$, then the resultant steady synaptic current equals the sum of Equations 3.53 and 3.54. Then Equations 3.45–3.52 apply when B_{inj} is replaced by

$$B_{\epsilon j} = (G_\epsilon + G_j)A/G_\infty \quad (3.55)$$

and E_r is replaced by the weighted mean

$$[G_\epsilon(E_r - E_\epsilon) + G_j(E_r - E_j)]/(G_\epsilon + G_j) \quad (3.56)$$

It may be noted that here any resting leakage, $G_r A(V_m - E_r)$, if present over area A, has been assumed negligible relative to synaptic current.

These results provide a means of determining the effects of a steady synaptic input at a discrete dendritic location, both with and without applied cur-

rent at $X = 0$. [For a somewhat different approach to such problems, see (34)].

Distribution of steady synaptic excitation to many discrete locations can be approximated as a uniform density of steady synaptic excitation over one or more regions of membrane surface area, and Equations 2.45–2.49 apply to each increment of cable length that corresponds to such a region. An illustration for two such regions is provided by the curve $T = \infty$ in Figure 5, based on the mathematical solution of Rall (141). Either this same method or a compartmental model (143) can be used to treat many regions having different densities of synaptic excitation and/or inhibition.

Case of Input to One Branch of Dendritic Neuron Model

Questions related to the input resistance that should be expected in a distal branch of an extensively branched dendritic tree have been noted and discussed elsewhere (3, 100, 105, 148, 150). To obtain explicit answers to many of these questions, it was found useful to construct (by means of superposition methods) a complete solution for an idealized neuron model (150). The most symmetrical version of this model was composed of N equal dendritic trees; each tree was equivalent to a cylinder of electrotonic length (L) and had M orders of symmetrical dendritic branching. The input current was injected at a single branch terminal.

Details of the superposition procedure used to solve this problem are discussed fully by Rall & Rinzel (150) and are not repeated here. The resulting steady-state solution (with k designating order of branching) can be expressed

$$V(X) = IR_{T\infty} \left\{ \frac{\cosh X}{N \sinh L} + \frac{A \sinh X}{N \cosh L} \right.$$
$$\left. \sum_{k=1}^{M} 2^{(k-1)} \frac{B_k \sinh (X - X_k)}{\cosh (L - X_k)} \right\} \quad (3.57)$$

where A and B_k are simple constants whose values are specified according to location, as follows

in the input tree	$A = N - 1$;
in the input branch	$B_k = 1$, for all k from 1 to M;
in the sister branch	same, except $B_M = -1$;
in the parent branch	same, except $B_M = 0$;
in first cousin branches	same, except $B_M = 0$, and $B_{M-1} = -1$;
in grandparent branch	same, except $B_M = 0$, and $B_{M-1} = 0$;
in the input trunk	$B_k = 0$, for all k;
in the other trees	$A = 1$, assuming, $X < 0$, and $B_k = 0$, for all k

This solution was used to compute the particular example illustrated in Figure 22, for the case of six dendritic trees with three orders of branching; that is, $N = 6$, M = 3, and $L = 1$, with length increments, $\Delta X = 0.25$ for all trunks and branches. It can be
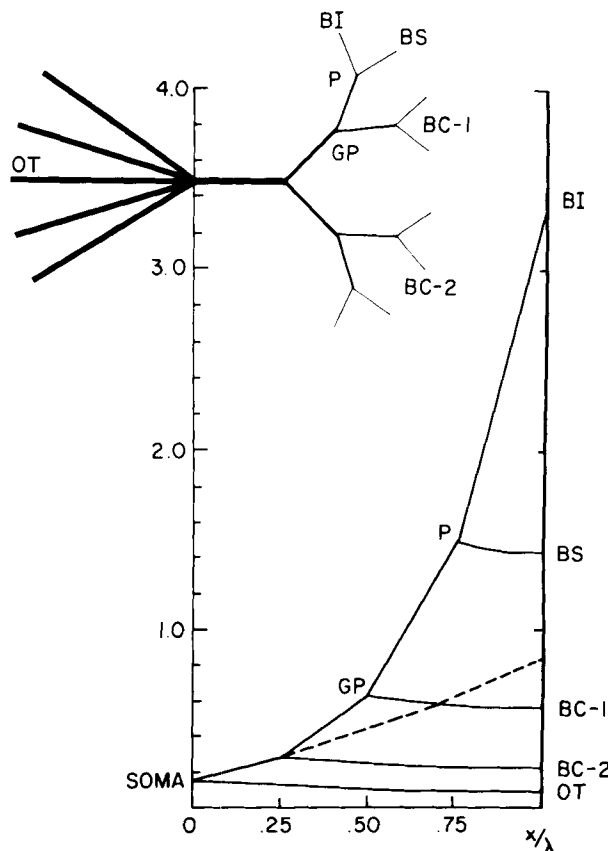
FIG. 22. Branching diagram (*upper left*) and graph (*below*) showing steady-state values of V as a function of X in all branches and trees of the neuron model, for steady current injected into the terminal of one branch. *BI* and *BS* designate the input branch and its sister branch, respectively; *P* and *GP* designate their parent and grandparent branch points, respectively; *BC-1* and *BC-2* designate first- and second-cousin branches, respectively, with respect to the input branch; *OT* designates the other trees of the neuron model. Model parameters are $N = 6$, $L = 1$, $M = 3$, with equal electrotonic length increments $\Delta X = 0.25$ assumed for all branches. Ordinates of graph express $V/IR_{T\infty}$ values, as defined by Eq. 3.57. [See (150).]

seen that the steepest gradient of membrane potential occurs in the input branch (BI). Most of the input current reaches the parent branch point (P); very little of this current flows into the sister branch (BS), whose sealed terminal is responsible for its low input conductance at P. Most of the current flows through the parent branch, where the gradient with respect to dimensionless X is about half as steep as in the input branch, because its $d^{3/2}$ value is doubled. In contrast to the steep gradients in the input branch and the parent and grandparent branches, the dashed curve in Figure 22 shows the smaller gradient that would be obtained if the same input current were equally divided between the eight terminal branches of that dendritic tree. The fact that this dashed curve coincides with the solid curve, for $X = 0$ to $X = 0.25$, illustrates an important and much more general property of this solution; the solution in the trunk of the input tree is the same for any apportionment of

the same total input current between these eight branch terminals. Of course, the solution in the five other trees (OT) also remains unaffected by any such reapportionment of input current within the input tree.

[It is noteworthy that the attenuation factor in the input branch is 2.4, while that in the sister branch (BS), about 1.04, is much smaller, even though these two branches have identical core resistance. This example should be helpful to those neurophysiologists whose intuitions misled them into believing that attenuation along a dendritic branch should be the same in centripetal and in centrifugal directions. Although the core resistance is the same in either direction, the boundary conditions are very different. The importance of the boundary condition to the resulting attenuation factor is also shown by Fig. 21 and Eq. 3.24.]

The input resistance at a branch location is considerably greater than the whole neuron input resistance (R_N) at the soma, or common point of origin of the N dendritic trees. For this idealized neuron model, it was shown (150) that the ratio of the branch input resistance (R_{BL}) at one branch terminal (where $X = L$) to the more familiar input resistance (R_N) can be expressed

$$\frac{R_{BL}}{R_N} = 1 + (N - 1)(\tanh L)^2 + N \tanh (L)$$

$$\cdot \sum_{k=1}^{M} 2^{(k-1)} \tanh (L - X_k) \tag{3.58}$$

This was used to compute the illustrative values shown in parentheses in Table 4; this table also includes corresponding values of the attenuation factor from the input branch terminal to the soma. These attenuation factors can be expressed

TABLE 4. *Input Resistance Ratio* and Steady-state Attenuation Factor†*

M	N = 6		L = 1.5	
	L = 1.0	L = 2.0	N = 6	N = 10
2	(9.5)	(17.4)	(14.3)	(23.6)
	14.7	65.5	33.6	55.4
3	(15.5)	(30.4)	(24.2)	(40.2)
	23.9	114	56.8	94.4
4	(26.0)	(53.6)	(41.7)	(69.4)
	40.1	202	98.0	163
5	(44.6)	(95.4)	(73.1)	(122)
	68.8	359	172	286
6	(78.0)	(172)	(130)	(216)
	120	647	305	508
7	(138)	(311)	(233)	(388)
	213	1170	548	912
8	(248)	(569)	(422)	(704)
	352	2140	992	1650

* Values in parentheses correspond to resistance ratio R_{BL}/R_N (Eq. 3.58).   † Values just below values in parentheses correspond to attenuation factor (Eq. 3.59).

$$AF_{BL/0} = \frac{V_{BL}}{V_0} = \frac{R_{BL}}{R_N} \cosh L \qquad (3.59)$$

which shows, explicitly, that this attenuation factor always exceeds the ratio R_{BL}/R_N. More general expressions that permit other input sites and also permit unequal trees and nonsymmetrical branching; as well as expressions for input impedance and for attenuation in AC steady states, are available elsewhere (150).

PASSIVE MEMBRANE POTENTIAL TRANSIENTS AND TIME CONSTANTS

In exploring transient cable properties of neurons, there has been concern with the interpretation of three quite different classes of experiments. Here the class concerned with action potential generation and propagation is excluded from further discussion. Other experiments make use of electrodes to apply (subthreshold) current, either brief current or prolonged constant current, to produce recordable voltage transients; the analysis of these transients involves estimation of the cable parameters (τ, λ, L, and input resistance) in relation to membrane parameters and geometric parameters of the neuron; this permits some assessment of how well the predictions of cable theory can account for transients obtained under various conditions. The third class of experiments involves the time course of synaptic potentials produced by various distributions of excitatory and inhibitory synaptic inputs over the soma and dendritic surfaces of a neuron; the extent to which cable theory predictions agree with these observations provides a contribution toward understanding "integrative" properties at the neuronal level.

Passive Decay Transients

The simplest membrane potential decay transient is proportional to the single exponential function, $\exp(-t/\tau)$, where τ is the passive membrane time constant. Such simple exponential decay to the resting potential should not be expected to occur in general; it occurs when several conditions are satisfied simultaneously: (a) all applied current must be turned off; (b) the membrane must nowhere be subjected to a voltage clamp, short circuit, or significant injury; (c) the membrane conductance, capacitance, and emf must remain at their resting values and be uniform over the membrane surface; and (d) the amount of membrane depolarization or hyperpolarization must be initially uniform over the membrane surface. Then all points of the membrane undergo identical decay of potential; each local element of membrane capacity discharges through its associated local element of membrane resistance; no current flows from one region of membrane to another; in fact, the net membrane current density (resistive

plus capacitive) is zero everywhere (see Eqs. 2.10, 2.11, and 2.16).

In contrast, when only the first three conditions are satisfied, but the initial polarization is not uniform, the decay transient is more complicated and it is different at different membrane locations. In those regions where the membrane potential has been displaced farthest from the resting value, the rate of decay will be initially more rapid than elsewhere and more rapid than for the case of uniform decay. The net membrane current density is not zero everywhere, because there is a flow of current between the more polarized regions and the less (or oppositely) polarized regions of the membrane surface. This current tends to redistribute charge on the membrane capacity and thus tends to equalize the membrane polarization toward a uniform distribution. This equalization takes place simultaneously with (and more rapidly than) the passive local discharge through local membrane resistance. The resultant decay transient at any point of the membrane is the sum of many component exponential decays with different time constants. This can be expressed

$$V = C_0 \exp(-t/\tau_0) + C_1 \exp(-t/\tau_1)$$
$$+ C_2 \exp(-t/\tau_2) + \ldots \qquad (4.1)$$

where the longest time constant

$$\tau_0 = R_m C_m \qquad (4.2)$$

is simply the passive membrane time constant, while the equalizing time constants, $(\tau_1, \tau_2, \ldots, \tau_n)$ are shorter, having values that depend on neuron geometry. For a cable of finite length, corresponding to a membrane cylinder with sealed ends, the mathematical solution (as expressed by Eq. 1.16), implies equalizing time constants defined by the expression

$$\tau_n = \frac{R_m C_m}{1 + (n\pi/L)^2} \qquad (4.3)$$

for positive integer values of n. The coefficients C_0, $C_1, \ldots, C_n$ have values that depend on the initial distribution of membrane polarization and on the point of observation chosen (see Eqs. 1.16–1.18); thus, for the membrane cylinder with sealed ends, the C_n of Equation 4.1 for any chosen point X have the values

$$C_n = B_n \cos(n\pi X/L) \qquad (4.4)$$

where the coefficients B_n represent the Fourier coefficients given by Equations 1.17 and 1.18.

The importance of these equations is that they provide a basis for estimating both τ_0 and L from experimental decay transients, provided that conditions a–c above are satisfied and that we are dealing either with a membrane cylinder having sealed ends or with a dendritic neuron that can be well approximated by an equivalent cylinder (141, 145, 146, 161) with sealed-end boundary conditions. It should be

added that the transient response to an applied current step contains the same time constants, but the values of the coefficients are changed in a systematic way (see Eqs. 4.10-4.15). Also, one should be warned that if a voltage clamp, short circuit, or significant injury is present, all the time constants become changed [see (145) for details].

Time Constant Ratios and Electrotonic Length

In favorable experiments, it is possible to obtain good estimates of the time constant ratio τ_0/τ_1 and sometimes of τ_0/τ_2 as well. Thus it is useful to note that Equations 4.2 and 4.3 imply that

$$\tau_0/\tau_n = 1 + (n\pi/L)^2 \qquad (4.5)$$

and

$$L = n\pi[\tau_0/\tau_n - 1]^{-1/2} \qquad (4.6)$$

It follows, for example, that a value of $L = \pi$ corresponds to $\tau_0/\tau_1 = 2$, while a value of $L = \pi/2 \cong 1.57$ corresponds to $\tau_0/\tau_1 = 5$. The method of estimating τ_0, τ_1, and τ_0/τ_1 by "peeling" exponential decays has been described elsewhere (145), together with comments on conditions that are favorable for such estimation.

This method has been applied to motoneurons of cat spinal cord in several laboratories (6, 7, 18, 119, 130). Two examples are shown in Figure 23. Such experiments have provided estimates of τ_0/τ_1 that range from about 3.5 to 11; this corresponds to a range of L values from 1 to 2 (with a mean value of
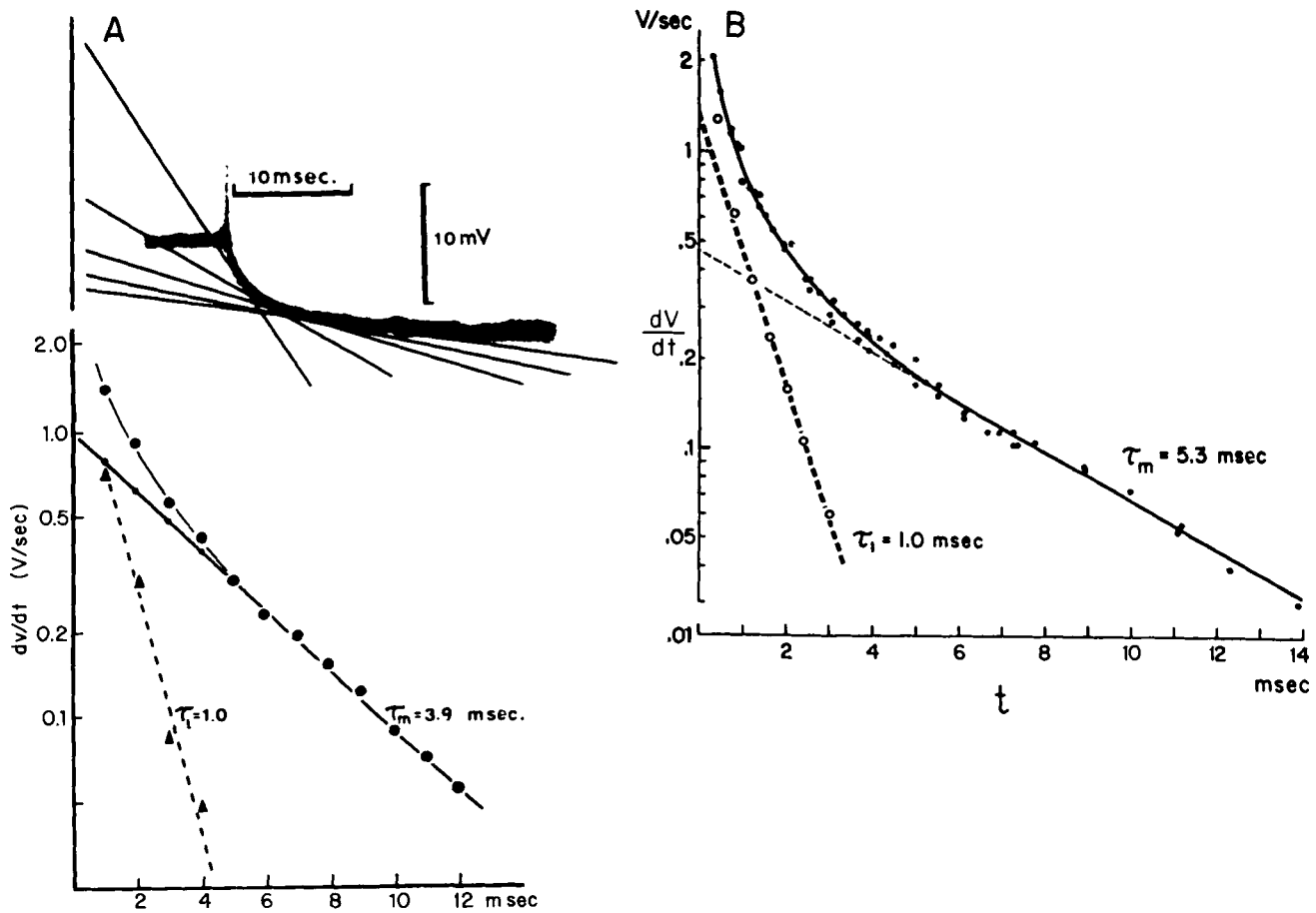

FIG. 23. Two examples of peeling the membrane time constant away from the first equalizing time constant, τ_1; data are slopes (dV/dt) of response at a motoneuron soma to an applied current step. A: top, start of the membrane potential response to hyperpolarizing current steps with 5 traces superimposed. Tangents on the slope are drawn at the 1st, 3rd, 5th, and 7th ms for dV/dt determinations. Plot of dV/dt on logarithmic scale vs. time shows an almost linear late part of its slope but considerable deviations from linearity in the initial part (bottom). Replots of these deviations during the initial 4 ms on logarithmic scale (▲) reveal the second-order time constant τ_1 (dashed line). [From Lux et al. (119).] B: semilogarithmic plot of the slope (dV/dt) vs. t, of the response to a constant current step applied to a motoneuron soma. ●, the dV/dt values plotted on a log scale; straight line through the tail has a slope implying $\tau_m = 5.3$ ms. ○, difference between the dV/dt values of the smooth curve and those of the dashed line extrapolated back from the straight tail. Heavier dashed line through ○ has a slope implying $\tau_1 = 1.0$ ms. [From Burke & ten Bruggincate (18).]

about 1.5) for the cylinders that are most nearly equivalent to these motoneurons. This agrees well with an earlier estimate of L between 1 and 2 that was made [(143, 145); cf. (139)] by considering the joint implications of both the range of input resistance values (R_N) found in electrophysiologically studied motoneurons and the range of anatomic measurements (1) made with a different sample of motoneurons.

In view of the uncertainties attached to using anatomic and electrophysiological data from different samples of motoneurons (139), it is noteworthy that two of the most recent studies have overcome this difficulty. Lux and his colleagues (119) used autoradiography, while Barrett & Crill (5, 6) used Procion dye injection, to help them make anatomic measurements of dendritic branching in the same individual motoneurons whose transient responses and input resistance they had measured electrophysiologically. They found quite good agreement between the two methods of estimating L; such agreement serves to increase one's confidence in the approximate validity and the usefulness of the underlying neuron model.

A somewhat different method of estimating L from transients has been described and illustrated by Jack and Redman and their colleagues (86, 89–93). They obtained a similar range of L values for cat spinal motoneurons. For the details of their methods, and for their assessment of these neuron models and of the distribution of synaptic input locations, their papers should be consulted directly.

The fact that some motoneurons of cat spinal cord do not fit the simple linear membrane model has been known for some time. Ito & Oshima (88) described a time constant of about 25 ms which is much larger than the passive membrane time constant; this corresponds to some incompletely understood slow process that underlies overshoots and undershoots and possibly also the anomalous rectification studied by Nelson & Frank (129). Such complications appear to be significant only in some motoneurons and negligible in others (18, 88, 130); possible errors resulting from this complication have been examined and discussed (18). It is noteworthy that the neurons of the red nucleus (183a) are free of such complications; their linear behavior and their special suitability for theoretical studies have recently been restudied and confirmed in much greater detail (183). An application of off-transient analysis to cultured muscle cells has been reported by Fischbach et al. (48b).

Effect of Large L and Infinite L

When the value of L is large, the value of π/L in Equations 4.3 and 4.5 is small, with the result that the succession of time constants $\tau_0, \tau_1, \ldots, \tau_n$ is closely spaced. Then these time constants cannot be

reliably separated experimentally. Also the sum of such closely spaced exponential decays becomes numerically very close to the solution for semi-infinite length; for this purpose, values of L greater than 4 are already rather large.

In the case of an initial point charge at $X = 0$, the solution (Eq. 4.1 or 1.16) at $X = 0$ can be expressed

$$V/(Q_0/\lambda c_m L) = \exp(-t/\tau_0)$$
$$+ 2 \sum_{n=1}^{\infty} \exp(-t/\tau_n) \tag{4.7}$$

where τ_n is defined by Equation 4.3 or 4.5. When L is very large, this infinite series becomes numerically very close to solution (Eq. 1.22) at $X = 0$, which can be expressed (for semi-infinite length)

$$V/(Q_0/\lambda c_m) = (\pi t/\tau)^{-1/2} \exp(-t/\tau) \tag{4.8}$$

where τ is the same as τ_0 above. To analyze experimental data, it is very useful to note the advantage of multiplying both sides of Equation 4.8 by the square root of t, and taking the natural log of both sides to obtain

$$\log_e[t^{1/2}V] = -t/\tau + \text{constant} \tag{4.9}$$

This provides a basis for estimating τ from experimental data where L is very large. In 1960, when dendritic trees were treated as though they were semi-infinite in length, such plotting [of dV/dt for the response to an applied current step; see Eqs. 4.24, 4.25] provided a basis for estimating the motoneuron membrane time constant from experimental data (140). Even now, where the value of L is known to lie in the range from 1 to 2, such plotting can provide information about the boundary condition at the dendritic terminals as discussed by Jack and Redman [see (92), Fig. 12 and (93), Fig. 7].

Transient Response to Applied Current Step, for Finite Length

If a constant current (I) is applied across the membrane at $X = 0$, beginning at $T = 0$, then the transient response for the cylinder with sealed ends can be expressed

$$V(X,T) = V(X,\infty)$$
$$- \sum_{n=0}^{\infty} B_n \cos(n\pi X/L) \exp(-t/\tau_n) \tag{4.10}$$

where the steady state is

$$V(X,\infty) = (IR_\infty \coth L) \frac{\cosh(L-X)}{\cosh L}$$
$$= IR_\infty \frac{\cosh(L-X)}{\sinh L} \tag{4.11}$$

the time constants are the same as before (Eqs. 4.2

and 4.3), and the Fourier coefficients (B_n) are defined by Equations 1.17 and 1.18 with $W(X)$ set equal to $V(X,\infty)$ of Equation 4.11, with the result that

$$B_0 = IR_x/L \tag{4.12}$$

and

$$B_n = 2B_0\,\tau_n/\tau_0 = \frac{2B_0}{1 + (n\pi/L)^2} \tag{4.13}$$

At $X = 0$, this transient response can be expressed more simply as

$$V(0,T) = IR_x \left[\coth L - \frac{\exp\,(-t/\tau_0)}{L} \right.$$
$$\left. - \frac{2}{L} \sum_{n=1}^{\infty} (\tau_n/\tau_0)\,\exp\,(-t/\tau_n) \right] \tag{4.14}$$

Because the experimental estimation of τ_0, τ_1, τ_0/τ_1, and L have made use of the slope, dV/dt, of such experimental transients, we note that Equation 4.14 implies

$$dV/dt = (IR_x/L\tau_0) \left[\exp\,(-t/\tau_0) \right.$$
$$\left. + 2 \sum_{n=1}^{\infty} \exp\,(-t/\tau_n) \right] \tag{4.15}$$

which is proportional to the time course of V in Equation 4.7 and hence proportional to what is known as the response function at $X = 0$ for an instantaneous point charge input at $X = 0$, $T = 0$.

The same time constants are present in Equations 4.7, 4.10, 4.14, and 4.15; however, the coefficient ratios are different. Both Equations 4.7 and 4.15 have $C_n/C_0 = 2$, but the corresponding ratio for the current step response is $B_n/B_0 = 2\tau_n/\tau_0$ in Equation 4.14 and $2(\tau_n/\tau_0)\,\cos\,(n\pi X/L)$ for the more general Equation 4.10. Because these coefficient ratios are beginning to be studied experimentally [(183); also N. Tsukahara, personal communication and L. van Keulen and R. de Jongh, personal communication], it is important to point out that these theoretical ratios are for an idealized point charge or point current at $X = 0$ of the finite cable, and, except for Equations 4.10 and 1.16, the point of observation is also assumed to be at $X = 0$.

If, for example, the initial charge is spread locally (i.e., constant from $X = 0$ to $X = A$ and zero from $X = A$ to $X = L$) then Equations 1.16 and 1.18 yield a coefficient ratio for the decay transient at any location (X) that can be expressed

$$C_n/C_0 = \frac{2\,\sin\,(n\pi A/L)}{n\pi A/L}\,\cos\,(n\pi X/L) \tag{4.16}$$

which reduces to 2.0 when $A = 0$ and also location $X = 0$.

On the other hand, when the theory explicitly includes a lumped soma at $X = 0$, with a dendritic/soma input conductance ratio (ρ) [see (145), p. 1492–1496], then Equation 4.10 becomes generalized to

$$V(X,T) = V(X,\infty) - \sum_{n=0}^{\infty} B_n\,\cos\,[\alpha_n\,(L-X)]$$
$$\cdot\exp\,[-(1 + \alpha_n^2)T] \tag{4.17}$$

where the steady state is

$$V(X,\infty) = IR_N\,\frac{\cosh\,(L - X)}{\cosh\,L} \tag{4.18}$$

Here the time constant ratios

$$\tau_0/\tau_n = 1 + \alpha_n^2 \tag{4.19}$$

are not as simple as Equation 4.5 because the values of α_n correspond to roots of the transcendental equation

$$\alpha L\,\cot\,(\alpha L) = -\rho\,L\,\coth\,L = -k \tag{4.20}$$

and the values of B_n in Equation 4.17 can be expressed

$$\frac{B_0}{IR_N} = \frac{\rho + 1}{k + 1} = \frac{\tanh\,L + L/k}{L + L/k} \tag{4.21}$$

and

$$B_n\,\cos\,(\alpha_n L) = \frac{2\,B_0\,\tau_n/\tau_0}{1 + (\alpha_n L)^2/(k^2 + k)} \tag{4.22}$$

where k is the positive constant defined in Equation 4.20. [For examples of roots of Eq. 4.20, see (21), Table II of Appendix IV gives values of their α, which correspond to αL here.] For the limiting case of dendritic dominance, $\rho = \infty = k$, and $\alpha_n = n\pi/L$; then the solution defined by Equations 4.17–4.22 simplifies to that of Equations 4.10–4.13. [It is noted that Eqs. 4.21 and 4.22 have not previously been published; my derivation made use of a modified orthogonality; recently L. van Keulen and R. de Jongh (personal communication) obtained equivalent expressions by a different method.]

Whether these theoretical expressions can be used to provide good experimental estimates of both L and ρ from an analysis of transients has not yet been established; this is a matter for future testing. Extensive computations and preliminary plotting (W. Rall, unpublished observations, 1962) using Equations 4.17–4.22 at $X = 0$, with several values of ρ and of L, did show that $\rho > 5$ and $L > 3$ give results that are very close in most respects to $\rho = \infty$ and $L = \infty$. Thus it was possible to make a preliminary judgment that the L values of motoneurons lie in a range (now known to be 1–2) where the transient is sensitive to the value of L (and thus provides a basis for estimating L from experiment), while the ρ values of motoneurons seem to lie in a range [usually >5; see (130)] where the transient is not very sensitive to the exact value of ρ (and thus provides a poor basis for estimating ρ from experimental transients).

It is important to point out that Jack & Redman (93) also obtained extensive numerical solutions for finite values of ρ and L. These were based on a

difficult mathematical solution [see their derivation in (93), Appendix], which is expressed as an infinite series involving parabolic cylinder functions. They showed that the limiting form of this series, as either L or ρ is increased to ∞, agrees with previously obtained results. Their theoretical solution, for the response to an instantaneous point charge, was then convolved numerically with a transient input current to obtain results thay have presented graphically and discussed in some detail [see (93), Figs. 4–8]. By means of these results, they have provided a detailed procedure for estimating τ, L, and ρ from experimental data; they also include a third parameter, α, which relates to the brevity of the input current. With their collaborators (86, 87, 89–93) they have provided a careful application of these procedures to motoneurons of cat spinal cord; this research provides not only valuable new data, but also valuable testing of the underlying theoretical model. Many of the data were found to fit the model well, confirming L values between 1 and 2 and ρ values greater than 3, but with considerable variability in the ρ values. Some of their data provide puzzling departures from theoretical predictions; sometimes increasing the value of ρ to ∞ does not result in a good fit. These discrepancies have been carefully discussed by Iansek & Redman (86), and they provide valuable clues for further study. They (86) have suggested that the resistivity of the soma membrane is lower than that of the dendrites, perhaps by a factor of 3 in some of these cases; they suggest tonic synaptic inhibitory input to the soma as an explanation. The possible contribution of an injury conductance (G_{inj}) at the site of microelectrode puncture may also need consideration as a source of such discrepancies in transient time course. Such explanations (either synaptic inhibition at the soma or G_{inj} at the soma) can be tested by additional experiments using voltage clamping at the soma; then any abnormal (but constant) conductance at the soma would be satisfied by the clamping circuit almost instantly; the remaining transient current would be determined only by the dendrites, independently of ρ and of any constant somatic conductances. Mathematical solutions for voltage clamping at the soma have been noted, both for dendritic cylinders of semi-infinite length (140) and those of finite length [(145); see also Eqs. 4.32–4.46]. Such solutions could also be obtained numerically by using the computational method suggested by Norman (131).

Applied Current Step with L Large or Infinite

Just as large values of L cause the sum of closely spaced exponentials in Equation 4.7 to become numerically close to Equation 4.8, large L also causes the corresponding Equation 4.14 for the response at $X = 0$ to a constant current step applied at $X = 0$, $T = 0$ to become numerically close to the following expression for semi-infinite length

$$V = IR_{\infty}\,\mathrm{erf}\,[(t/\tau)^{1/2}] \qquad (4.23)$$

Where the error function is defined

$$\mathrm{erf}(x) \equiv \frac{2}{\sqrt{\pi}}\int_{0}^{x} \exp\,(-y^2)\mathrm{d}y$$

and is available as a tabulated function [e.g., see Appendix II, (21)]. It may be noted that $\mathrm{erf}(0) = 0$, $\mathrm{erf}(\infty) = 1$, and $\mathrm{erf}(-x) = -\mathrm{erf}(x)$. Differentiation of Equation 4.23 with respect to t yields an expression for the slope

$$\mathrm{d}V/\mathrm{d}t = \frac{IR_{\infty}}{\tau\sqrt{\pi}}\,(t/\tau)^{-1/2}\exp\,(-t/\tau) \qquad (4.24)$$

As should be expected, this slope is proportional to Equation 4.8 for the response function at $X = 0$ for an instantaneous point charge at $X = 0$. Thus, as noted with Equation 4.9, here the expression

$$\log_e\,[t^{1/2}\mathrm{d}V/\mathrm{d}t] = -t/\tau + \text{constant} \qquad (4.25)$$

provides the basis for a plot of LRT $\mathrm{d}V/\mathrm{d}t$ (i.e., log of root T times $\mathrm{d}V/\mathrm{d}t$, plotted vs. t) to estimate τ where L is very large. A discussion of such plotting, together with theoretical expressions for the complication provided by a lumped soma (140), and by both lumped soma and finite length, can be found in the studies by Jack & Redman [(92, 93); see also (91)].

It should be emphasized that Equation 4.23 represents a useful special case (at $X = 0$) of a more general and more complicated expression for the transient response at any X, for a current step applied at $X = 0$. This more general expression has been well established since 1946 by the classic studies of Hodgkin & Rushton (80) and Davis & Lorente de Nó (33). For the semi-infinite region $(0 \leq X \leq \infty)$ this solution can be expressed

$$\frac{V(X,T)}{V(0,\infty)}$$
$$= \begin{cases} + (1/2)\,\exp(-X)\mathrm{erfc}(X/2\sqrt{T} - \sqrt{T}) \\ - (1/2)\,\exp(+X)\mathrm{erfc}(X/2\sqrt{T} + \sqrt{T}) \end{cases} \qquad (4.26)$$

where $V(0,\infty) = IR_{\infty}$ for a semi-infinite length having a sealed end at $X = 0$, or $V(0,\infty) = IR_{\infty\infty} = (1/2)IR_{\infty}$ for a doubly infinite length that extends from $-\infty$ to $+\infty$, and I is current applied across the membrane at $X = 0$; the complementary error function is defined $\mathrm{erfc}(x) = 1 - \mathrm{erf}(x)$; it decreases monotonically from $\mathrm{erfc}(-\infty) = 2$, through $\mathrm{erfc}(0) = 1$, to $\mathrm{erfc}\,(+\infty) = 0$. Equation 4.26 corresponds to previously published equations [(80), Eq. 4.1, Table 1, and Fig. 2C; also (33), Eq. 37 and Fig. 6] and is illustrated here by Figure 24.

It should be noted that the rather complicated expression on the right side of Equation 4.26 becomes greatly simplified for either $T = \infty$ or $X = 0$. When $T = \infty$, we see that $\mathrm{erfc}(-\infty) = 2$ and $\mathrm{erfc}(+\infty) = 0$ reduce the right side of Equation 4.26 simply to

$\exp(-X)$, which is the well-known steady-state decrement with distance for semi-infinite length. For $X = 0$, one obtains $(1/2)[1 - \mathrm{erf}(-\sqrt{T}) - 1 + \mathrm{erf}(\sqrt{T})]$, which reduces simply to $\mathrm{erf}(\sqrt{T})$, in confirmation of Equation 4.23. This transient, at $X = 0$, rises steeply for small values of T. On the other hand, the transient at large values of X rises very slowly for small values of T and is effectively delayed (Fig. 24); when X is large enough and T is small enough that the values of $(X/2\sqrt{T} \pm \sqrt{T})$ are large (e.g., >2.8), then both the complementary error functions in Equation 4.26 have very small values (e.g., $<10^{-4}$). Furthermore the effect of distance X on the slope dV/dT is shown explicitly by differentiating Equation 4.26 and rearranging terms to obtain

$$\frac{dV/dT}{V(0,x)} = (\pi T)^{-1/2} \exp\left(- \frac{X^2}{4T} - T\right) \quad (4.27)$$

It should be noted that this expression is proportional, as it should be, to the fundamental solution (Eq. 1.22) for an instantaneous point source. Thus the several useful properties that are pointed out next for Equation 4.27 have a related meaning for Equation 1.22.

Equation 4.27 shows that, for any given value of
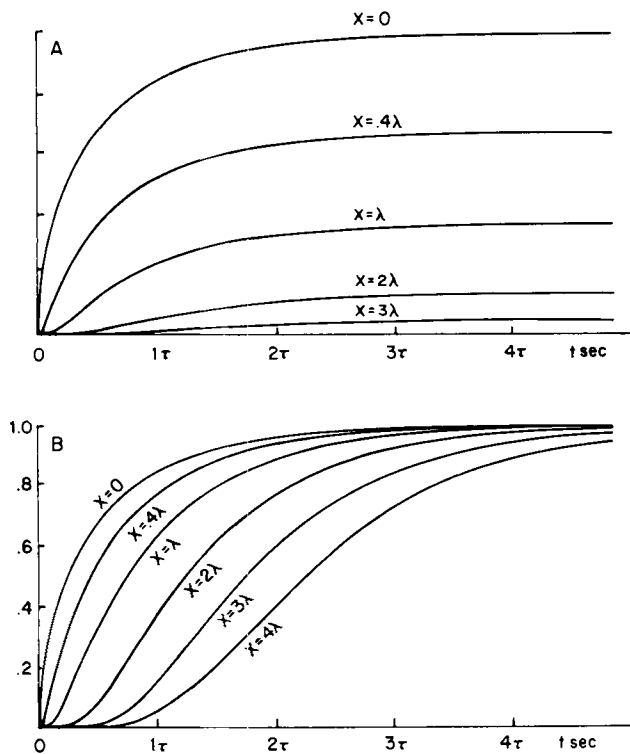
FIG. 24. Two different graphs based on Eq. 4.26, as plotted by Davis & Lorente de Nó (33). A: curves plotted to the same amplitude scale show both slowing and reduced amplitude with distance. B: curves replotted relative to the steady-state value at each location [i.e., $V(X, T)/V(X, \infty)$] to highlight the changing shape of the delayed rise.

T, the slope dV/dT is smaller at distance X than at $X = 0$, by the factor

$$\frac{dV/dT \text{ at } (X,T)}{dV/dT \text{ at } (0,T)} = \exp\left(-\frac{X^2}{4T}\right) \quad (4.28)$$

Thus, when $T = 0.1$, this slope factor equals 0.082 for $X = 1$ and 0.000045 for $X = 2$. Also, by taking the natural log of Equation 4.28 and rearranging, we can obtain the expression

$$x^2 = (\lambda^2/\tau)4t \log_e \left\{\frac{dV/dt \text{ at } (0,t)}{dV/dt \text{ at } (x,t)}\right\} \quad (4.29)$$

which can be used to plot paired experimental values of x^2 versus $4t \log_e \{dV/dt \text{ ratio}\}$ to fit a straight line having a slope of λ^2/τ. If τ has already been determined from the transient at $x = 0$, or by some other method, this provides an estimate of λ^2; conversely, if λ has already been determined from the steady state, this provides an estimate of τ.

A different, but somewhat similar relation can be obtained from a consideration of the point of inflection in each of the transients defined by Equation 4.26. Such points of inflection are found mathematically by differentiating Equation 4.27 with respect to T and setting this equal to zero. [This is equivalent to finding the paired values of X and T for the electrotonically spreading peak of Eq. 1.22, as previously presented by Fatt and Katz (47, pp. 332 and 363).]

The resulting relation of such paired values can be expressed

$$x^2 = (\lambda^2)(4T^2 + 2T) \quad (4.30)$$

When τ has already been estimated, one can use Equation 4.30 as the basis for a plot of paired values of x^2 versus $(4T^2 + 2T)$ to fit a straight line having a slope of λ^2.

A still different property of this kind was noted and used by Hodgkin & Rushton (80). From the theoretical curves of Equation 4.26 it was found that there is an almost linear relation between each value of X and its corresponding value of T for which the transient V at X reaches half its steady-state value $V(X, \infty)$; a plot of such paired values of X and T has a slope $\Delta X/\Delta T \cong 2$; this means that a plot of paired experimental x and t values would be expected to fit a slope

$$\Delta x/\Delta t \cong 2\lambda/\tau \quad (4.31)$$

This provides an alternate means of estimating either λ or τ when the other has already been estimated. Also, for example, the ratio of λ^2/τ from Equation 4.29 and $2\lambda/\tau$ from Equation 4.31 yields $\lambda/2$, without knowing τ; this estimate of λ can be compared with that obtained from steady-state decrement with distance.

Clearly there are several different but interrelated ways to estimate the values of τ and λ, as was

emphasized also by Hodgkin & Rushton (80), as well as by Fatt and Katz (47, 98). The more closely the experimental conditions fit the idealized assumptions of the mathematical physics, the better should be the agreement between the different ways of estimating τ and λ. As already noted in the discussion of input resistance, the earlier experiments (80, 98) were performed with extracellular electrodes and involved estimation of both r_i and r_c (for the extracellular layer under the oil) and the various ratios such as $r_c/(r_c + r_i)$; subsequent experiments using intracellular electrodes and a large extracellular volume (47) could treat r_c as negligible and thus make use of simpler expressions for λ and input resistance and lead to simpler estimation of R_i or diameter and resulting estimates of R_m and C_m (see Table 1 and Eqs. 3.15–3.22).

It may be noted that when a lumped soma is placed at $x = 0$, Equations 4.23–4.27 are replaced by more complicated expressions, which are not reproduced here (92, 93, 140); the solution was by means of Laplace transforms (21, 91–93, 140). The generalization of Equation 4.26 to a three-dimensional problem has recently been reported (132).

Voltage Clamp at X = 0, with Infinite L

When a voltage clamp is suddenly applied at $X = 0$ to a previously resting cable of semi-infinite or infinite length, the solution is closely related to Equation 4.26 and can be expressed

$$\frac{V(X,T)}{V(0,\text{clamp})}$$

$$= \begin{cases} + (1/2)\exp(-X)\text{erfc}(X/2\sqrt{T} - \sqrt{T}) \\ + (1/2)\exp(+X)\text{erfc}(X/2\sqrt{T} + \sqrt{T}) \end{cases} \quad (4.32)$$

[A corresponding expression can be found in Carslaw & Jaeger (21), Eq. 7, p. 135, and Laplace transform no. 19, Appendix V.] It may be noted that, as with Equation 4.26, here also setting $T = \infty$ reduces the right side to $\exp(-X)$, the steady-state solution; however, setting $X = 0$ reduces the right side to unity, as it must for the voltage-clamping boundary condition.

Here, differentiation with respect to T yields, on rearrangement, the expression

$$\frac{dV/dT}{V(0,\text{clamp})} = (\pi T^3)^{-1/2}(X/2) \exp\left(-\frac{X^2}{4T} - T\right) \quad (4.33)$$

which differs somewhat from Equation 4.27. At any T, the ratio of slopes at any two locations $(X_1$ and $X_2)$ can be expressed

$$\frac{dV/dT, \text{ at } (X_1,T)}{dV/dT, \text{ at } (X_2,T)} = \left(\frac{X_1}{X_2}\right) \exp\left(\frac{X_2^2 - X_1^2}{4T}\right) \quad (4.34)$$

By taking natural logs of both sides, one can obtain

$$x_2^2 - x_1^2$$

$$= (\lambda^2/\tau)4t \, \log_e\left\{\left(\frac{x_2}{x_1}\right) \frac{dV/dt \text{ at } (x_1,t)}{dV/dt \text{ at } (x_2,t)}\right\} \quad (4.35)$$

for voltage clamping at $X = 0$, for semi-infinite length (cf. Eq. 4.29 for the applied current step). This could be used to estimate the value of (λ^2/τ) from experiments where the slopes of the transients (Eq. 4.32) can be measured for several values of x and t. However, if measurements are possible only at $X = 0$, one must measure the clamping current transient that is proportional to $(-dV/dX)$ at $X = 0$. Differentiation of Equation 4.32 with respect to X yields

$$\frac{dV/dX}{V(0,\text{clamp})} = \begin{cases} - (\pi T)^{-1/2} \exp\left(-\frac{X^2}{4T} - T\right) \\ - \text{ expression on right side} \\ \quad \text{of Eq. 4.26} \end{cases} \quad (4.36)$$

and setting $X = 0$ yields the following proportionality for the time course of the current supplied by the voltage clamp

$$I \propto (\pi T)^{-1/2} \exp(-T) + \text{erf}(T^{1/2}) \quad (4.37)$$

in agreement with a result obtained in 1960 [(140), p. 529–530 and p. 515]; as then noted [(140), p. 515], such a clamping current has a time derivative that can be expressed by the proportionality

$$dI/dt \propto - (t)^{-3/2} \exp(-t/\tau) \quad (4.38)$$

This provides a basis for plotting $\log_e [t^{3/2} (-dI/dt)]$ versus t to obtain a slope equal to $-(1/\tau)$ for voltage clamping at $X = 0$, with semi-infinite length, assuming membrane properties remain passive. These results also provide a basis for analyzing data obtained when voltage clamping a neuron soma, if dendritic electrotonic length is very large and the membrane remains passive. Results for finite dendritic length are considered next.

Voltage Clamp with Finite Length

There may be considerable future application of a voltage clamp at $X = 0$, with a sealed end at $X = L$; also a pair of equal voltage clamps at $X = 0$ and $X = 2L$, with observations made at $X = L$ or other intermediate locations, has the merit of testing only the region of core conductor between the paired voltage clamps. The solution (145) of both problems, in the region from $X = 0$ to $X = L$, can be expressed

$$\frac{V(X,T)}{V(0,\text{clamp})} = \frac{\cosh(L - X)}{\cosh L}$$

$$+ \sum_{n=1}^{\infty} A_n \sin(\alpha_n X) \exp(-t/\tau_n) \quad (4.39)$$

where $\qquad \alpha_n = (2n - 1)\pi/2L$ $\qquad$ (4.40)

and

$$\tau_n = R_m C_m/(1 + \alpha_n^2) \qquad (4.41)$$

are not the same as those for the current step with sealed end at $X = L$. For a zero initial condition, the Fourier coefficients (A_n) are calculated for $F(X)$ equal to minus the steady state; then

$$A_n = -\frac{2\alpha_n}{(1 + \alpha_n^2)L} = \frac{-4}{(2n - 1)\pi(1 + \alpha_n^{-2})} \qquad (4.42)$$

where the second version facilitates comparison with a result given by Carslaw & Jaeger |(21), Eq. 8, p. 135; there is agreement when careful consideration is given to the effect of shifting from their voltage-clamp locations, at $\pm$ ℓ, to the locations, $X = 0$ and $X = 2L$, used here|. Here the summation runs from $n = 1$ to ∞, because there is no term having the passive membrane time constant, $\tau_0 = R_m C_m$, in the presence of a voltage clamp or short circuit (145).

At $X = L$, $\sin(\alpha_n L) = -(-1)^n$, and the transient can be expressed

$$\frac{V(L,T)}{V(0,\text{clamp})} = \frac{1}{\cosh L}$$

$$+ \frac{2}{L} \sum_{n=1}^{\infty} \frac{(-1)^n \alpha_n}{(1 + \alpha_n^2)} \exp(-t/\tau_n) \qquad (4.43)$$

where α_n and τ_n are given by Equations 4.40 and 4.41. When such a transient is recorded midway between a pair of voltage clamps, one should explore estimating at least τ_1 and τ_2, and then $2L$; perhaps even more complete curve fitting can be carried out. It may be noted that for $L = \pi/2$, $\tau_1 = \tau_0/2$ and $\tau_2 = \tau_0/10$, implying that $\tau_1/\tau_2 = 5$; for $L = \pi$, $\tau_1 = \tau_0/1.25$, and $\tau_2 = \tau_0/3.25$, implying a value of 2.6 for the ratio τ_1/τ_2. However, to estimate L directly from τ_1 and τ_2, one can make use of the relation

$$2L = \pi \left[\frac{9\tau_2 - \tau_1}{\tau_1 - \tau_2} \right]^{1/2} \qquad (4.44)$$

At $X = 0$, the transient current supplied by the voltage clamp to the region from $X = 0$ to $X = L$ is proportional to $(-dV/dX)$ at $X = 0$. This current time course is proportional to

$$\tanh L + \frac{2}{L} \sum_{n=1}^{\infty} \frac{\alpha_n^2}{(1 + \alpha_n^2)} \exp(-t/\tau_n) \qquad (4.45)$$

and this current has a time derivative

$$dI/dt \propto -\sum_{n=1}^{\infty} \alpha_n^2 \exp(-t/\tau_n) \qquad (4.46)$$

For very large values of L, these two expressions can be expected to become numerically proportional to the corresponding expressions (Eqs. 4.37 and 4.38)

for semi-infinite length. Future testing is needed to verify the expected usefulness of these expressions; they have the merit that (with good voltage clamping) the presence of a lumped soma membrane at $X = 0$, and even the added complication of either a low somatic R_m value or a somatic injury conductance, G_{inj} (provided they remain constant), would not be expected to modify these transients after the initial instant. This contrasts with the case of an applied current step.

A very recent study of various voltage-clamping arrangements, including active membrane properties, has been reported by Moore et al. (125a).

Transient Response to Current Injected at One Branch of Model

The response function, for an instantaneous point charge delivered to one branch terminal of an idealized neuron model, has been derived (using superposition methods), and explicit expressions have been provided, both in the Laplace transform domain and in the time domain (161). The full details and notation are not repeated here. The mathematical expressions in the time domain are infinite series of two types: one converges rapidly for large values of T, while the other converges well for small values of T; computations with both expressions were used to obtain the solid curve displayed in Figure 25 with semi-log scaling.

Useful physical intuitive insight can be obtained
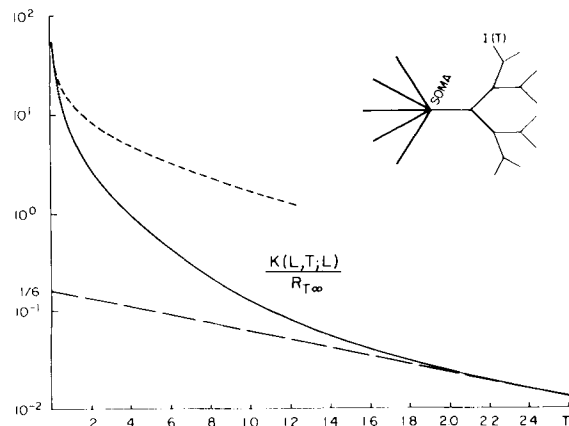
FIG. 25. Response function at the input branch terminal (*solid curve*), compared with 2 asymptotic cases (*dashed curves*); ordinates are plotted on a logarithmic scale. *Inset*, neuron model with input injected at one branch terminal. Solid curve represents the response function as $T \to \infty$ (Eq. 4.47); its left intercept represents 1.0, and $N = 6$. Lower dashed curve is a straight line representing uniform decay and representing the asymptotic behavior of the response function as $T \to \infty$ (Eq. 4.47); its left intercept represents a value of $1/6$ because $NL = 6$. Upper dashed curve represents the asymptotic behavior as $T \to 0$; this also represents the response for a semi-infinite length of terminal branch (Eq. 4.48). For any combination that makes $Q_0 R_{T_\infty}/\tau = 1$ mV, the values of the functions plotted here would correspond to V in millivolts. |See (161).|

by understanding the reasons why this response function (at the site of charge injection) approaches the upper dashed curve of Figure 25 for very small values of T, and why it approaches the lower dashed straight line for very large values of T. The straight line corresponds to

$$V(T) = \frac{Q_0}{NL\lambda c_m} \exp(-T) \qquad (4.47)$$

This limiting case corresponds to the simple exponential decay that would occur at all locations if the original charge were distributed evenly over the entire neuron model; it may be noted that $NL\lambda c_m$ represents the total membrane capacity of this neuron model, where each of N equivalent cylinders has a length λL and a membrane capacity per unit length c_m. The solid curve approaches the lower dashed line as the distribution of charge gradually becomes equalized over the entire surface (161). The upper dashed curve represents the response to an instantaneous charge (Q_0) placed at the terminal of an Mth order branch, for the limiting case when the branch length is extended to very great length. In agreement with Equations 1.22, 1.23, and 4.8, this transient can be expressed

$$V(T) = A_0(\pi T)^{-1/2} \exp(-T) \qquad (4.48)$$

where

$$A_0 = \frac{Q_0 2^M R_{T\alpha}}{\tau} = \frac{Q_0 2^M}{\lambda c_m}$$

because, with M orders of symmetrical branching, the R_α value of an Mth order branch is 2^M times that $(R_{T\alpha})$ of the trunk; similarly, the capacity per λ length of the branch is 2^{-M} times that (λc_m) of the trunk. This limiting transient (upper dashed curve in Fig. 25) agrees with that in the neuron model during the earliest time, before significant charge has spread to the point where the input branch takes origin from its parent branch. The earliest deviation of the solid curve from this dashed curve is due, physically, to the fact that further spread of charge is facilitated by the lower resistance provided by the larger diameter parent branch, in parallel with the sister branch. All such effects, at all branch points, are provided for in the complete response function (161) and account for the way in which the solid curve in Figure 25 passes from early agreement with Equation 4.48 to late agreement with the uniform decay of Equation 4.47.

When this response function is convolved with the brief input current transient shown at upper left of Figure 26, the resulting voltage transient at the input location is shown as $V(L,T)$ in Figure 26. Also convolution with the response function at the soma $(X = 0)$ for $I(T)$, applied (in any proportions) to one or more branch terminals, resulted in the voltage transient shown as $V(0,T)$ in Figure 26; the ampli-

tude of this transient has been amplified 200 times relative to $V(L,T)$. The same transients, plotted to a logarithmic amplitude scale, are included in Figure 27, which also shows the voltage transients computed at several other locations. It can be seen that, with increasing electrotonic distance from the input branch terminal (BI), to the parent node (P), on
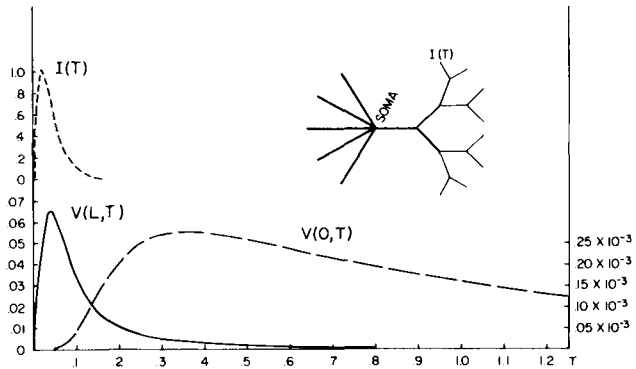

FIG. 26. Computed voltage time course at the input-receiving branch terminal (solid curve) and at the soma (lower dashed curve) for a particular time course $[I(T)]$ of injected current (upper dashed curve). Neuron model is shown at upper right, and parameters used were $N = 6$, $M = 3$, $X_1 = 0.25$, $X_2 = 0.5$, $X_3 = 0.75$, and $L = 1$. Ordinate values for the solid curve using scale at left represent dimensionless values of $V(L, T)/(2^M R_{T\alpha}I_p e)$ [see (161)]. Soma response (lower dashed curve) has been amplified 200 times; the ordinate values, using scale at right, represent dimensionless values of $V(0, T)/(2^M R_{T\alpha}I_p e)$ [see (161)]. Factor $2^M R_{T\alpha}I_p e$ equals $8 \times (4.56 R_N) \times (I_p e)$ which is approximately equal to 100 times the product R_N and I_p. For example, if $R_N = 10^6$ Ω and $I_p = 10^{-8}$ A, the above factor is approximately 1 V; then the left-hand scale can be read in volts for $V(L, T)$ and the right-hand scale can be read in volts for $V(0, T)$.
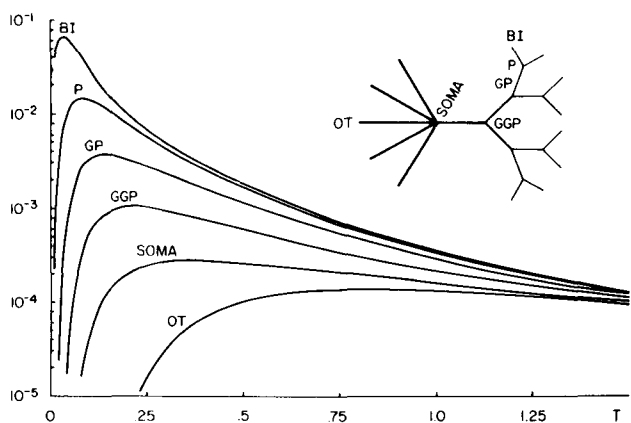

FIG. 27. Semi-log plots of transient membrane potential vs. T at successive sites along the mainline in the neuron model for transient current injected into the terminal of one branch. BI designates the input branch terminal, while P, GP, and GGP designate the parent, grandparent, and great grandparent nodes, respectively, along the mainline from BI to the soma. Response at the terminals of the trees not receiving input directly is labeled OT. Model parameters, neuron branching diagram, and current time course are the same as in Fig. 26. Ordinate values represent dimensionless values of $V(X, T)/(2^M R_{T\alpha}I_p e)$ where $V(X, T)$ was obtained as the convolution of $I(T)$ with $K(X, T; L)$ defined in reference (161).
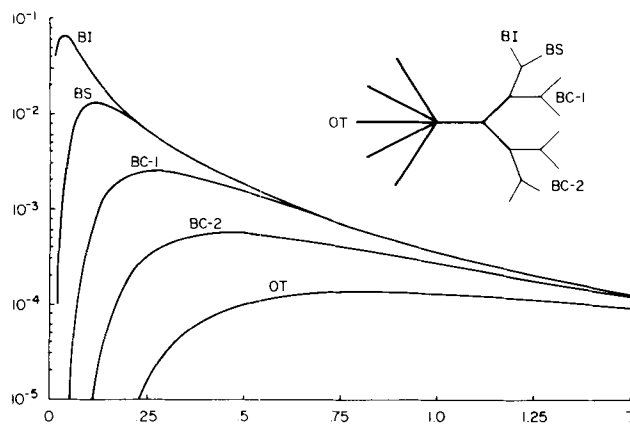
FIG. 28. Semi-log plots of voltage vs. T at all the branch terminals in the neuron model for transient current injected into the terminal of one branch. Refer to Fig. 26 for model parameters and input current time course. BI and BS designate the input branch terminal and the sister branch terminal, respectively. BC-1 and BC-2 designate the terminals of the 2 first-cousin and the 4 second-cousin branches, respectively, in the input tree, while OT designates the branch terminals of the other 5 trees. Transients are computed and scaled as indicated in Fig. 27. [See (161).]

through to the soma and to the terminals of the other trees (OT), the time of peak becomes increasingly delayed and the peak amplitude becomes increasingly attenuated. These peak times and attenuation factors have been collected in Table 5, together with those at the other branch terminals. In Figure 28 the transients computed for these other branch terminals are displayed; the membrane potential in the sister branch (BS) becomes equalized most rapidly with that in the input branch (BI); equalization with the first-cousin branches (BC-1) takes longer and with the second-cousin branches (BC-2) takes even longer. These equalizations are governed by time constants that depend on the electrotonic distances between these branch terminals. Further discussion of these results can be found in the original paper (161). Other calculations and discussion of transient attenuation have been provided by Barrett & Crill (7), Redman (159), and Rall (144, 148).

RELATIONS BETWEEN NEURON MODEL PARAMETERS

The background and assumptions of dendritic neuron models are discussed in the section DENDRITIC ASPECTS OF NEURONS, with comments on the experi-

mental testing and the biophysical insights that have resulted. In subsequent sections the mathematical results of cable theory that are needed for the interpretation of electrophysiological experiments both with axons and with dendritic neurons are developed. Here these results are used to summarize the relations between various neuron parameters, especially with regard to the interpretation of experiments made with motoneurons of cat spinal cord.

Input Resistance and Membrane Resistivity

The neuron input resistance (R_N) is a basic measured parameter; however, the resting membrane resistivity (R_m) must be estimated by means of geometric and cable considerations. For simplicity, it has usually been assumed that R_m has the same value for the soma and all the dendritic branches. However, there have been early suggestions (46b, 139, 140) that the value of R_m could be different at different locations, and quite recently it has been pointed out that the value at the soma might be significantly lower than in the dendrites (6, 86). Also it has been recognized that R_m may not be at its resting value in a given experiment, because there may be background synaptic activity (excitatory and/or inhibitory) impinging on the neuron, possibly with a nonuniform distribution over the surface. Even for resting conditions, R_m must be regarded as an effective value for an overall surface area that is partly occluded by a high density of inactive synaptic endings.

In general, the neuron input conductance $(G_N = 1/R_N)$ can be expressed

$$G_N = G_S + G_A + \sum_j G_{Dj} \qquad (5.1)$$

where G_S is the soma conductance, G_A is the input conductance of the axon, and the last expression represents the combined dendritic input conductance where G_{Dj} represents the input conductance of the jth dendritic tree and the summation symbol implies a summation composed of all the dendritic trees. Usually G_A is not explicitly included, either because it is the smallest component or because it may be regarded as included with the dendrites.

It is useful to define the dendritic-to-soma conductance ratio

$$\rho = \sum_j G_{Dj}/G_S \qquad (5.2)$$

TABLE 5. *Transient Attenuation Factors and Peak Times and Steady-state Attenuation Factors*

Location	BI	P	GP	GGP	Soma	BS	BC-1	BC-2	OT
Peak time	0.04	0.085	0.135	0.21	0.35	0.12	0.27	0.46	0.84
Peak value × 10³	64.8	14.5	3.75	1.05	0.276	12.8	2.54	0.557	0.135
Transient attenuation factor	1.0	4.5	17.3	62	235	5.1	25	116	479
Steady-state attenuation factor	1.0	2.3	5.3	12.0	23.9	2.4	6.0	15.5	34.0

Peak times and values from Figs. 27 and 28.

Although it has been difficult to determine values of ρ precisely, the fact that the more recent estimates of ρ usually exceed 5 and often exceed 10 or 15 provides an order of magnitude measure of dendritic dominance. If we neglect G_A, Equations 5.1 and 5.2 imply that

$$G_N = (\rho + 1)G_S \qquad (5.3)$$

and

$$G_N = \left(\frac{\rho + 1}{\rho}\right) \sum_j G_{Dj} \qquad (5.4)$$

The soma conductance can be expressed

$$G_S = A_S/R_{mS} + G_{inj} \qquad (5.5)$$

where A_S represents the soma membrane area and G_{inj} represents an injury conductance that is zero only when the membrane seals perfectly around the microelectrode. Some electrode penetrations result in injury currents that reduce the measured resting potential; when such reduction is to half the normal resting potential, one can conclude that G_{inj} is as large as the intact value of G_N. Those experiments are rejected, but what about a smaller injury conductance, such as one that reduces the resting potential by 10%? This might not be detected and not be rejected. Yet it would be responsible for much more than a 10% change in the effective values of G_S and ρ. For example, if the uninjured neuron had a ρ value of 9, implying that $G_N = 10\, G_S$, then the injury that increased G_N by 10% would have increased G_S by 100%. Such doubling of G_S must halve the value of ρ from 9 to 4.5; these changed values can also be summarized as

$$G_N/G_S = 110/20 = 5.5 = \rho + 1$$

Such effects of injury may well be responsible for some of the variability found in experimental estimates of ρ.

Although Equations 5.3 and 5.5 can be used to obtain the expression

$$R_{mS} = \frac{(\rho + 1)\, A_S R_N}{1 - G_{inj}/G_S} \qquad (5.6)$$

its usefulness is limited by the uncertainties in the values of G_{inj}/G_S and ρ. For experimentally estimated values of A_S and R_N, one can use Equation 5.6 to assess the implications of various hypothetical values of G_{inj}/G_S and ρ. For example, consider $R_N = 2$ MΩ and $A_S = 10^{-4}$ cm^2. Then for $\rho = 10$ with $G_{inj} = 0$, Equation 5.6 implies $R_{mS} = 2,200\ \Omega$ cm^2. However, if $\rho = 10$ with $G_{inj}/G_S = 0.5$, it implies $R_{mS} = 4,400\ \Omega$ cm^2; on the other hand, if ρ is halved while G_{inj} is assumed zero, then Equation 5.6 would yield $R_{mS} = 1,200\ \Omega$ cm^2.

Dendritic Tree Input Resistance and Membrane Resistivity

Valuable simplification occurs when dendritic trees are treated as equivalent cylinders (see subsection *Results for Trees Equivalent to Cylinders*). Here results are given for more general dendritic trees. The input conductance of the jth dendritic tree can be expressed

$$G_{Dj} = G_{\infty j}B_{0j} \qquad (5.7)$$
$$= (\pi/2)(R_{mD}R_i)^{-1/2}\, B_{0j}\, (d_{0j})^{3/2}$$

where d_{0j} is its trunk diameter and B_{0j} is a factor that depends on the diameters and the electrotonic lengths of its branches in a manner explained in 1959 [(139); see Eqs. 3.37–3.41]. If the branches were equivalent to an extension of the trunk to infinite length, then $B_{0j} = 1$, while, for an equivalent cylinder of finite length, $B_{0j} = \tanh(L_j)$, where L_j represents the electrotonic length of this dendritic tree, and it has been assumed that the dendritic terminals are sealed. In general the value of B_{0j} depends on the branch lengths and diameters and on the value of R_{mD}. The values of R_{mD} and of R_i are needed for the λ values in the dendritic branches of different diameters. When complete anatomic information is available, one can calculate the values of B_{0j} for several tentative values of R_{mD} [e.g., see (4a, 6, 119, 139)]. Then comparison with experimentally measured input resistance (R_N) permits one to estimate a range of compatible values for R_{mD}.

Here it is useful to combine Equations 5.4 and 5.7 as though the B_{0j} values were already known; then the dendritic membrane resistivity can be expressed in terms of its square root

$$R_{mD}^{1/2} = \left(\frac{\pi(\rho + 1)}{2\rho\, (R_i)^{1/2}}\right) R_N \sum_j B_{0j}(d_{0j})^{3/2} \qquad (5.8)$$

For example, suppose that $\rho \cong 10$ and $R_i \cong 70\ \Omega$ cm; then the factor in large parentheses equals about 0.2 $(\Omega$ cm$)^{-1/2}$. If $B_{0j} = 0.8$ for all trees, then a large motoneuron with a combined dendritic trunk $d^{3/2}$ value of 600×10^{-6} cm$^{3/2}$ with an R_N value of 0.5 MΩ would imply an R_{mD} value of 2,300 Ω cm^2, while a smaller motoneuron having a $\Sigma d^{3/2}$ value of 200×10^{-6} cm$^{3/2}$ with an R_N value of 2.5 MΩ would imply an R_{mD} value of 6,400 Ω cm^2. The experimental sample of Lux et al. (119) has mean values of $R_N = 1.07$ MΩ, $\Sigma d^{3/2} = 335 \times 10^{-6}$ cm$^{3/2}$, and $R_m = 2,750\ \Omega$ cm^2, suggesting an average B_{0j} value around the 0.8 value used above. The experimental sample of Barrett & Crill (6) showed reduction of $\Sigma d^{3/2}$ with electrotonic distance from the soma (this implies a smaller value of B_{0j}, but the initial taper also makes it difficult to decide where the trunk diameters should be measured); they obtained an estimate of at least 1,800 Ω cm^2 for R_m and suggested that R_{mD} could easily be as large as 8,000 Ω cm^2, if the value of R_{mS} is small.

Results for Trees Equivalent to Cylinders

It may be noted that the dendritic surface area is not explicit in Equation 5.8, because it is buried in complicated cable considerations. This can be remedied when each dendritic tree satisfies the constraints for representation as an equivalent cylinder with a sealed end (119, 141-143, 148). Then it can be shown for each tree that

$$G_D = \frac{A_D}{R_{mD}} \frac{\tanh (L)}{L} \tag{5.9}$$

where $A_D = \ell \pi d$ is the membrane surface area of the equivalent cylinder, which also equals the surface area of the original dendritic tree (141-143). [To obtain Eq. 5.9 from Eq. 5.7, with subscript j deleted, note that

$$G_\infty = \frac{\lambda}{r_m} = \frac{\lambda A_D}{r_m \ell \pi d} = \frac{A_D}{R_{mD} L}$$

and that $B_0 = \tanh (L)$ for an equivalent cylinder having a sealed end (see Eqs. 3.6, 3.29, and 3.37).] For small values of $L = \ell/\lambda$, the value of $\tanh(L)$ is close to L; that is, if $L < 0.4$, the discrepancy is less than 5%. Then Equation 5.9 reduces to

$$G_D \simeq \frac{A_D}{R_{mD}}, \text{ for } L \text{ small} \tag{5.10}$$

which agrees with the simple intuitive concepts of surface area and membrane resistivity when the membrane potential is nearly uniform: electrotonic decrement is negligible for small L with a sealed end. In contrast, for very large values of L, the value of $\tanh(L)$ is very close to 1.0, and Equation 5.9 reduces to

$$G_D \simeq \frac{A_D}{R_{mD} L} = \frac{\lambda \pi d}{R_{mD}}, \text{ for } L \text{ large} \tag{5.11}$$

Here, as $L \to \infty$, $G_D \to G_\infty$ and the surface area of the cylinder becomes infinite; however, the numerator of Equation 5.11 corresponds to the finite surface area for a length (λ) of this cylinder.

For dendritic trees equivalent to cylinders of intermediate electrotonic length, Equation 5.9 is used with Equation 5.4 to obtain the expression

$$R_{mD} = \left(\frac{\rho + 1}{\rho}\right) (R_N) \sum_j A_{Dj} \frac{\tanh(L_j)}{L_j} \tag{5.12}$$

where A_{Dj} and L_j are the surface area and the electrotonic length, respectively, of the jth dendritic tree or of its equivalent cylinder. If these trees all have the same electrotonic length (L_D), this expression is further simplified to

$$R_{mD} = (1 + 1/\rho)R_N A_{\Sigma D} \tanh (L_D)/L_D \tag{5.13}$$

where $A_{\Sigma D}$ represents the summed surface area of these dendritic trees or their equivalent cylinders.

Having obtained this result, one can simplify further to obtain Equation 5.16. First, however, it seems worthwhile to note that the assumptions made so far provide useful expressions for ρ and also for the ratio of combined dendritic surface area to the combined $d^{3/2}$ value of the dendritic trunks. Thus Equations 5.7-5.13 can be used to obtain the ratio

$$A_{\Sigma D}/\Sigma d_{0j}^{3/2} = (\pi/2)L_D(R_{mD}/R_i)^{1/2} \tag{5.14}$$

Also Equations 5.2, 5.5, 5.9, and 5.13 can be used to express the value of ρ in terms of the dendritic and somatic values of surface area and membrane resistivities

$$\rho = \frac{R_{mS}A_{\Sigma D} \tanh (L_D)}{R_{mD}(A_S + G_{inj}R_{mS})L_D} \tag{5.15}$$

provided that the dendritic trees are all equivalent to cylinders of the same electrotonic length. Suppose, for example, that $L_D = 1.5$, implying $\tanh(L_D)/L_D = 0.6$; then a surface area ratio $(A_{\Sigma D}/A_S)$ of 20 would imply $\rho = 12$, if $G_{inj} = 0$ and $R_{mS} = R_{mD}$; however, it would imply $\rho = 6$, if $G_{inj} = 0$ with R_{mS} equal to half R_{mD}, or if $G_{inj} = A_S/R_{mS}$ with $R_{mS} = R_{mD}$.

Result for Neuron Equivalent to Cylinder

When the dendritic trees are equivalent to cylinders of the same electrotonic length and when ρ is large, but not accurately known, a useful overall estimate of R_m can be obtained

$$R_m \simeq R_N A_N \tanh (L_N)/L_N \tag{5.16}$$

where A_N and L_N represent the surface area and the electrotonic length of that cylinder most nearly equivalent to the whole neuron (i.e., soma plus dendrites). Here A_N equals $A_{\Sigma D}$ plus A_S, and L_N exceeds L_D by only a small amount when ρ is large (145, 148).

The usefulness of Equation 5.16 is greatly enhanced by the fact that the value of L_N can be estimated from an analysis of transients [(91-93, 145, 146); see Eq. 4.6]. Such estimates of L_N seem to be more reliable than the estimates of ρ (6, 86, 119, 145). The range of values, from 1 to 2 for L_N of cat spinal motoneurons implies a range, from 0.76 to 0.48 for the value of $\tanh(L_N)/L_N$ in Equation 5.16. The estimates of L_N and R_N can be made electrophysiologically; however, the estimate of soma-dendritic surface area (A_N) requires careful histological study and measurement of the same neuron. This experimental feat has been achieved by Lux et al. (119) and by Barrett & Crill (5, 6). Such measurements provide not only estimates of A_N, but also estimates of A_S and $\Sigma d^{3/2}$. Also the measurements of branch diameters permit an assessment of how well the dendritic trees satisfy the $d^{3/2}$ constraint for equivalence to a cylinder; in their analysis of 50 branchings, Lux et al. (119) found approximate satisfaction

of this constraint; however, Barrett & Crill (6) reported decreasing $\Delta d^{3/2}$ with distance away from the soma. In any case, when detailed anatomic measurements are available, one can use Eq. 5.16 to provide an initial estimate of R_m; then this estimate can be tested together with the best estimate of R_i, by carrying out a detailed computation of the input conductance of each dendritic tree (6, 119, 139) to see how nearly this combined dendritic input conductance can account for the whole neuron input conductance. Even after refinement by such testing, the resulting estimated range of values for R_m should be qualified by noting such possible sources of error as shrinkage (or swelling) between the time of the electrical measurements and the histological meas-

urements, as well as the possibility of injury or of different soma membrane resistivity noted with Equations 5.5, 5.6, and 5.15 [see (6, 119, 139, 145)].

Estimation of Motoneuron Parameters

The equations needed for estimation of membrane time constants are presented and discussed extensively in the preceding section. A full set of parameter estimates for motoneurons of cat spinal cord appears in Table 3. Mutually consistent representative values were selected for the first eight parameters (ranges are based on experiment). The last four representative values are consistent when dendritic trees are assumed equivalent to cylinders.

REFERENCES

1. AITKEN, J. T., AND J. E. BRIDGER. Neuron size and neuron population density in the lumbosacral region of the cat's spinal cord. *J. Anat.* 95: 38–53, 1961.
2. ARAKI, T., AND T. OTANI. Response of single motoneurons to direct stimulation in toad's spinal cord. *J. Neurophysiol.* 18: 472–485, 1955.
3. ARSHAVSKII, Y. I., M. B. BERKINBLIT, S. A. KOVALEV, V. V. SMOLYANINOV, AND L. M. CHAILAKHYAN. The role of dendrites in the functioning of nerve cells. *Dokl. Akademii Nauk SSSR* 163: 994–997, 1965. [Translation in *Dokl. Biophys.* Consultants Bureau, New York, 1965.]
4. BARNWELL, G. M., AND B. J. CERIMELE. A mathematical model of the effects of spatio-temporal patterns of dendritic input potentials on neuronal somatic potentials. *Kybernetik* 10: 144–155, 1972.
4a. BARRETT, J. N. Motoneuron dendrites: role in synaptic integration. *Federation Proc.* 34: 1398–1407, 1975.
5. BARRETT, J. N., AND W. E. CRILL. Specific membrane resistivity of dye-injected cat motoneurons. *Brain Res.* 28: 556–561, 1971.
6. BARRETT, J. N., AND W. E. CRILL. Specific membrane properties of cat motoneurones. *J. Physiol. London* 239: 301–324, 1974.
7. BARRETT, J. N., AND W. E. CRILL. Influences of dendritic location and membrane properties on the effectiveness of synapses on cat motoneurones. *J. Physiol. London* 239: 325–345, 1974.
8. BERNSTEIN, J. Untersuchungen zur Thermodynamik der bioelektrischen Ströme. *Pflueger's Arch. Ges. Physiol.* 92: 521–562, 1902.
9. BINSTOCK, L., AND L. GOLDMAN. Current and voltage clamped studies on *Myxicola* giant axons. *J. Gen. Physiol.* 54: 730–740, 1969.
10. BISHOP, G. H. Natural history of the nerve impulse. *Physiol. Rev.* 36: 376–399, 1956.
10a. BISHOP, G. H., AND J. L. O'LEARY. The polarity of potentials recorded from the superior colliculus. *J. Cellular Comp. Physiol.* 19: 289–300, 1942.
11. BOK, S. T. *Histonomy of the Cerebral Cortex.* Amsterdam: Elsevier, 1959.
12. BRAZIER, M. A. B. The historical development of neurophysiology. In: *Handbook of Physiology. Neurophysiology,* edited by H. W. Magoun. Washington, D.C.: Am. Physiol. Soc., 1959, sect. 1, vol. I, p. 1–59.
13. BRINLEY, F. J., JR. Sodium, potassium, and chloride concentrations and fluxes in the isolated giant axon of *Homarus. J. Neurophysiol.* 28: 742–772, 1965.
14. BROCK, L. G., J. S. COOMBS, AND J. C. ECCLES. The recording of potentials from motoneurones with an intracellular electrode. *J. Physiol. London* 117: 431–460, 1952.

15. BULLOCK, T. H. Neuron doctrine and electrophysiology. *Science* 129: 997–1002, 1959.
16. BURKE, R. E. Motor unit types of cat triceps surae muscle. *J. Physiol. London* 193: 141–160, 1967.
17. BURKE, R. E. Composite nature of the monosynaptic excitatory postsynaptic potential. *J. Neurophysiol.* 30: 1114–1136, 1967.
18. BURKE, R. E., AND G. TEN BRUGGENCATE. Electrotonic characteristics of alpha motoneurones of varying size. *J. Physiol. London* 212: 1–20, 1971.
19. BUTZ, E. G., AND J. D. COWAN. Transient potentials in dendritic systems of arbitrary geometry. *Biophys. J.* 14: 661–689, 1974.
20. CALVIN, W. H. Dendritic synapses and reversal potentials: theoretical implications of the view from the soma. *Exptl. Neurol.* 24: 248–264, 1969.
20a. CARPENTER, D. O., M. M. HOVEY, AND A. F. BAK. Measurements of intracellular conductivity in *Aplysia* neurons: evidence for organization of water and ions. *Ann. NY Acad. Sci.* 204: 502–530, 1973.
21. CARSLAW, H. S., AND J. C. JAEGER. *Conduction of Heat in Solids.* London: Oxford, 1959.
21a. CLARE, M. H., AND G. H. BISHOP. Properties of the dendrites; apical dendrites of the cat cortex. *Electroencephalog. Clin. Neurophysiol.* 7: 85–98, 1955.
22. CLARK, J., AND R. PLONSEY. The extracellular potential field of the single active nerve fiber in a volume conductor. *Biophys. J.* 8: 842–864, 1968.
23. COLE, K. S. Dynamic electrical characteristics of the squid giant axon membrane. *Arch. Sci. Physiol.* 3: 253–258, 1949.
24. COLE, K. S. *Membranes, Ions and Impulses.* Berkeley: Univ. of California Press, 1968.
25. COLE, K. S., AND H. J. CURTIS. Electric impedance of the squid giant axon during activity. *J. Gen. Physiol.* 22: 649–670, 1939.
26. COLE, K. S., AND H. J. CURTIS. Bioelectricity: electric physiology. In: *Medical Physics,* edited by O. Glasser. Chicago: Year Book, vol. II, 1950, p. 82–90.
27. COLE, K. S., AND A. L. HODGKIN. Membrane and protoplasm resistance in the squid giant axon. *J. Gen. Physiol.* 22: 671–687, 1939.
28. COOMBS, J. S., J. C. ECCLES, AND P. FATT. The electrical properties of the motoneurone membrane. *J. Physiol. London* 130: 291–325, 1955.
29. COOMBS, J. S., J. C. ECCLES, AND P. FATT. The inhibitory suppression of reflex discharges from motoneurones. *J. Physiol. London* 130: 396–413, 1955.
30. CREMER, M. Zum Kernleiterproblem. *Z. Biol.* 37: 550–553, 1899; *Z. Biol.* 40: 393–418, 1900.
31. CURTIS, H. J., AND K. S. COLE. Transverse electric imped-

ance of the squid giant axon. *J. Gen. Physiol.* 21: 757-765, 1938.

32. CURTIS, D. R., AND J. C. ECCLES. Time courses of excitatory and inhibitory synaptic actions. *J. Physiol. London* 145: 529-546, 1959.

33. DAVIS, L., JR., AND R. LORENTE DE NÓ. Contribution to the mathematical theory of the electrotonus. *Studies Rockefeller Inst. Med. Res.* 131: 442-496, 1947.

34. DIAMOND, J. The activation and distribution of GABA and L-glutamate receptor on goldfish *Mauthner* neurons: an analysis of remote dendritic inhibition (with appendix by A. F. Huxley). *J. Physiol. London* 194: 669-723, 1968.

35. DODGE, F. A., AND J. W. COOLEY. Action potential of the motoneuron. *IBM J. Res. Develop.* 17: 219-229, 1973.

36. DU BOIS-REYMOND, E. *Untersuchungen über Thierische Elektricität.* Berlin: Reimer, vol. I, 1848; vol. II, 1849.

37. ECCLES, J. C. *The Physiology of Nerve Cells.* Baltimore: Johns Hopkins Press, 1957.

38. ECCLES, J. C. Neuron physiology. In: *Handbook of Physiology. Neurophysiology,* edited by H. W. Magoun. Washington, D.C.: Am. Physiol. Soc., 1959, sect. 1, vol. I, p. 59-74.

39. ECCLES, J. C. Membrane time constants of cat motoneurones and time courses of synaptic action. *Exptl. Neurol.* 4: 1-22, 1961.

40. ECCLES, J.C. *The Physiology of Synapses.* Berlin: Springer, 1964.

41. EISENBERG, R. S., AND E. A. JOHNSON. Three dimensional electrical field problems in physiology. *Progr. Biophys.* 20: 1-65, 1970.

42. ENGEL, E., V. BARCILON, AND R. S. EISENBERG. The interpretation of current-voltage relations recorded with a single microelectrode. *Biophys. J.* 12: 384-403, 1972.

43. EVANS, J. W., AND N. SHENK. Solutions to axon equations. *Biophys. J.* 10: 1090-1101, 1970.

44. FADIGA, E., AND J. M. BROOKHART. Monosynaptic activation of different portions of the motor neuron membrane. *Am. J. Physiol.* 198: 693-703, 1960.

45. FALK, G., AND P. FATT. Linear electrical properties of striated muscle fibres observed with intracellular electrodes. *Proc. Roy. Soc. London Ser. B* 160: 69-123, 1964.

46. FATT, P. Biophysics of junctional transmission. *Physiol. Rev.* 34: 674-710, 1954.

46a.FATT, P. Electric potentials occurring around a neurone during its activation. *J. Neurophysiol.* 20: 27-60, 1957.

46b.FATT, P. Sequence of events in synaptic activation of a motoneurone. *J. Neurophysiol.* 20: 61-80, 1957.

47. FATT, P., AND B. KATZ. An analysis of the end-plate potential recorded with an intracellular electrode. *J. Physiol. London* 115: 320-370, 1951.

48. FATT, P., AND B. KATZ. The effect of inhibitory nerve impulses on a crustacean muscle fibre. *J. Physiol. London* 121: 374-389, 1953.

48a.FERNALD, R. D. A neuron model with spatially distributed synaptic input. *Biophys. J.* 11: 323-340, 1971.

48b.FISCHBACH, G. D., M. NAMEROFF, AND P. G. NELSON. Electrical properties of chick skeletal muscle fibers developing in cell culture. *J. Cell Physiol.* 78: 289-300, 1971.

49. FITZHUGH, R. Impulses and physiological states in theoretical models of nerve membrane. *Biophys. J.* 1: 445-466, 1961.

50. FITZHUGH, R. Computation of impulse initiation and saltatory conduction in a myelinated nerve fiber. *Biophys. J.* 2: 11-21, 1962.

51. FITZHUGH, R. Mathematical models of excitation and propagation in nerve. In: *Biological Engineering,* edited by H. P. Schwan. New York: McGraw Hill, 1969, p. 1-85.

52. FITZHUGH, R. Dimensional analysis of nerve models. *J. Theoret. Biol.* 40: 517-541, 1973.

53. FRANK, K., AND M. C. BECKER. Microelectrodes for recording and stimulation. In: *Physical Techniques in Biological Research,* edited by W. L. Nastuk. New York: Academic, 1964, vol. V, p. 22-87.

54. FRANK, K., AND M. G. F. FUORTES. Stimulation of spinal

motoneurones with intracellular electrodes. *J. Physiol. London* 134: 451-470, 1956.

55. FOURIER, J. *The Analytical Theory of Heat.* New York: Dover, 1955. [French original, 1822; English translation, 1878.]

56. GELFAN, S., G. KAO, AND D. S. RUCHKIN. The dendritic tree of spinal neurons. *J. Comp. Neurol.* 139: 385-411, 1970.

57. GESELOWITZ, D. B. Comment on the core conductor model. *Biophys. J.* 6: 691-692, 1966.

57a.GILBERT, D. S. Axoplasm architecture and physical properties as seen in the *Myxicola* giant axon. *J. Physiol. London* 253: 257-301, 1975.

58. GOLDMAN, D. E. Potential, impedance, and rectification in membranes. *J. Gen. Physiol.* 27: 37-60, 1943.

59. GOLDMAN, L. The effects of stretch on cable and spike parameters of single nerve fibres; some implications for the theory of impulse propagation. *J. Physiol. London* 175: 425-444, 1964.

60. GOLDMAN, L., AND J. S. ALBUS. Computation of impulse conduction in myelinated fibres; theoretical basis of the velocity diameter relation. *Biophys. J.* 8: 596-607, 1968.

61. GOLDMAN, L., AND C. L. SCHAUF. Quantitative description of sodium and potassium currents and computed action potentials in *Myxicola* giant axons. *J. Gen. Physiol.* 61: 361-384, 1973.

62. GOLDSTEIN, S. S., AND W. RALL. Changes of action potential shape and velocity for changing core conductor geometry. *Biophys. J.* 14: 731-757, 1974.

62a.GRAHAM, J., AND R. W. GERARD. Membrane potentials and excitation of impaled single muscle fibers. *J. Cellular Comp. Physiol.* 28: 99-117, 1946.

63. GRANIT, R. *The Basis of Motor Control.* New York: Academic, 1970.

64. GRUNDFEST, H. Electrical inexcitability of synapses and some consequences in the central nervous system. *Physiol. Rev.* 37: 337-361, 1957.

64a.HARMON, L. D., AND E. R. LEWIS. Neural modeling. *Physiol. Rev.* 46: 513-591, 1966.

65. HELLERSTEIN, D. Passive membrane potentials: a generalization of the theory of electrotonus. *Biophys. J.* 8: 358-379, 1968.

66. HENNEMAN, E., G. G. SOMJEN, AND D. D. CARPENTER. Functional significance of cell size in spinal motoneurons. *J. Neurophysiol.* 28: 599-620, 1965.

67. HERMANN, L. Allgemeine Nervenphysiologie. In: *Handbuch der Physiologie,* edited by L. Hermann. Leipzig: Vogel, 1879, vol. 2, parts 1 and 3.

68. HERMANN, L. Zur Theorie der Erregungsleitung und der elektrischen Erregung. *Pflueger's Arch. Ges. Physiol.* 75: 574-590, 1899.

69. HERMANN, L. Beiträge zur Physiologie und Physik des Nerven. *Pflueger's Arch. Ges. Physiol.* 109: 95-144, 1905.

70. HERMANN, L., AND O. WEISS. Ueber die Entwicklung des Elektrotonus. *Pflueger's Arch. Ges. Physiol.* 71: 237-295, 1898.

71. HODGKIN, A. L. Evidence for electrical transmission in nerve. Parts I and II. *J. Physiol. London* 90: 183-232, 1937.

72. HODGKIN, A. L. The subthreshold potentials in a crustacean nerve fibre. *Proc. Roy. Soc. London Ser. B* 126: 87-121, 1938.

73. HODGKIN, A. L. The membrane resistance of a non-medullated nerve fibre. *J. Physiol. London* 106: 305-318, 1947.

74. HODGKIN, A. L. The ionic basis of electrical activity in nerve and muscle. *Biol. Rev.* 26: 339-409, 1951.

75. HODGKIN, A. L. Ionic movements and electrical activity in giant nerve fibres (The Croonian Lecture). *Proc. Roy. Soc. London Ser. B* 148: 1-37, 1958.

76. HODGKIN, A. L. *The Conduction of the Nervous Impulse.* Springfield, Ill.: Thomas, 1964.

77. HODGKIN, A. L., AND A. F. HUXLEY. A quantitative description of membrane current and its application to conduction and excitation in nerve. *J. Physiol. London* 117: 500-544, 1952.

78. HODGKIN, A. L., A. F. HUXLEY, AND B. KATZ. Measurement of current-voltage relations in the membrane of the giant axon of the *Loligo*. *J. Physiol. London* 116: 424-448, 1952.

79. HODGKIN, A. L., AND B. KATZ. The effect of sodium ions on the electrical activity of the giant axon of the squid. *J. Physiol. London* 108: 37-77, 1949.

80. HODGKIN, A. L., AND W. A. H. RUSHTON. The electrical constants of a crustacean nerve fibre. *Proc. Roy. Soc. London Ser B* 133: 444-479, 1946.

81. HOORWEG, J. L. Ueber die elektrischen Eigenschaften der Nerven. *Pflueger's Arch. Ges. Physiol.* 71: 128-157, 1898.

82. HUBBARD, J. I., R. LLINÁS, AND D. M. J. QUASTEL. *Electrophysiological Analysis of Synaptic Transmission*. London: Arnold, 1969.

83. HUMPHREY, D. R. Re-analysis of the antidromic cortical response. II. On the contribution of cell discharge and PSPs to the evoked potentials. *Electroencephalog. Clin. Neurophysiol.* 25: 421-442, 1968.

84. HUXLEY, A. F., AND R. STÄMPFLI. Evidence for saltatory conduction in peripheral myelineated nerve fibres. *J. Physiol. London* 108: 315-339, 1949.

85. HUXLEY, A. F., AND R. STÄMPFLI. Direct determination of membrane resting potential and action potential in single myelinated nerve fibres. *J. Physiol. London* 112: 476-495, 1951.

86. IANSEK, R., AND S. J. REDMAN. An analysis of the cable properties of spinal motoneurones using a brief intracellular current pulse. *J. Physiol. London* 234: 613-636, 1973.

87. IANSEK, R., AND S. J. REDMAN. The amplitude, time course and charge of unitary excitatory post-synaptic potentials evoked in spinal motoneurone dendrites. *J. Physiol. London* 234: 665-688, 1973.

88. ITO, M., AND T. OSHIMA. Electrical behaviour of the motoneurone membrane during intracellularly applied current steps. *J. Physiol. London* 180: 607-635, 1965.

89. JACK, J. J. B., S. MILLER, R. PORTER, AND S. J. REDMAN. The distribution of group Ia synapses on lumbosacral spinal motoneurones in the cat. In: *Excitatory Synaptic Mechanisms*, edited by P. Andersen and J. K. S. Jansen. Oslo: Universitetsforlaget, 1970, p. 199-205.

90. JACK, J. J. B., S. MILLER, R. PORTER, AND S. J. REDMAN. The time course of minimal excitatory post-synaptic potentials evoked in spinal motoneurones by group Ia afferent fibres. *J. Physiol. London* 215: 353-380, 1971.

91. JACK, J. J. B., D. NOBLE, AND R. W. TSIEN. *Electric Current Flow in Excitable Cells*. London: Oxford, 1975.

92. JACK, J. J. B., AND S. J. REDMAN. The propagation of transient potentials in some linear cable structures. *J. Physiol. London* 215: 283-320, 1971.

93. JACK, J. J. B., AND S. J. REDMAN. An electrical description of the motoneurone and its application to the analysis of synaptic potentials. *J. Physiol. London* 215: 321-352, 1971.

94. JACOBSON, S., AND D. A. POLLEN. Electrotonic spread of dendritic potentials in feline pyramidal cells. *Science* 161: 1351-1353, 1968.

95. KAPLAN, S., AND D. TRUJILLO. Numerical studies of the partial differential equations governing nerve impulse conduction: the effect of Lieberstein's inductance term. *Math. Biosci.* 7: 379-404, 1970.

96. KATZ, B. Experimental evidence for a non-conducted response of nerve to subthreshold stimulation. *Proc. Roy. Soc. London Ser. B* 124: 244-276, 1937.

97. KATZ, B. *Electric Excitation of Nerve*. Oxford, 1939.

98. KATZ, B. The electrical properties of the muscle fibre membrane. *Proc. Roy. Soc. London Ser. B* 135: 506-534, 1948.

99. KATZ, B. *Nerve, Muscle, and Synapse*. New York: McGraw Hill, 1966.

100. KATZ, B., AND R. MILEDI. A study of spontaneous potentials in spinal motoneurones. *J. Physiol. London* 168: 389-422, 1963.

101. KELVIN, W. T. On the theory of the electric telegraph. *Proc. Roy. Soc.* 7: 382-399, 1855; also *Phil. Mag. Ser.* 4, 11: 146-160, 1856 and *Kelvin's Collected Papers*.

102. KERNELL, D. Input resistance, electrical excitability, and size of ventral horn cells in cat spinal cord. *Science* 152: 1637-1640, 1966.

103. KERNELL, D. The repetitive impulse discharge of a simple neurone model compared to that of spinal motoneurones. *Brain Res.* 11: 685-687, 1968.

103a.KHODOROV, B. I., AND E. N. TIMIN. Nerve impulse propagation along nonuniform fibers. *Progr. Biophys. Mol. Biol.* 30: 145-184, 1975.

103b.KLEE, M., AND W. RALL. Computed potentials of cortically arranged populations of neurons. *J. Neurophysiol.* In Press.

104. KOLES, Z. J., AND M. RASMINSKY. A computer simulation of conduction in demyelinated nerve fibres. *J. Physiol. London* 227: 351-364, 1972.

105. KUNO, M. Quantum aspects of central and ganglionic synaptic transmission in vertebrates. *Physiol. Rev.* 51: 647-678, 1971.

106. KUNO, M., AND R. LLINÁS. Enhancement of synaptic transmission by dendritic potentials in chromatolyzed motoneurones of the cat. *J. Physiol. London* 210: 807-821, 1970.

107. LEWIS, E. R. The iron-wire model of the neuron: a review. In: *Cybernetic Problems in Bionics*, edited by H. L. Oestreicher. New York: Gordon and Breach, 1968.

107a.LEWIS, E. R. Using electronic circuits to model simple neuroelectric interactions. *Proc. IEEE* 56: 931-949, 1968.

108. LING, G., AND R. W. GERARD. The normal membrane potential of frog sartorius fibers. *J. Cellular Comp. Physiol.* 34: 383-396, 1949.

109. LIEBERSTEIN, H. M. On the Hodgkin-Huxley partial differential equation. *Math. Biosci.* 1: 45-69, 1967.

110. LLINÁS, R., AND C. NICHOLSON. Electrophysiological properties of dendrites and somata in alligator Purkinje cells. *J. Neurophysiol.* 34: 532-551, 1971.

111. LLOYD, D. P. C. Integrative pattern of excitation and inhibition in two-neuron reflex arcs. *J. Neurophysiol.* 9: 439-444, 1946.

112. LORENTE DE NÓ, R. Synaptic stimulation as a local process. *J. Neurophysiol.* 1: 194-206, 1938.

113. LORENTE DE NÓ, R. A study of nerve physiology. *Studies Rockefeller Inst. Med. Res.* 131 and 132, 1947.

114. LORENTE DE NÓ, R. Action potential of the motoneurons of the hypoglossus nucleus. *J. Cellular Comp. Physiol.* 29: 207-287, 1947.

115. LORENTE DE NÓ, R. Conduction of impulses in the neurons of the oculomotor nucleus. In: *The Spinal Cord*, edited by J. L. Malcolm and J. A. B. Cray. Boston: Little, Brown, 1953. (Ciba Found. Symp.)

116. LORENTE DE NÓ, R., AND G. A. CONDOURIS. Decremental conduction in peripheral nerve; integration of stimuli in the neuron. *Proc. Natl. Acad. Sci. US* 45: 592-617, 1959.

117. LUX, H-D. Eigenschaften eines Neuron-Modells mit Dendriten begrenzter Länge. *Pflueger's Arch. Ges. Physiol.* 297: 238-255, 1967.

118. LUX, H-D., AND D. A. POLLEN. Electrical constants of neurons in the motor cortex of the cat. *J. Neurophysiol.* 29: 207-220, 1966.

119. LUX, H-D., P. SCHUBERT, AND G. W. KREUTZBERG. Direct matching of morphological and electrophysiological data in cat spinal motoneurons. In: *Excitatory Synaptic Mechanisms*, edited by P. Andersen and J. K. S. Jansen. Oslo: Universitetsforlaget, 1970, p. 189-198.

120. MARMONT, G. Studies on the axon membrane. 1. A new method. *J. Cellular Comp. Physiol.* 34: 351-382, 1949.

121. MARTIN, A. R. A further study of the statistical composition of the end-plate potential. *J. Physiol. London* 130: 114-122, 1955.

122. MATTEUCCI, M. C. Sur le pouvoir électro-moteur secondaire des nerfs, et son application à l'électro-physiologie. *Compt. Rend.* 56: 760, 1863.

123. MENDELL, L. M., AND E. HENNEMAN. Terminals of single Ia fibers: location, density, and distribution within a pool of

300 homonymous motoneurons. *J. Neurophysiol.* 34: 171–187, 1971.

124. MIROLLI, M., AND S. R. TALBOTT. The geometrical factors determining the electrotonic properties of a molluscan neurone. *J. Physiol. London* 227: 19–34, 1972.

125. MOORE, J. W., AND K. S. COLE. Voltage clamp techniques. In: *Physical Techniques in Biological Research*, edited by W. L. Nastuk. New York: Academic, 1963, vol. 6, p. 263–321.

125a. MOORE, J. W., F. RAMÓN, AND R. W. JOYNER. Axon voltage-clamp simulations. *Biophys. J.* 15: 11–69, 1975.

126. NASTUK, W. L., AND A. L. HODGKIN. The electrical activity of single muscle fibres. *J. Cellular Comp. Physiol.* 35: 39–73, 1950.

127. NELSON, P. G. Interaction between spinal motoneurons of the cat. *J. Neurophysiol.* 29: 275–287, 1966.

128. NELSON, P. G., AND K. FRANK. Extracellular potential fields of single spinal motoneurons. *J. Neurophysiol.* 27: 913–927, 1964.

129. NELSON, P. G., AND K. FRANK. Anomalous rectification in cat spinal motoneurons and effect of polarizing currents on excitatory post synaptic potential. *J. Neurophysiol.* 30: 1097–1113, 1967.

130. NELSON, P. G., AND H-D. LUX. Some electrical measurements of motoneuron parameters. *Biophys. J.* 10: 55–73, 1970.

131. NORMAN, R. S. Cable theory for finite length dendritic cylinders with initial and boundary conditions. *Biophys. J.* 12: 25–45, 1972.

132. PESKOFF, A., AND R. S. EISENBERG. A point source in a cylindrical cell: potential for a step-function of current inside an infinite cylindrical cell in a medium of finite conductivity. *UCLA Engr. School Rep.* No. 7421, April 1974.

133. PFLÜGER, E. *Physiologie des Electrotonus.* Berlin: Hirschwald, 1859.

134. PICKARD, W. F. A contribution to the electromagnetic theory of the unmyelinated axon. *Math. Biosci.* 2: 111–121, 1968.

134a. PICKARD, W. F. Electrotonus on a cell of finite dimensions. *Math. Biosci.* 10: 201–213, 1971.

135. PLONSEY, R. Volume conductor fields of action currents. *Biophys. J.* 4: 317–328, 1964.

136. PLONSEY, R. *Bioelectric Phenomena.* New York: McGraw Hill, 1969.

137. POTTALA, E. W., T. R. COLBURN, AND D. R. HUMPHREY. A dendritic compartment model neuron. *IEEE Trans. Biomed. Engr. BME* 20: 132–139, 1973.

138. RALL, W. Membrane time constant of motoneurons. *Science* 126: 454, 1957.

139. RALL, W. Branching dendritic trees and motoneuron membrane resistivity. *Exptl. Neurol.* 1: 491–527, 1959.

140. RALL, W. Membrane potential transients and membrane time constant of motoneurons. *Exptl. Neurol.* 2: 503–532, 1960.

141. RALL, W. Theory of physiological properties of dendrites. *Ann. NY Acad. Sci.* 96: 1071–1092, 1962.

142. RALL, W. Electrophysiology of a dendritic neuron model. *Biophys. J.* 2, no. 2, part 2: 145–167, 1962.

143. RALL, W. Theoretical significance of dentritic trees for neuronal input-output relations. In: *Neural Theory and Modeling*, edited by R. Reiss. Stanford: Stanford Univ. Press, 1964, p. 73–97.

144. RALL, W. Distinguishing theoretical synaptic potentials computed for different soma-dendritic distributions of synaptic input. *J. Neurophysiol.* 30: 1138–1168, 1967.

145. RALL, W. Time constants and electrotonic length of membrane cylinders and neurons. *Biophys. J.* 9: 1483–1508, 1969.

146. RALL, W. Distributions of potential in cylindrical coordinates and time constants for a membrane cylinder. *Biophys. J.* 9: 1509–1541, 1969.

147. RALL, W. Dendritic neuron theory and dendrodendritic synapses in a simple cortical system. In: *The Neurosciences: Second Study Program*, edited by F. O. Schmitt. New York: Rockefeller, 1970, p. 552–565.

148. RALL, W. Cable properties of dendrites and effects of synaptic location. In: *Excitatory Synaptic Mechanisms*, edited by P. Andersen and J. K. S. Jansen. Oslo: Universitetsforlag, 1970, p. 175–187.

149. RALL, W., R. E. BURKE, T. G. SMITH, P. G. NELSON, AND K. FRANK. Dendritic location of synapses and possible mechanisms for the monosynaptic EPSP in motoneurons. *J. Neurophysiol.* 30: 1169–1193, 1967.

150. RALL, W., AND J. RINZEL. Branch input resistance and steady attenuation for input to one branch of a dendritic neuron model. *Biophys. J.* 13: 648–688, 1973.

151. RALL, W., AND G. M. SHEPHERD. Theoretical reconstruction of field potentials and dendrodendritic synaptic interactions in olfactory bulb. *J. Neurophysiol.* 31: 884–915, 1968.

152. RALL, W., G. M. SHEPHERD, T. S. REESE, AND M. W. BRIGHTMAN. Dendro-dendritic synaptic pathway for inhibition in the olfactory bulb. *Exptl. Neurol.* 14: 44–56, 1966.

152a. RAMÓN, F., R. W. JOYNER, AND J. W. MOORE. Propagation of action potentials in inhomogeneous axon regions. *Federation Proc.* 34: 1357–1363, 1975.

153. RAMÓN MOLINER, E. An attempt at classifying nerve cells on the basis of their dendritic patterns. *J. Comp. Neurol.* 119: 211–227, 1962.

154. RAMÓN MOLINER, E. The morphology of dendrites. In: *The Structure and Function of the Nervous System*, edited by G. H. Bourne. New York: Academic, 1968. vol. 1.

155. RAMÓN Y CAJAL, S. *Histologie du Systeme Nerveux de l'Homme et des Vertebres* (translated by L. Asoulay). Paris: Maloine, 1911.

156. RANCK, J. B., JR. Analysis of specific impedance of rabbit cerebral cortex. *Exptl. Neurol.* 7: 153–174, 1963.

157. RASHBASS, C., AND W. A. H. RUSHTON. The relation of structure to the spread of excitation in the frog's sciatic trunk. *J. Physiol. London* 110: 110–135, 1949.

158. RASMUSSEN, G. L. Selective silver impregnation of synaptic endings. In: *New Research Techniques of Neuroanatomy*, edited by W. F. Windle. Springfield, Ill.: Thomas, 1957.

159. REDMAN, S. J. The attenuation of passively propagating dendritic potentials in a motoneurone cable model. *J. Physiol. London* 234: 637–664, 1973.

160. RINZEL, J., AND J. B. KELLER. Traveling wave solutions of a nerve conduction equation. *Biophys. J.* 13: 1313–1337, 1973.

161. RINZEL, J., AND W. RALL. Transient response in a dendritic neuron model for current injected at one branch. *Biophys. J.* 14: 759–790, 1974.

162. RUSHTON, W. A. H. The effect upon the threshold for nervous excitation of the length of nerve exposed and the angle between current and nerve. *J. Physiol. London* 63: 357–377, 1927.

163. RUSHTON, W. A. H. Initiation of the propagated disturbance. *Proc. Roy. Soc. London Ser. B* 124: 210–243, 1937.

164. RUSHTON, W. A. H. A theory of the effects of fibre size in medullated nerve. *J. Physiol. London* 115: 101–122, 1951.

165. SCHEIBEL, M. E., AND A. B. SCHEIBEL. Of pattern and place in dendrites. *Intern. Rev. Neurobiol.* 13: 1–26, 1970.

166. SCHWAN, H. P. Electrical properties of tissue and cell suspensions. In: *Advances in Biological and Medical Physics*, edited by J. H. Lawrence and C. A. Tobias. New York: Academic, 1957, vol. 5, p. 147–209.

167. SCHWAN, H. P. Determination of biological impedances. In: *Physical Techniques in Biological Research*, edited by W. L. Nastuk. New York: Academic, 1963, vol. 6, p. 323–407.

168. SCHWAN, H. P., AND K. S. COLE. Bioelectricity: alternating current admittance of cells and tissues. In: *Medical Physics*, edited by O. Glasser. Chicago: Yearbook, 1960, vol. 3, p. 52–56.

168a. SCHWINDT, P. C., AND W. H. CALVIN. Nature of conductances underlying rhythmic firing in cat spinal motoneurons. *J. Neurophysiol.* 36: 955–973, 1973.

169. SCOTT, A. C. Effect of the series inductance of a nerve axon upon its conduction velocity. *Math. Biosci.* 11: 277–290, 1971.

169a. SCOTT, A. C. The electrophysics of a nerve fiber. *Rev. Mod.*

Physics 47: 487–533, 1975.

170. SHEPHERD, G. M. The olfactory bulb as a simple cortical system: experimental analysis and functional implications. In: *The Neurosciences: Second Study Program*, edited by F. O. Schmitt. New York: Rockefeller, 1970, p. 539–552.

171. SHEPHERD, G. W. *The Synaptic Organization of the Brain*. London: Oxford, 1974.

172. SHEPHERD, G. M., AND L. B. HABERLY. Partial activation of olfactory bulb: analysis of field potentials and topographic relation between bulb and lateral olfactory tract. *J. Neurophysiol.* 33: 643–653, 1970.

173. SHOLL, D. A. *The Organization of the Cerebral Cortex*. New York: Wiley, 1956.

174. SMITH, T. G., R. B. WUERKER, AND K. FRANK. Membrane impedance changes during synaptic transmission in cat spinal motoneurons. *J. Neurophysiol.* 30: 1072–1096, 1967.

175. SPENCER, W. A., AND E. R. KANDEL. Electrophysiology of hippocampal neurons. III. Firing level and time constant. *J. Neurophysiol.* 24: 260–271, 1961.

176. STÄMPFLI, R. Bau und Funktion isolierter markhaltiger Nervenfasern. *Ergeb. Physiol.* 47: 70–165, 1952.

177. TAKAHASHI, K. Slow and fast groups of pyramidal tract cells and their respective membrane properties. *J. Neurophysiol.* 28: 908–924, 1965.

178. TASAKI, I. The electrosaltatory transmission of the nerve impulse and the effect of narcosis upon the nerve fiber. *Am. J. Physiol.* 127: 211–227, 1939.

179. TASAKI, I. *Nervous Transmission*. Springfield, Ill.: Thomas, 1953.

180. TASAKI, I. New measurements of the capacity and the resistance of the myelin sheath and the nodal membrane of the isolated frog nerve fiber. *Am. J. Physiol.* 181: 639–650, 1955.

181. TASAKI, I. Conduction of the nerve impulse. In: *Handbook of Physiology. Neurophysiology*, edited by H. W. Magoun. Washington, D.C.: Am. Physiol. Soc., 1959, sect. 1, vol. I, p. 75–121.

182. TAYLOR, R. E. Cable theory. In: *Physical Techniques in Biological Research*, edited by W. L. Nastuk. New York: Academic, 1963, vol. 6, chapt. 4, p. 219–262.

183. TSUKAHARA, N., F. MURAKAMI, AND H. HULTBORN. Electrical constants of neurons of the red nucleus. *Exptl. Brain Res.* 23: 49–64, 1975.

183a. TSUKAHARA, N., K. TOYAMA, AND K. KOSAKA. Electrical activity of red nucleus neurones investigated with intracellular microelectrodes. *Exptl. Brain Res.* 4: 18–33, 1967.

183b. VALDIOSERA, R., C. CLAUSEN, AND R. S. EISENBERG. Measurement of the impedance of frog skeletal muscle fibers. *Biophys. J.* 14: 295–315, 1974.

184. WEBER, H. Ueber die stationären Strömungen der Elektricität in Cylindern. *J. Reine Angewandte Math.* 76: 1–20, 1873.

185. WEIDMANN, S. The electrical constants of Purkinje fibres. *J. Physiol. London* 118: 348–360, 1952.

186. WEINBERG, A. M. Weber's theory of the Kernleiter. *Bull. Math. Biophys.* 3: 39–55, 1941.

187. WOODBURY, J. W., AND H. D. PATTON. Electrical activity of single spinal cord elements. *Cold Spring Harbor Symp. Quant. Biol.* 17: 185–188, 1952.

188. WYCKOFF, R. W. G., AND J. Z. YOUNG. The motoneuron surface. *Proc. Roy. Soc. London Ser. B* 144: 440–450, 1956.

189. YOUNG, J. Z. Structure of nerve fibres and synapses in some invertebrates. *Cold Spring Harbor Symp. Quant. Biol.* 4: 1–6, 1936.

190. ZUCKER, R. S. Field potentials generated by dendritic spikes and synaptic potentials. *Science* 165: 409–413, 1969.

191. ZUCKER, R. S. Theoretical implications of the size principle of motoneurone recruitment. *J. Theoret. Biol.* 38: 587–596, 1973.